Multiphase flow in spout fluidized bed granulators

Multiphase Flow in Spout Fluidized Bed Granulators

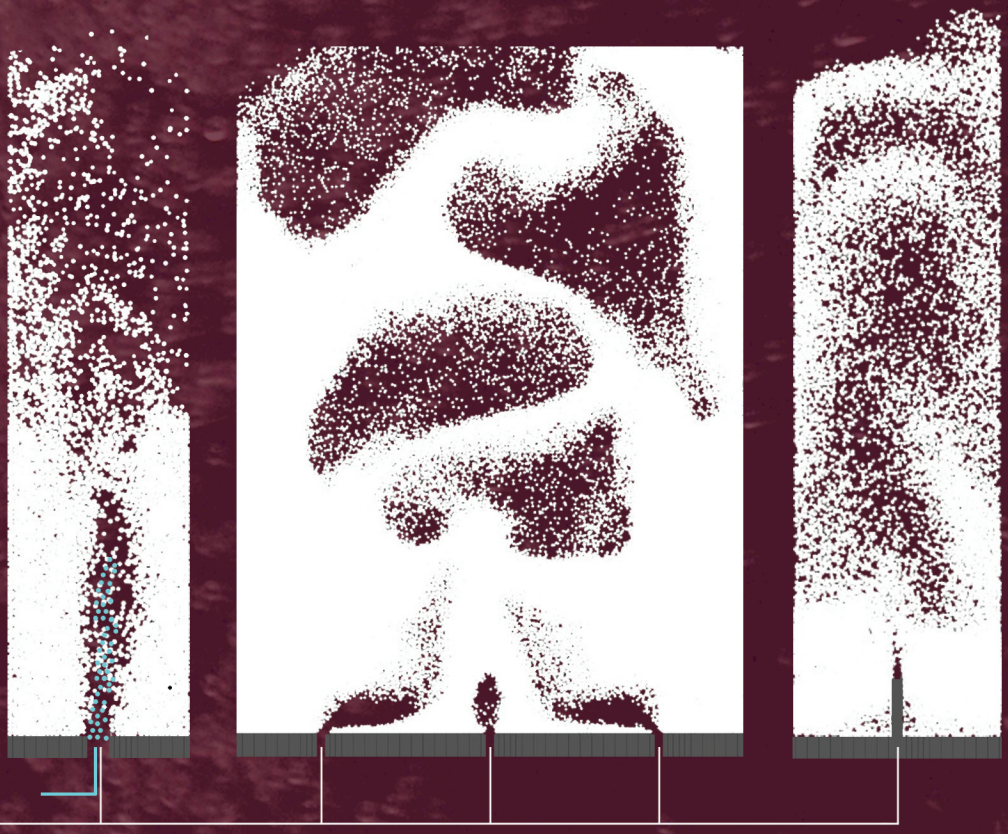

M.S. van Buijtenen - Tiemersma

Multiphase Flow in Spout Fluidized Bed Granulators

Samenstelling promotiecommissie:

Prof.dr. P.J. Lemstra, voorzitter	Technische Universiteit Eindhoven
Prof.dr.ir. J.A.M Kuipers, promotor	Technische Universiteit Eindhoven
Dr.ir. N.G Deen, copromotor	Technische Universiteit Eindhoven
Prof.dr. J.P.K. Seville	University of Warwick
Prof.dr.–Ing habil. S. Heinrich	Technische Universität Hamburg-Harburg
Prof.dr.ir. J.C. Schouten	Technische Universiteit Eindhoven
Prof.dr. R.F. Mudde	Technische Universiteit Delft
Dr. R. van Belzen	Yara Technology Center Sluiskil

This research was financially supported by the FOM-STW-EZ research programme 'Dispersed multiphase flow' (05MFS53, workgroup STW (TPC.7507)) and Yara Technology Center Sluiskil, the Netherlands.

Publisher:
Ipskamp Drukkers B.V., P.O box 333, 7500 AH, Enschede, the Netherlands
A catalogue record is available from the Eindhoven University of Technology Library
ISBN: 978-90-386-2459-4

Multiphase Flow in Spout Fluidized Bed Granulators

PROEFSCHRIFT

ter verkrijging van de graad van doctor aan de
Technische Universiteit Eindhoven, op gezag van de
rector magnificus, prof.dr.ir. C.J. van Duijn, voor een
commissie aangewezen door het College voor
Promoties in het openbaar te verdedigen
op donderdag 19 mei 2011 om 16.00 uur

door

Maria Suzanna van Buijtenen

geboren te Warnsveld

Dit proefschrift is goedgekeurd door de promotor:

prof.dr.ir. J.A.M. Kuipers

Copromotor:
dr.ir. N.G. Deen

Summary

Multiphase Flow in Spout Fluidized Bed Granulators

Spout fluidized beds are frequently used for the production of granules or particles through granulation, which are widely applied, for example, in the production of detergents, pharmaceuticals, food and fertilizers (Mörl et al. 2007). Spout fluidized beds have a number of advantageous properties, such as high mobility of the particles preventing undesired agglomeration and enabling excellent heat transfer control. Additionally, liquid can easily be sprayed into the bed through the spout, making spout fluidized beds very suitable for coating and layer wise growth of particles. During the granulation process, particles contain different loadings of melt which results in altered collision properties in time and space across the bed. This change in collision properties influences the bed dynamics, and consequently the granule quality. To improve the performance of the spout fluidized bed granulator, it is very important to understand the interplay of collision properties and bed dynamics, and is therefore studied in this work. The particle-particle interactions were first studied in a 3D system, using the Discrete Element Model (DEM). Several test cases were defined, where the particles possessed a different restitution coefficient for each case, and the examined flow regimes comprised the intermediate / spout-fluidization regime (B1), spouting-with-aeration regime (B2) and the jet-in-fluidized-bed regime (B3). The pressure drop and the vertical particle velocity were compared to experimental data obtained by Link et al. (2007). The computed results with $e_n = 0.97$ resembled the experimental results very well. It was shown that a decreasing restitution coefficient produces more vigorous bubbling and more pronounced heterogeneity (instability). The particle velocity and RMS (root mean square) profiles confirm the effect on the stability of the bed and reveal that the spout channel for cases B1 and B3 becomes unstable when the restitution coefficient decreases. For case B2, a transition occurred from the spouting-with-aeration to the intermediate/spout-fluidization regime at low restitution coefficient. These findings demonstrate the profound influence of the restitution coefficient on the dynamics of the bed. During the granulation process, when the particles contain different moisture contents, regions in the bed exist that contain particles with different restitution coefficients. These regions thus experience different dynamics, resulting in complex overall dynamic behaviour of the spout fluidized bed granulator.

To verify if the same features are observed in experiments, different particle systems with *a.o.* different restitution coefficients were investigated in a pseudo-2D spout fluidized bed. This was done for different flow regimes: the spout-fluidization regime (case B1), the spouting-with-aeration regime (case B2) and

the jet-in-fluidized-bed regime (case B3). The considered particle systems comprise glass beads, γ-alumina oxide and zeolite 4A particles, which are all classified as Geldart D particles. A non-intrusive measurement technique was used, *viz.* particle image velocimetry (PIV) to obtain the particle flow field in a pseudo two-dimensional (2D) spout fluidized bed. Additionally, digital images were analyzed using a newly developed digital image analysis (DIA) algorithm to evaluate the particle volume fraction. It is demonstrated that the new proposed DIA algorithm provides reliable information on the particle volume fraction distribution, showing that it is a powerful tool when combined with PIV. The added value of DIA is confirmed by comparing the particle velocity fields and volumetric particle fluxes. The particle flux obtained with the combined PIV/DIA technique was used to validate DEM simulation results of the jet-in-fluidized-bed regime (case B3) for all three particle systems. It was found that the vertical particle fluxes obtained from the simulations were slightly overpredicted higher up in the bed and in the annulus region, which most likely is due to the more pronounced wall effect in pseudo-2D beds. Simulations with a larger friction coefficient for particle-wall interactions with glass beads showed (for this examined system) a better resemblance to the computed downward flux in the annulus compared to the experimental results. The effect of the collision properties for glass beads, γ-alumina oxide and zeolite 4A particles has been studied in the three flow regimes and for each flow regime, the particle volume fraction profiles show small differences among the different particle systems. For the γ-alumina oxide and zeolite 4A particles, the spout channel is less stable for the cases B1 and B2. The particle fluxes also display small differences between the particle systems for each flow regime.

The simulated cases mimicked different stages of wetting during granulation processes, and they revealed that the bed dynamics is highly affected by differences in the restitution coefficient. During granulation processes, however, regions of wet particles and dry particles prevail at different locations inside the bed and at different time-scales. Therefore, a variable restitution coefficient was considered, to study the effect of the inter-particle interaction on the bed dynamics. The restitution coefficient is varied in time and space depending on the moisture content due to the particle-droplet interaction and evaporation. For this study, the DEM was extended by incorporating the moisture content into the (effective) restitution coefficient where both droplets and particles were considered as discrete elements. The same flow regimes were examined and for all flow regimes, the averaged bed height increased with decreasing restitution coefficient. Moreover, the averaged

bed height for a variable restitution coefficient was larger for all flow regimes compared to a case with a constant restitution coefficient, indicating that the spatial distribution of the restitution coefficient influences the bed dynamics. The effect of evaporation on the distribution of the restitution coefficient was only observed for the jet-in-fluidized-bed regime (B3), where the background velocity is relatively high leading to enhanced evaporation from the particles in the annulus region. This is reflected in the averaged bed height for the evaporation test case, which is larger compared to a test case without evaporation. A larger bed height for cases with variable restitution coefficient is due to the pressure build up in the spout region caused by the longer closing period of the spout channel. This is confirmed by the recorded pressure fluctuation signal and its root mean square which are larger for the cases with the variable restitution coefficient.

To the author's knowledge, most of the research on spout fluidized beds done so far had been focussed on single-spout fluidization. However, multiple spouts are present in industrial granulators, and little was known about the effect of multiple spouts on the bed dynamics. Therefore, the objective of this work was to study the effect of two and three spouts on the bed dynamics of a pseudo-2D spout fluidized bed, by employing the DEM and applying Particle Image Velocimetry (PIV) and Positron Emission Particle Tracking (PEPT) techniques on a pseudo-2D spout fluidized bed. A flow regime map was constructed, revealing new regimes that were not reported so far. The multiple-interacting-spouts regime (C) has been studied in detail for a double- and triple-spout fluidized bed, where the corresponding fluidization regime for a single-spout fluidized bed has been studied as a reference case. The experimental results obtained with PIV and PEPT agreed very well for all the three cases, showing the good performance of these techniques. The DEM simulation results slightly deviated from the experiments which was attributed to particle-wall effects that are more dominant in pseudo-2D beds than in 3D systems. The investigated multiple-interacting-spouts regime is a fully new flow regime that does not appear in single-spout fluidized beds. Two flow patterns have been observed, *viz.* particle circulation in between the spouts near the bottom of the bed, and an apparent single-spout fluidization motion at a higher location upwards in the bed. These findings show that the presence of multiple spouts in a spout fluidized bed highly affect the flow behaviour, which cannot be distinguished by solely investigating single-spout fluidized beds.

A second geometric feature in industrial spout fluidized bed granulators is that the spouts are slightly elevated from the bottom plate to facilitate efficient the

injection of the liquid. The influence on the bed dynamics was investigated as well. The experiments were conducted in a pseudo-2D and a cylindrical 3D spout fluidized bed, where Positron Emission Particle Tracking (PEPT) and Particle Image Velocimetry (PIV) were applied to the pseudo-2D bed, and PEPT and Electrical Capacitance Tomography (ECT) to the cylindrical 3D bed. A discrete element model (DEM) was used to perform full 3D simulations of the bed dynamics. Several cases were studied, *i.e.* beds with spout heights of 0, 2 and 4 cm. In the pseudo-2D bed the spout-fluidization and jet-in-fluidized-bed regime were considered first, and it was shown that in the spout-fluidization regime the expected dead zones appeared in the annulus near the bottom of the bed in case the spout is elevated. However, in the jet-in-fluidized-bed regime the circulation pattern of the particles is affected, without the development of stagnant zones. The jet-in-fluidized-bed regime was further investigated, and additionally the experimental results obtained with PIV and PEPT were compared with the DEM simulation results. The experimental results obtained with PIV and PEPT agreed mutually very well, and in addition agreed well wtih the DEM results, although the velocities in the annulus region were slightly overpredicted. The latter is probably due to the particle-wall effects that are more dominant in pseudo-2D systems compared to 3D systems. In the jet-in-fluidized-bed regime the background gas velocity is relatively high, producing bubbles in the annulus that interact with the spout channel. In case of a non-elevated spout, this interaction occurs near the bottom of the bed. As the spout is elevated, this interaction is shifted upwards in the bed, which allows the bubbles to remain undisturbed providing the motion of the particles in the annulus near the bottom of the bed. As a result, no dead zones are created and additionally, circulation patterns are vertically stretched. These findings were also obtained for the cylindrical 3D bed, though, the effects were less pronounced. In the cylindrical 3D bed the PEPT results show that the effect on the bed dynamics starts at $h_{spout} = 4$ cm, which is confirmed by the ECT results. Additionally, ECT measurements were conducted for $h_{spout} = 6$ cm to verify if indeed the effect prevails at larger spout heights. The root mean square of the particle volume fraction slightly increased at $h_{spout} = 2$ cm, while a larger increase is found at $h_{spout} = 4$ and 6 cm, showing that indeed more bubbles are formed. The presented results have not been reported so far and form valuable input information for improving industrial granulators.

Samenvatting

Meerfase Stroming in Spout Wervelbed Granulatoren

Spout wervelbedden worden vaak gebruikt voor de productie van deeltjes door middel van granulatie. Deze deeltjes worden breed toegepast in de productie van, bijvoorbeeld, waspoeders, pharmaceutische producten, voeding en kunstmest (Mörl et al. 2007). Spout wervelbedden hebben een groot aantal voordelen, waaronder een hoge mate van mobiliteit van de deeltjes zodat ongewenste agglomeratie voorkomen wordt en warmteoverdracht zeer goed gecontroleerd kan worden. Daarbij kan een vloeistof eenvoudig via de spout in het bed gesproeid worden, wat spout wervelbedden zeer geschikt maakt voor het coaten en het laten groeien van deeltjes dat laag voor laag plaatsvindt. Gedurende het granulatieproces bevatten de deeltjes verschillende hoeveelheden vocht wat resulteert in variërende botsingseigenschappen in tijd en plaats in het bed. Deze verandering van botsingseigenschappen beïnvloedt de beddynamica, en dus ook de kwaliteit van het product. Om de prestatie van de spout wervelbed granulator te verbeteren, is het zeer belangrijk om de wisselwerking tussen botsingseigenschappen en beddynamica te begrijpen en daarom is deze wisselwerking onderzocht in dit proefschrift. De deeltjes-deeltjes interactie is eerst bestudeerd in een 3D systeem, waarbij gebruik is gemaakt van het "Discrete Element Model" (DEM). Hiertoe zijn verschillende systemen gedefinieerd waarbij voor elk systeem de deeltjes een andere restitutiecoëfficiënt hadden. De bestudeerde stromingsregimes bestonden uit het spout-gefluïdiseerde regime (B1), spouten-met-beluchting regime (B2) en het straal-in-gefluïdiseerd-bed regime (B3). De drukval en verticale deeltjes snelheden zijn vergeleken met experimentele data die verkregen zijn door Link et al. (2007). De met DEM berekende resultaten met $e_n = 0.97$ komen goed overeen met de experimentele resultaten. Tevens is aangetoond dat wanneer de restitutiecoëfficiënt daalt, meer bellen aanwezig zijn die meer heterogeniteit (instabiliteit) in het bed veroorzaken. De mate waarin dit plaatsvindt is afhankelijk van het stromingsregime waarin geopereerd wordt. De deeltjes snelheid en RMS (standaarddeviatie) profielen bevestigen het effect op het bed en laten zien dat het spoutkanaal voor de B1 en B3 systemen instabiel wordt wanneer de restitutiecoëfficiënt daalt. Voor systeem B2 vindt er bij lage restitutiecoëfficiënt een overgang plaats van spouten-met-beluchting naar het spout-fluïdisatie regime. Deze bevindingen laten zien dat de invloed van de restitutiecoëfficiënt op de beddynamica van groot belang is. Tijdens het granulatieproces, wanneer de deeltjes verschillende hoeveelheden vocht bevatten, bestaan er gebieden in het bed waarbij de deeltjes verschillende waarden van de restitutiecoëfficiënt hebben. Deze gebieden ondervinden een andere dynamica hetgeen resulteert in een gewijzigde

prestatie van de spout wervelbed granulator.

Om na te gaan of dezelfde trends in de experimenten worden waargenomen, zijn verschillende deeltjessystemen onderzocht met *o.a.* verschillende restitutiecoëfficiënten in een pseudo-2D spout wervelbed. Dit is gedaan voor verschillende stromingsregimes: het spout-fluïdisatie regime (case B1), het spouten-met-beluchting regime (case B2) en het straal-in-gefluïdiseerd-bed regime (case B3). De onderzochte deeltjessystemen zijn glasdeeltjes, γ-alumina-oxide en zeoliet 4A deeltjes, die allen als Geldart D deeltjes zijn geclassificeerd. De techniek "Particle Image Velocimetry" (PIV) is gebruikt, waarmee het stomingsveld van de deeltjes in een pseudo twee-dimensionaal (2D) bed wordt verkregen zonder de stroming te verstoren. De digitale beelden (verkregen middels PIV) zijn geanalyseerd met behulp van een nieuw ontwikkeld algoritme om de deeltjes volumefractie te bepalen. Middels deze "Digital Image Analysis" (DIA) techniek is aangetoond dat betrouwbare informatie over de deeltjes volumefractie verdeling wordt verkregen. De combinatie van DIA met PIV vormt een krachtige methode voor het verkrijgen van de volumetrische deeltjesfluxen. De verwachtte toegevoegde waarde werd bevestigd door de deeltjes snelheid en de volumetrische deeltjesfluxen te vergelijken. De deeltjesflux verkregen met de gecombineerde PIV/DIA techniek is gebruikt om de DEM simulatieresultaten te valideren voor het straal-in-gefluïdiseerd-bed regime (case B3) voor de drie deeltjessystemen. De verticale deeltjesfluxen verkregen met de simulaties worden enigszins overschat bovenin het bed en in de annulus, hetgeen veroorzaakt kan zijn door het wandeffect dat groter is in pseudo-2D bedden. Simulaties met een hogere waarde van de frictiecoëfficiënt voor deeltje-wand interacties met glasdeeltjes lieten zien dat (voor dit bestudeerde systeem) de in de simulaties bepaalde neergaande flux in de annulus beter overeenkwam met de experimentele resultaten. Het effect van de botsingseigenschappen voor glas, γ-alumina-oxide en zeoliet 4A deeltjes is bestudeerd in de drie stromingsregimes en voor elk stromingsregime bleek dat de deeltjes volumefractie kleine verschillen gaf tussen de verschillende deeltjessystemen. Voor de γ-alumina-oxide en zeoliet 4A deeltjes is het spoutkanaal minder stabiel voor de B1 en B2 cases. De deeltjesfluxen lieten ook kleine verschillen zien tussen de deeltjessystemen voor elk stromingsregime.

De gesimuleerde systemen representeren verschillende stadia van bevochtiging die tijdens granulatieprocessen optreden, en het bleek dat de beddynamica heel erg beïnvloed wordt door de verschillen in de restitutiecoëfficiënt. Gedurende granulatieprocessen, zijn daarentegen zones van natte en droge deeltjes gelijktijdig aan-

wezig op verschillende plaatsen in het bed. Daarom is tevens een systeem bekeken met variabele restitutiecoëfficiënten, zodat het effect van de deeltjes-deeltjes interactie op de beddynamica bestudeerd kan worden. De restitutiecoëfficiënt verandert in tijd en plaats tengevolge van verschillen in de vochtbelading van het deeltje, hetgeen het gevolg is van de interactie tussen druppel en deeltje, en verdamping. Voor dit onderzoek is de DEM uitgebreid door de vochtbelading te verdisconteren in de restitutiecoëfficiënt, waarbij zowel druppels als deeltjes beschouwd worden als discrete elementen. Dezelfde stromingsregimes zijn bestudeerd en voor elk stromingsregime stijgt de gemiddelde bedhoogte bij dalende restitutiecoëfficiënt. Bovendien is de verandering van de gemiddelde bedhoogte groter wanneer de restitutiecoëfficiënt variabel is dan wanneer de restitutiecoëfficiënt constant is, wat voor elk stromingsregime het geval blijkt te zijn. Dit houdt in dat de beddynamica ook beïnvloed wordt door de verdeling van de restitutiecoëfficiënt in het bed. De invloed van verdamping op de verdeling van de restitutiecoëfficiënt is alleen waargenomen voor het straal-in-gefluïdiseerd-bed regime (B3), waar de achtergrondsnelheid relatief hoog is en dientengevolge in de annulus tot meer verdamping van het vocht op de deeltjes leidt. Dit is terug te vinden in de gemiddelde bedhoogte voor het systeem met verdamping, die hoger is dan de bedhoogte in het systeem zonder verdamping. Een grotere bedhoogte voor de systemen met variabele restitutiecoëfficiënt is het gevolg van de drukopbouw die in het spoutkanaal ontstaat doordat het spoutkanaal voor een langere periode gesloten is. Dit wordt bevestigd door het drukfluctuatiesignaal en de bijbehorende standaarddeviatie, welke hoger zijn voor de systemen met variabele restitutiecoëfficiënt.

Voor zover bij de auteur bekend, is het onderzoek aan spout wervelbedden voornamelijk geconcentreerd op enkelvoudige-spout fluïdisatie. Echter, in industriële granulatoren zijn meerdere spouts aanwezig, waarbij weinig bekend is over het effect van meerdere spouts op de beddynamica. Daarom is het doel van dit onderzoek om de invloed van twee en drie spouts op de beddynamica van een pseudo-2D spout wervelbed te bestuderen. Dit is onderzocht op basis van DEM simulaties en PIV en "Positron Emission Particle Tracking" (PEPT) metingen voor een pseudo-2D bed. Een stromingsregimediagram is opgesteld waarbij nieuwe stromingsregimes zijn ontdekt die tot dusver nog niet zijn gerapporteerd. Het interactie-van-meerdere-spouts-regime (C) is in detail onderzocht voor een dubbele- en drievoudige-spout wervelbed, waarbij het overeenkomstige spout-fluïdisatie regime voor een enkelvoudige-spout wervelbed bestudeerd is als referentie. De experimentele resultaten verkregen met PIV en PEPT komen zeer

goed met elkaar overeen voor alle drie de systemen, waaruit blijkt dat beide technieken betrouwbare resultaten genereren. De DEM simulatieresultaten wijken licht af van de experimenten, hetgeen te wijten is aan de deeltje-wand effecten die in pseudo-2D bedden meer overheersen dan in 3D systemen. Het onderzochte interactie-van-meerdere-spouts-regime (C) is een volledig nieuw stromingsregime dat niet voorkomt in enkelvoudige-spout wervelbedden. Er zijn twee stromingspatronen waargenomen, namelijk een deeltjescirculatie tussenin de spouts en nabij de bodem, en een schijnbare enkelvoudige-spout fluïdisatie beweging bovenin het bed. Deze bevindingen laten zien dat meerdere spouts in een spout wervelbed in hoge mate het stromingsgedrag beïnvloeden, wat niet aan het licht komt wanneer louter enkelvoudige-spout wervelbedden bestudeerd worden.

Een tweede kenmerk van industrïele spout wervelbed granulatoren is de verhoogde spouts ten opzichte van de bodemplaat, ten behoeve van optimale vloeistofinjectie. Derhalve is het effect van de verhoogde spout op de beddynamica ook bestudeerd is. De experimenten zijn uitgevoerd in een pseudo-2D en een cylindrisch 3D spout wervelbed, waarbij "Positron Emission Particle Tracking" (PEPT) en "Particle Image Velocimetry" (PIV) zijn toegepast op het pseudo-2D bed, en PEPT en "Electrical Capacitance Tomography" (ECT) op het cylindrisch 3D bed. Al deze technieken hebben de eigenschap dat de stroming in het bed niet wordt verstoord. Een "Discrete Element Model" (DEM) is gebruikt om volledige 3D simulaties uit te voeren voor het pseudo-2D bed. Verscheidene systemen zijn bestudeerd, zoals bedden met spouthoogtes van 0, 2, en 4 cm. In het pseudo-2D bed, zijn het spout-fluïdisatie en straal-in-gefluïdiseerd-bed regime eerst onderzocht, en het bleek dat in het spout-fluïdisatie regime de verwachtte dode zones in de annulus dichtbij de bodem ontstaan zodra de spout enigszins is verhoogd. Echter, in het straal-in-gefluïdiseerd-bed regime wordt het circulatie patroon van de deeltjes beïnvloed, zonder dat er dode zones ontstaan. Het straal-in-gefluïdiseerd-bed regime is daarom verder onderzocht, waarbij de experimentele resultaten verkregen met PIV en PEPT vergeleken werden met DEM simulatieresultaten. De experimentele PIV en PEPT resultaten kwamen onderling zeer goed overeen, en strookten eveneens met de DEM resultaten hoewel de snelheden in de annulus enigszins overschat werden. Dit laatste is waarschijnlijk het gevolg van deeltje-wand effecten die in pseudo-2D systemen van groter belang zijn dan in 3D systemen. In het straal-in-gefluïdiseerd-bed regime is de achtergrondsnelheid relatief hoog, zodat er meer bellen in de annulus geproduceerd worden die het spoutkanaal meer beïnvloeden. In het geval van een niet verhoogde spout vindt

deze interactie plaats tussen de bellen en het spoutkanaal dichtbij de bodemplaat. Zodra de spout is verhoogd, verschuift deze interactie naar een hogere positie in het bed, wat ervoor zorgt dat de bellen onverstoord blijven waardoor de deeltjes in de annulus dichtbij de bodem in beweging worden gebracht. Dit resulteert in het uitblijven van dode zones en het verticaal uitrekken van de circulatie patronen. Deze conclusies zijn ook verkregen bij het cylindrische 3D bed, hoewel de effecten minder uitgesproken waren. In het cylindrische 3D bed lieten de PEPT resultaten zien dat het effect op de beddynamica begint bij $h_{spout} = 4$ cm en dit werd bevestigd door ECT resultaten. Daarnaast zijn ECT metingen uitgevoerd voor $h_{spout} = 6$ cm teneinde te verifiëren of het effect daadwerkelijk bij grotere spouthoogtes plaatsvindt. De standaarddeviatie van de deeltjes volumefractie was licht gestegen bij $h_{spout} = 2$ cm, terwijl een grotere stijging was gevonden bij $h_{spout} = 4$ and 6 cm, wat inderdaad impliceert dat er meer bellen worden gevormd. De gepresenteerde resultaten zijn tot nog toe niet gerapporteerd en ze vormen waardevolle informatie voor het verbeteren van industriële granulatoren.

Contents

1 Introduction

1.1 Granulation Process

Granulation processes are widely applied for example in the production of detergents, pharmaceuticals, food and fertilizers, and aim to produce granules with particular properties, such as size, mechanical strength (to ease product handling) and chemical composition (purity). Two types of granulation processes can roughly be distinguished, *viz*. dry and wet granulation.

Dry granulation is based on compression of powders, without the addition of binder for agglomeration. This type of granulation is particularly used for powders that are sensitive to moisture and heat, and finds its application mainly in the pharmaceutical industry. Examples of dry granulation are roller compaction and tabletting.

In wet granulation, a liquid is involved which can either act as a binder between powders to form agglomerates or as a building block in the granule by solification on a single particle (Mörl et al. 2007). According to Iveson et al. (2001), different mechanisms should be distinguished during agglomeration, namely nucleation, consolidation and growth, and breakage. Knowledge of these mechanisms is vital

to control the entire process. Agglomeration processes are often applied in the production of food and detergents, where fine powders are involved. Examples are rotating drum mixers, high shear mechanical mixers and fluidized bed granulators with bottom or top spray. In a fluidized bed, particles are brought into motion by an upward flowing gas stream, and due to the particle-fluid and particle-particle interaction the particles display a behaviour that is normally encountered in fluids. The gas velocity at which this behaviour first emerges is defined as the minimum fluidization velocity. Fluidization behaviour of particles depends strongly on particle size and density, which is classified by Geldart (1973). Wet granulation without agglomeration, *i.e.* coating or layer wise particle growth, is often applied for larger particles (diameter $\sim$ 1 - 7 mm) which are classified as Geldart class D. Such large particles are most efficiently produced in fluidized bed reactors, however, they are difficult to fluidize since large bubbles are formed reaching dimensions of the vessel, leading to slugs. Therefore spouted beds or spout fluidized beds are used (see for a schematic representation Figure 1.1).

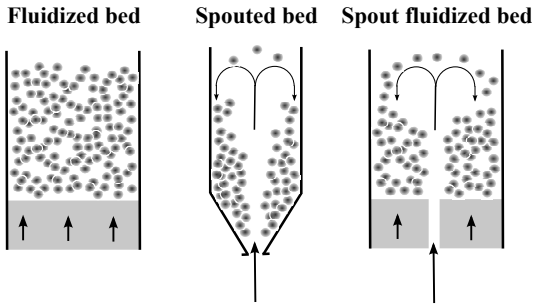

Figure 1.1: Schematic of a fluidized bed (left), a spouted bed (centre) and spout fluidized bed (right).

The spout, which is a high speed gas jet, enables the particles to move without creating slugs, which improves the particle circulation. In a spouted bed motion of the particles is solely induced by a spout, and a spout fluidized bed combines the favourable properties of both spouted and fluidized beds, enabling high mobility of the particles, preventing undesired agglomeration and providing excellent heat transfer control. Additional advantage of spout fluidized beds is, that liquid can easily be sprayed into the bed through the spout. Spout fluidized beds are also often applied for a wide variation of 'dry' purposes such as burning of solid fuels, drying of food *e.g.* vegetables, fruit, cereals, and roasting of *a.o.* coffee beans.

Coating processes via spout fluidized bed granulators are found in coating of pharmaceuticals, production of plastics and fertilizers. The latter forms the basis for this work. Urea is mainly applied as fertilizer, and is used all over the world. The demand for this product is quite large, as reported by the International Fertilizer Industry Association, where the estimated global production in 2008 was 146×10^6 ton and is expected to rise to 175×10^6 ton in 2013 (Mavrovic et al. 2010). These large amounts ask for large (and efficient) production capacities, for which the spout fluidized bed granulator is very suitable. Additionally, the required large particle sizes and their resistance to crushing during transport can be achieved in a spout fluidized bed granulator. In Figure 1.2, a schematic drawing of a continuous spout fluidized bed is presented for the production of fertilizers.

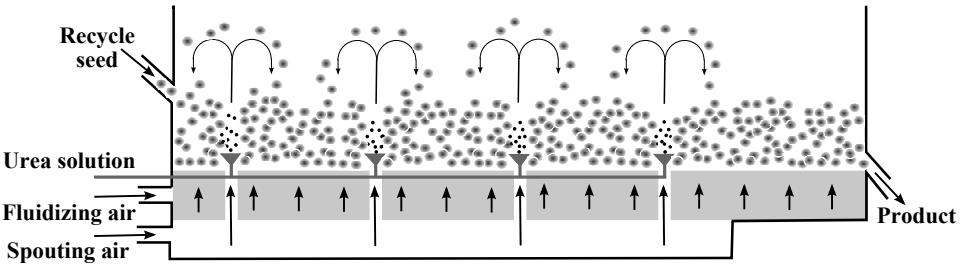

Figure 1.2: Schematic of a spout fluidized bed granulator for the production of urea granules.

A spout fluidized bed comprises a bed filled with urea particles, in which hot molten urea solution is introduced as small droplets along with a carrier gas through the spout. To keep the granular material in the bed in motion, fluidizing gas is distributed via the bottom plate. The droplets will stick to the particles, resulting in particle growth. Particles that have sufficiently grown leave the bed. Subsequently, the produced particles are sieved to sort the product from oversize and undersize particles. Oversize particles are ground to yield small particles, which are recycled along with the undersize particles. Although the spout fluidized bed granulator is the favourable technology to produce fertilizers, the recycle stream is still large, energy losses are quite extensive and improvement of product quality is still necessary. Consequently, understanding of the phenomena inside a spout fluidized bed is crucial to improve the efficiency of the granulator.

1.2 Objective of this Thesis

The performance of the granulator depends on the particle mixing, and thus particle motion, which is therefore of considerable importance. If, for instance, particles remain too long in the spout region, particles become too wet resulting in undesired agglomeration. During the granulation process, particles contain different loadings of melt which results in altered collision properties distributed in time and space across the bed. This change in collision properties influences the bed dynamics, and consequently influences the granule quality. To improve the performance of the spout fluidized bed granulator, it is very important to understand the interplay of collision properties and bed dynamics, which is therefore studied in this work.

Most of the research done so far had been focussed on single-spout fluidization. However, as shown in Figure 1.2 multiple spouts are present in the industrial granulator, and it was not clear yet what the effect is on the bed dynamics. Consequently, this is the second topic of this research.

Furthermore, the spouts are slightly elevated from the bottom to ease the injection of the liquid. This geometric feature is also examined to reveal the effect on the dynamics of the spout fluidized bed.

1.3 Approach

Little is known about the details of the granulation process. This is mainly due to the fact that the granulation process is not visually accessible. The use of measurement probes is also hampered, since it disturbs the flow and thus the granulation process. Furthermore, the measurement probes would soon be covered with a layer of granulate material, making this kind of measurements problematic. An alternative to investigate the granulation behaviour in detail is the usage of non-intrusive measurement tools and fundamental, deterministic models.

The non-intrusive measurement techniques used in this work are Particle Image Velocimetry (PIV) combined with Digital Image Analysis (DIA) to measure the particle motion and particle volume fraction in a pseudo-2D spout fluidized bed, Positron Emission Particle Tracking (PEPT) to determine the particle velocity in both the pseudo-2D and cylindrical 3D bed, and Electrical Capacitance Tomography (ECT) to capture the particle volume fraction in the cylindrical 3D spout fluidized bed. These experiments were conducted to gain insight of the phenom-

ena that occur in the spout fluidized bed, and to compare experimental results to simulation results obtained with the Discrete Element Model (DEM).

The Discrete Element Model is a simulation model that is embedded in the multi-level modeling approach, as shown in Figure 1.3.

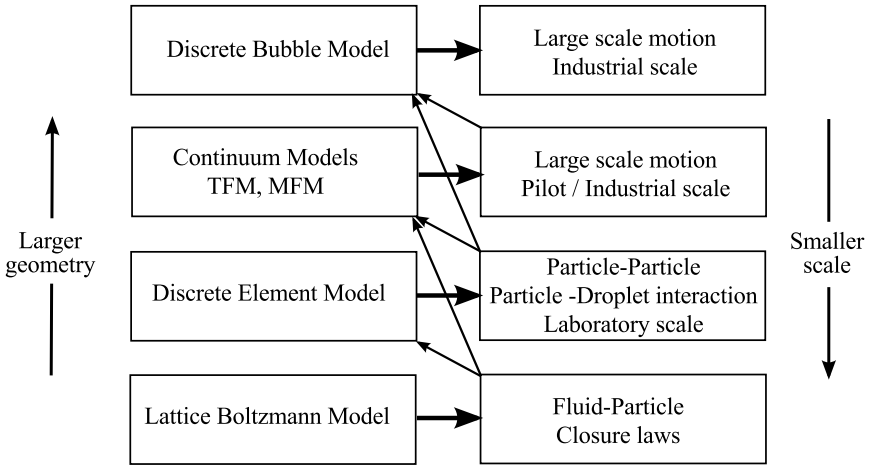

Figure 1.3: Schematic representation of the multi-level modeling approach demonstrating the available models that describe gas-solid flows with increasing detail from top to bottom.

Since the macroscopic circulation patterns in (spout) fluidized beds are governed by microscopic interactions, such as particle-particle and particle-fluid interactions, several simulation models are necessary to describe these phenomena at the required level of detail. Therefore, a multi-level modeling strategy is adopted in our group (Van der Hoef et al. 2008), which distincts four levels of modeling.

At the most detailed level of description the gas flow field is modeled at scales smaller than the particle size with the Lattice Boltzmann Model (LBM). The momentum exchange between the particles and the gas phase is determined, which can be used in the higher scale models.

At the intermediate level, the flow field is modeled at a larger scale than the particles size, where a grid cell typically contains in the order of 10 - 100 particles. This is done with the Discrete Element Model (DEM), originally named as the Discrete Particle Model (DPM, Hoomans et al. (1996)). However, in this work an additional discrete phase is present, namely, the droplets. The DEM consists of two parts: a Lagrangian description of the positions and velocities of the solid

particles and droplets from Newton's law, and an Eulerian description for the local gas density and velocity from the Navier-Stokes equations. The advantage of DEM is that the particle-wall and particle-particle (and particle-droplet) interactions are accounted for in a realistic manner, where the system size is about $O(10^6)$ particles, which is sufficiently large to allow for a direct comparison with laboratory-scale experiments. Hence, DEM is used in this work.

The third model is the continuum model, *i.e.* the Two Fluid Model (TFM) or the Multi Fluid Model (MFM), where two or multiple phases are considered as interpenetrating continua that are described by the Navier-Stokes equations. This Euler-Euler model is based on the Kinetic Theory of Granular Flow (KTGF) and requires closures for the particle-fluid and particle-particle interactions, which are obtained from LBM and DEM. With TFM and MFM, bed behaviour of gas-solid flows can be predicted at intermediate pilot-industrial scale.

At the highest level, industrial scale fluidized bed reactors are simulated with the Discrete Bubble Model (DBM), where the voids or bubbles are considered as discrete elements (similar to the particles in DEM) and the emulsion phase as the continuum phase.

1.4 Outline of this Thesis

The organisation of this thesis is as follows: In Chapter 2 the particle-particle interactions are studied in a 3D system, using the Discrete Element Model (DEM). Several test cases are defined, where the particles possess a different restitution coefficient mimicking different degrees of wetting. The effect of the restitution coefficient is studied for three flow regimes, *viz.* intermediate/spout-fluidization, spouting-with-aeration and jet-in-fluidized-bed regime. The particle-particle interactions are experimentally studied in a pseudo-2D bed in Chapter 3, using combined Particle Image Velocimetry / Digital Image Analysis (PIV/DIA). A new DIA algorithm was developed and will be discussed in chapter 3. Three particle systems were considered, namely glass beads, γ-alumina oxide and zeolite 4A particles, and investigated in the intermediate/spout-fluidization, spouting-with-aeration and jet-in-fluidized-bed regime. In Chapter 4 the DEM is extended to study the particle-particle interactions during granulation. In this work, the granulation process is studied on basis of water spray into a spout fluidized bed containing glass beads. The water droplets stick on the particles, causing variation of the particles restitution coefficient in time and space in the bed. Simulations

were conducted for a 3D system, for the intermediate/spout-fluidization, spouting-with-aeration and jet-in-fluidized-bed regime, in accordance with the simulations as presented in Chapter 2. Subsequently, these results were compared to the results obtained in Chapter 2. Chapter 5 describes the effect of double- and triple-spouts in a pseudo-2D spout fluidized bed. Experiments were conducted using PIV and Positron Emission Particle Tracking (PEPT), and the results were compared mutually and to DEM simulations. The study on spout elevation is reported in Chapter 6. Experiments were carried out in a pseudo-2D and a cylindrical 3D spout fluidized bed. PIV and PEPT were applied to the pseudo-2D bed, whereas PEPT and Electrical Capacitance Tomography (ECT) were applied to the cylindrical 3D bed. DEM simulations were run for the pseudo-2D case and compared to the experimental results. The last Chapter comprises an Epilogue, which discusses the results and its relevance for industry, and gives recommendations for future work.

Acknowledgement

The authors would like to thank FOM, STW and Yara Sluiskil, The Netherlands, for their financial support to the project.

2

Discrete Simulation Study on the Effect of Dry Particle-Particle Interactions

This chapter is based on:
M.S. van Buijtenen, N.G. Deen, S. Heinrich, S. Antonyuk and J.A.M. Kuipers, Discrete simulation study on the influence of the restitution coefficient on spout fluidized-bed dynamics, *Chemical Engineering Technology* **2009**, *32 (3)*, 454.

Abstract

Spout fluidized beds are largely applied in granulation processes in industry, in which efficient contacting between large particles, droplets and gas is of paramount importance. However, detailed understanding of the complex behaviour of these systems is lacking. Therefore, the effect of the inter-particle interaction on the bed dynamics is studied in this chapter, by investigating the bed height, pressure drop and vertical particle velocity as function of the restitution coefficient. In addition, the amplitude of the fluctuations of these quantities is displayed in terms of the root mean square (RMS). This is done computationally, with the use of an extended discrete element model (DEM). The examined flow regimes comprise the intermediate / spout-fluidization regime (B1), spouting-with-aeration regime (B2) and the jet-in-fluidized-bed regime (B3). The pressure drop and the vertical particle velocity are compared to experimental data obtained by Link et al. (2007). The computed results with $e_n = 0.97$ resemble the experimental results. It is shown that if the restitution coefficient decreases, more bubbles are present causing more pronounced heterogeneity (instability) in the overall flow structure of the bed, in more or less extent dependent on the flow regime. The particle velocity and RMS profiles confirm the effect on the stability of the bed and show that the spout channel for cases B1 and B3 becomes unstable when the restitution coefficient decreases. For case B2, a transition occurs from the spouting-with-aeration to the intermediate/spout-fluidization regime at low restitution coefficient. These findings show the great importance of the influence of the restitution coefficient on the dynamics of the bed. During the granulation process, when the particles contain different moisture contents, regions in the bed exist that contain particles with different restitution coefficients. These regions thus experience different dynamics, resulting in varying performance of the spout fluidized bed granulator.

2.1 Introduction

This chapter describes the effect of the inter-particle interaction on the bed dynamics in a spout fluidized bed. During the granulation process, particles contain different loadings of moisture which results in altered collision properties in time and location across the bed. This change in collision properties influences the bed dynamics, and consequently influences the granule quality. To improve the performance of the spout fluidized bed granulator, it is very important to understand the interplay of collision properties and bed dynamics. This has been shown by Passos and Mujumdar (2000) and Vieira and Rocha (2004), who experimentally investigated the flow behaviour in spouted beds with dry respectively wet particles. They both observed a decrease of the particle velocity in the annulus with increasing moisture content, keeping constant all the operating conditions during a coating experiment. In addition, the bed pressure drop was found to decrease with increase of the instantaneous bed saturation degree. The stable spout pressure drop in the dry bed was found to be higher than that in the wet bed. Fu et al. (2004) also studied the effect of the moisture content on collision properties experimentally. The collision properties between particles are captured in the restitution coefficient which is the ratio of the velocities associated with impact and rebound. They found that the restitution coefficient decreases with increasing moisture content, which they attributed to the reduction of Young's modulus. Mangwandi et al. (2007) experimentally investigated the impact behaviour of three different types of granules, *viz.* wet, melt and binderless granules. Wet granules are defined as granules in which the primary particles are held together by liquid bridges; the melt granules are wet granules with solidified binder. The binderless granules are granules without binder. They also found differences in restitution coefficients for the different types of granules. Research has thus shown that the moisture content in spout fluidized beds has a great influence on the inter-particle collision properties and hence on the flow behaviour. It may therefore be concluded that a detailed description of the influence of the restitution coefficient on the bed dynamics is of great importance. However, such a description has not yet been obtained due to the practical problems faced in the experimental study of spouted beds, such as unfeasible non-intrusive access of the spout channel. Therefore, computational methods provide a powerful and attractive alternative for laborious experimental studies. A discrete element model (DEM) is used, which describes the dynamics of the continuous gas-phase and the discrete particles. The model is based on the DEM originally developed by Hoomans et al. (1996) and extended by Link et al.

(2007) for the simulation of spout fluidized beds. The objective is to gain insight in the effect of the restitution coefficient on the flow behaviour of spout fluidized beds at different flow regimes using the DEM. The simulation results are compared with experimental data obtained by Link et al. (2007). The organization of this chapter is as follows: first, the DEM is briefly discussed. Then, the studied test cases are described, followed by an explanation of the experimental procedure conducted by Link et al. (2007). Finally, the simulation results are discussed and compared with the experiments.

2.2 Numerical Model

The simulations are conducted with a discrete element model that describes the dynamics of the continuous gas-phase on an Eulerian grid and those of the particles on Lagrangian coordinates. For each element momentum balances are solved. The momentum transfer among each of the phases is described in detail at the level of individual elements, and the inter-particle collisions are described using a soft sphere approach. To exchange the property values from Eulerian grid cells to Lagrangian coordinates and vice versa, Euler-Lagrange coupling is necessary.

2.2.1 Gas Phase

The gas phase flow field is computed from the volume-averaged Navier-Stokes equations given by:

$$\frac{\partial}{\partial t}(\varepsilon_f \rho_f) + \nabla \cdot (\varepsilon_f \rho_f \mathbf{u}_f) = 0 \tag{2.1}$$

$$\frac{\partial}{\partial t}(\varepsilon_f \rho_f \mathbf{u}_f) + \nabla \cdot (\varepsilon_f \rho_f \mathbf{u}_f \mathbf{u}_f) = -\varepsilon_f \nabla p - \nabla \cdot (\varepsilon_f \boldsymbol{\tau}_f) - \mathbf{S}_p + \varepsilon_f \rho_f \mathbf{g} \tag{2.2}$$

where the fluid density, ρ_f, is determined using the ideal gas law and the viscous stress tensor, $\boldsymbol{\tau}_f$ is assumed to obey the general form for a Newtonian fluid (Bird et al. (1960)):

$$\boldsymbol{\tau}_f = -\left[\left(\lambda_f - \frac{2}{3}\mu_f\right)(\nabla \cdot \mathbf{u}_f)\mathbf{I} + \mu_f\left((\nabla \mathbf{u}_f) + (\nabla \mathbf{u}_f)^{\mathbf{T}}\right)\right] \tag{2.3}$$

Two-way coupling is achieved via the sink term, $\mathbf{S}_p$, which is computed from:

$$\mathbf{S}_p = \frac{1}{V_{cell}} \sum_{\forall\, i \,\in\, cell} \frac{V_i \beta}{(1-\varepsilon_f)} (\mathbf{u}_f - \mathbf{v}_i) D(\mathbf{r} - \mathbf{r}_i) \tag{2.4}$$

The distribution function, D, distributes the reaction force acting on the gas phase to the velocity nodes in the staggered Eulerian grid, and β represents the interphase momentum transfer coefficient due to drag, which is calculated using a drag relation proposed by Koch and Hill (2001) that is based on lattice-Boltzmann simulations:

$$\beta = \frac{18 \mu_f \varepsilon_f^2 (1-\varepsilon_f)}{d_p^2} \left(F_0 (1-\varepsilon_f) + \frac{1}{2} F_3 (1-\varepsilon_f) Re_p \right) \tag{2.5}$$

where $\varepsilon_f + \varepsilon_p = 1$ and Re_p is given by:

$$Re_p = \frac{\varepsilon_f \rho_f |\mathbf{u}_f - \mathbf{v}_p| d_p}{\mu_f} \tag{2.6}$$

and with:

$$F_0(1-\varepsilon_f) = \begin{cases} \frac{1+3\sqrt{\frac{(1-\varepsilon_f)}{2}} + \frac{135}{64}(1-\varepsilon_f)\ln(1-\varepsilon_f) + 16.14(1-\varepsilon_f)}{1+0.681(1-\varepsilon_f) - 8.48(1-\varepsilon_f)^2 + 8.16(1-\varepsilon_f)^3} & \text{if } (1-\varepsilon_f) < 0.4 \\ \frac{10(1-\varepsilon_f)}{\varepsilon_f^3} & \text{if } (1-\varepsilon_f) \geq 0.4 \end{cases} \tag{2.7}$$

$$F_3(1-\varepsilon_f) = 0.0673 + 0.212(1-\varepsilon_f) + \frac{0.0232}{\varepsilon_f^5} \tag{2.8}$$

2.2.2 Particle Motion

The translational and rotational motion of each individual particle present in the system is calculated from the Newtonian equations of motion:

$$m_p \frac{d\mathbf{v}_\mathrm{p}}{dt} = -V_p \nabla p + \frac{V_p \beta}{(1-\varepsilon_f)} (\mathbf{u}_f - \mathbf{v}_p) + m_p \mathbf{g} + \sum_{N_p} \mathbf{F}_{p \leftrightarrow p} + \sum_{N_w} \mathbf{F}_{p \leftrightarrow w} \tag{2.9}$$

$$I_p \frac{d\boldsymbol{\omega}_p}{dt} = \mathbf{T}_p \tag{2.10}$$

where the moment of inertia of the particle is defined as:

$$I_p = \frac{2}{5} m_p r_p^2 \tag{2.11}$$

2.2.3 Particle-Particle Interaction

The contact forces during particle-wall and inter-particle collisions are calculated with the soft sphere approach, which was originally proposed by Cundall and Strack (1979) for flow problems arising in the geophysical domain. In this approach, the particles are assumed to undergo deformation during their contact, where the contact forces are calculated from a simple mechanical analogue involving a spring, a dash-pot and a slider. This allows for energy dissipation due to non-ideal particle interaction by means of the empirical coefficients of normal and tangential restitution, and the coefficient of friction. In case a particle is in contact with several other particles the net contact force follows from the addition of all binary contributions:

$$\mathbf{F}_{contact,a} = \sum_{\forall b \in contactlist} (\mathbf{F}_{ab,n} + \mathbf{F}_{ab,t}) \tag{2.12}$$

The contact force $\mathbf{F}_{contact,a}$ is used to resolve the Newtonian equations of motion for particle a (equation 2.9). $\mathbf{F}_{ab,n}$ and $\mathbf{F}_{ab,t}$ represent the normal and tangential component of the contact force between particle a and b, respectively.
The torque is defined as:

$$\mathbf{T}_a = \sum_{\forall b \in contactlist} (r_a \mathbf{n}_{ab} \times \mathbf{F}_{ab,t}) \tag{2.13}$$

The normal unit vector of the two contacting particles a and b is defined as:

$$\mathbf{n}_{ab} = \frac{\mathbf{r}_b - \mathbf{r}_a}{|\mathbf{r}_b - \mathbf{r}_a|} \tag{2.14}$$

where the normal unit vector thus points in the direction from the centre of particle a to the centre of particle b, with $\mathbf{r}_a$ as the point of origin.
To determine the normal component of the contact force a simple linear spring/dash-pot model is used, as described in equation 2.15.

$$\mathbf{F}_{ab,n} = -k_n \delta_n \mathbf{n}_{ab} - \eta_n \mathbf{v}_{ab,n} \tag{2.15}$$

where k_n is the stiffness of the normal spring and the overlap δ_n is given by:

$$\delta_n = (r_a + r_b) - |\mathbf{r}_a - \mathbf{r}_b| \tag{2.16}$$

The normal damping coefficient η_n is described as:

$$\eta_n = \begin{cases} \frac{-2\ln(e_n)\sqrt{m_{ab}k_n}}{\sqrt{\pi^2+\ln^2(e_n)}} & \text{if} \quad e_n \neq 0 \\ 2\sqrt{m_{ab}k_n} & \text{if} \quad e_n = 0 \end{cases} \tag{2.17}$$

where m_{ab} is the effective mass, which is formulated as:

$$m_{ab} = \left(\frac{1}{m_a} + \frac{1}{m_b} \right)^{-1} \tag{2.18}$$

In particle-wall collisions the mass of particle b (*i.e.* the wall) is infinitely large, resulting in $m_{ab} = m_a$. The coefficient of normal restitution e_n is described as $(0 \leq e_n \leq 1)$:

$$\mathbf{v}_{ab} \cdot \mathbf{n}_{ab} = -e_n (\mathbf{v}_{ab,0} \cdot \mathbf{n}_{ab}) \tag{2.19}$$

The relative particle velocity is described in equation 2.20 and can be decomposed in a normal (equation 2.21) and a tangential component (equation 2.22).

$$\mathbf{v}_{ab} = (\mathbf{v}_a - \mathbf{v}_b) + (r_a \boldsymbol{\omega}_a + r_b \boldsymbol{\omega}_b) \times \mathbf{n}_{ab} \tag{2.20}$$

$$\mathbf{v}_{ab,n} = (\mathbf{v}_{ab} \cdot \mathbf{n}_{ab}) \mathbf{n}_{ab} \tag{2.21}$$

$$\mathbf{v}_{ab,t} = \mathbf{v}_{ab} - \mathbf{v}_{ab,n} \tag{2.22}$$

The tangential unit vector is given by:

$$\mathbf{t}_{ab} = \frac{\mathbf{v}_{ab,t}}{|\mathbf{v}_{ab,t}|} \tag{2.23}$$

The tangential component of the contact force is defined by two types of collisions, *i.e.* sticking and sliding, which are respectively described in equation 2.24.

$$\mathbf{F}_{ab,t} = \begin{cases} -k_t \boldsymbol{\delta}_t - \eta_t \mathbf{v}_{ab,t} & \text{if} \quad |\mathbf{F}_{ab,t}| \leq \mu |\mathbf{F}_{ab,n}| \\ -\mu |\mathbf{F}_{ab,n}| \mathbf{t}_{ab} & \text{if} \quad |\mathbf{F}_{ab,t}| > \mu |\mathbf{F}_{ab,n}| \end{cases} \tag{2.24}$$

k_t is the stiffness of the tangential spring and μ is the friction coefficient that is described as:

$$|\mathbf{n}_{ab} \times \mathbf{J}_{ab}| = -\mu (\mathbf{n}_{ab} \cdot \mathbf{J}_{ab}) \tag{2.25}$$

The tangential damping coefficient η_t is:

$$\eta_t = \begin{cases} \frac{-2\ln(e_t)\sqrt{\frac{2}{7} m_{ab} k_t}}{\sqrt{\pi^2 + \ln^2(e_t)}} & \text{if} \quad e_t \neq 0 \\ 2\sqrt{\frac{2}{7} m_{ab} k_t} & \text{if} \quad e_t = 0 \end{cases} \tag{2.26}$$

where e_t is the coefficient of tangential restitution $(0 \leq e_t \leq 1)$:

$$\mathbf{v}_{ab} \cdot \mathbf{t}_{ab} = -e_t (\mathbf{v}_{ab,0} \cdot \mathbf{t}_{ab}) \tag{2.27}$$

The tangential overlap is given by:

$$\boldsymbol{\delta}_t = \begin{cases} \boldsymbol{\delta}_{t,0}\mathbf{H} + \int_{t_0}^{t}(v_{ab,t})\,dt & \text{if} \quad |\mathbf{F}_{ab,t}| \leq \mu|\mathbf{F}_{ab,n}| \\ \frac{\mu}{k_t}|\mathbf{F}_{ab,n}|\mathbf{t}_{ab} & \text{if} \quad |\mathbf{F}_{ab,t}| > \mu|\mathbf{F}_{ab,n}| \end{cases} \tag{2.28}$$

with

$$\mathbf{H} = \begin{bmatrix} (1-\cos\phi)h_x^2 + \cos\phi & (1-\cos\phi)h_x h_y - h_z\sin\phi & (1-\cos\phi)h_x h_z - h_y\sin\phi \\ (1-\cos\phi)h_x h_y + h_z\sin\phi & (1-\cos\phi)h_y^2 + \cos\phi & (1-\cos\phi)h_y h_z - h_x\sin\phi \\ (1-\cos\phi)h_x h_z - h_y\sin\phi & (1-\cos\phi)h_y h_z + h_x\sin\phi & (1-\cos\phi)h_z^2 + \cos\phi \end{bmatrix} \tag{2.29}$$

$$\mathbf{h} = \frac{\mathbf{n}_{ab} \times \mathbf{n}_{ab,0}}{|\mathbf{n}_{ab} \times \mathbf{n}_{ab,0}|} \tag{2.30}$$

$$\phi = \arcsin\left(|\mathbf{n}_{ab} \times \mathbf{n}_{ab,0}|\right) \tag{2.31}$$

For further details on the collision model the interested reader is referred to the work of Hoomans et al. (1996) and Deen et al. (2007).

2.2.4 Euler-Lagrange Coupling

The particle velocity is calculated from the force balance of a single particle (equation 2.9), which requires properties of the gas phase on the Lagrangian coordinates, while these are defined on the Eulerian grid. Hence, mapping to the particle Lagrangian coordinates is necessary as described by Godlieb (2010). Since the particles are relatively large compared to the size of the Eulerian grid cells, the particles cover several cells hampering mapping over one cell. Therefore, to enable mapping over several grid cells a cube around each particle is defined. Within this cube, the properties in grid cells near the particle are more affected by the Euler-Lagrange coupling than at larger distance, which can be described by different mapping functions such as for example Gaussian functions, described by Deen et al. (2004). However, these functions are computationally quite expensive and hence a triangular description is used, differing only slightly from Gaussian mapping as shown by Godlieb (2010). The weight in x-direction is defined as:

$$D(x - x_i) = \frac{n - |x - x_i|}{n^2} \tag{2.32}$$

and the total weight:

$$D(\mathbf{r} - \mathbf{r}_i) = D(x - x_i)D(y - y_i)D(z - z_i) \tag{2.33}$$

where x_i is the position of particle i, x is the position of the cell and n is the semi-width of the cubic mapping domain:

$$n = 5 \cdot r_p \tag{2.34}$$

For particles near a wall, the cube could (partly) overlap the wall resulting in unrealistic mapping outside the computational domain. A method to prevent this from happening is proposed by Link (2006), where the cube that covers the wall is folded back into the computational domain (Figure 2.1).

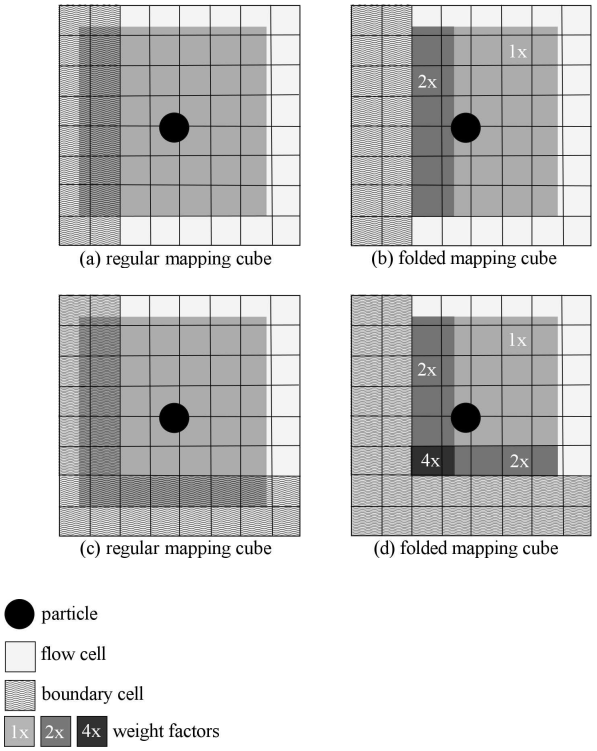

Figure 2.1: Illustration of the cubic volume folding at the boundaries of the computational domain.

2.2.5 Numerical Algorithm

In the soft sphere approach, the deformation of particles during contact is fully resolved, requiring a separate time step besides the main time step that is used to solve the Navier-Stokes equations and inter-phase coupling. The main time step Δt_{flow} is divided into a number of time steps Δt_{coll} to calculate the particle collisions. Δt_{coll} should be chosen sufficiently small to ensure that the contact lasts several time steps to satisfy conservation of energy during numerical integration. A schematic scheme of the numerical algorithm is presented in Figure 2.2.

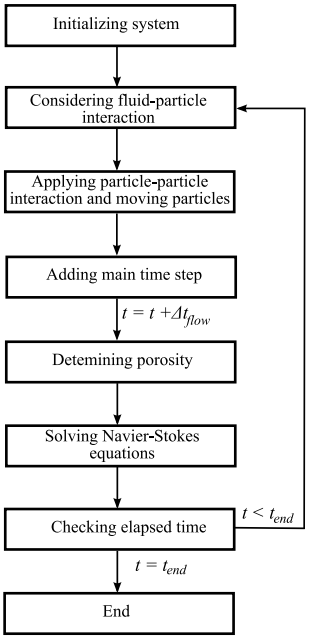

Figure 2.2: Flow diagram of the numerical algorithm of the discrete element model.

The motion of particles is resolved fully 3D in the DEM with first order (Euler) integration of the Newtonian equations of motion according to Hoomans et al. (1996), which is shown in equation 2.35.

$$\begin{aligned} \mathbf{v}^{n+1} &= \mathbf{v}^n + \Delta t_{coll} \frac{\sum \mathbf{F}^n}{m_p} \\ \mathbf{x}^{n+1} &= \mathbf{x}^n + \Delta t_{coll} \cdot \mathbf{v}^{n+1} \\ \boldsymbol{\omega}^{n+1} &= \boldsymbol{\omega}^n + \Delta t_{coll} \frac{\sum \mathbf{T}^n}{I} \end{aligned} \tag{2.35}$$

2.3 Test Cases

The objective of this work is to study the effect of the restitution coefficient on the bed dynamics. Therefore several simulations have been conducted using different values of the restitution coefficient, ranging from 0.2 to 0.97. In addition, its influence is investigated for various flow regimes, which are chosen in accordance with the experiments of Link et al. (2007). In Table 2.1 the particle properties are listed, the studied flow regimes are shown in Table 2.2, whereas the numerical settings and time step per simulation are listed in Table 2.3 and Table 2.4, respectively.

Table 2.1: Particle properties.

Property	Value	Unit
d_p	4.0	mm
ρ_p	2526	kg/m^3
$e_{n,p\leftrightarrow p}$	0.20-0.97	-
$e_{n,p\leftrightarrow w}$	0.20-0.97	-
$e_{t,p\leftrightarrow p}$	0.33	-
$e_{t,p\leftrightarrow w}$	0.33	-
$\mu_{p\leftrightarrow p}$	0.10	-
$\mu_{p\leftrightarrow w}$	0.10	-

Table 2.2: Flow regimes.

Case	Flow regime	u_{bg} [m/s]	$\frac{u_{bg}}{u_{mf}}$	u_{sp} [m/s]	$\frac{u_{sp}}{u_{mf}}$	u_{sup} [m/s]	$\frac{u_{sup}}{u_{mf}}$
B1	Intermediate / spout-fluidization	2.5	1.4	60	34	3.7	2.1
B2	Spouting-with-aeration	2.5	1.4	90	51	4.3	2.4
B3	Jet-in-fluidized-bed	3.5	2.0	65	37	4.8	2.7

Table 2.3: Numerical settings.

Property	Value	Unit
N_x	21	-
N_y	14	-
N_z	100	-
t_{end}	20	s
N_p	$4.48 \cdot 10^4$	-
k_n	10^4	N/m

Table 2.4: Time step used in the simulations.

e_n [-]	Δt_{B1} [s]	Δt_{B2} [s]	Δt_{B3} [s]
0.2	10^{-5}	10^{-5}	$5 \cdot 10^{-5}$
0.4	10^{-5}	10^{-5}	$5 \cdot 10^{-5}$
0.6	10^{-5}	10^{-5}	$2.5 \cdot 10^{-5}$
0.8	10^{-5}	10^{-5}	$2.5 \cdot 10^{-5}$
0.97	10^{-5}	10^{-5}	$2.5 \cdot 10^{-5}$

2.4 Experimental Methods

Link et al. (2007) used positron emission particle tracking (PEPT) as a non-intrusive measuring technique, which supplies detailed information about the particle motion. PEPT tracks the motion of a single activated particle in a spout fluidized bed over a long period of time in a non-intrusive manner. For further details on the experimental method the interested reader is referred to the work of Link et al. (2007). The 3D spout fluidized bed set-up used by Link et al. (2007) consists of a gas-fluidized bed, which is schematically represented in Figure 2.3.

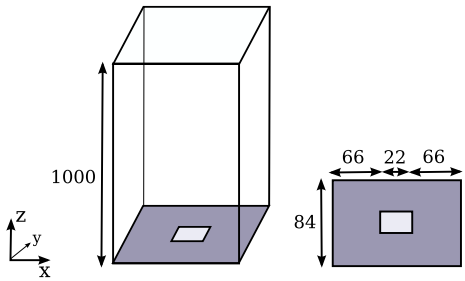

Figure 2.3: Schematic representation of the geometry of the 3D spout fluidized bed; dimensions are given in mm.

The side walls of the bed are made of aluminum, while the front and back walls are made of polycarbonate. Pressurized air was fed to the bed through three separate sections. A 2 mm thick porous plate with an average pore size of 100 μm provided a homogeneous gas distribution over the two fluidization sections. Figure 2.3 shows that the bed contains a spout section, which is covered by a 0.5 mm metal gauze and located on the border between the two fluidization sections at the geometrical centre of the bottom plate. The particles possess the same properties as given in Table 2.1 and the true normal restitution coefficient in the experiments is 0.97. The experiments conducted by Link et al. (2007) provide results of the time-averaged vertical particle velocity and the root mean square (RMS) belonging to the flow regimes B1, B2 and B3. These results will be compared with the results obtained from the DEM simulations.

2.5 Results and Discussion

To study the effect of the restitution coefficient on the bed dynamics, the following aspects will be examined:

- Bed height
- Pressure drop fluctuations
- Particle velocity

The bed height and pressure drop fluctuations are presented to study the overall bed dynamics, and the particle velocity to capture more details of the particle motion in the bed as function of the restitution coefficient. The experimental results reported by Link et al. (2007) are used to validate the simulated results. First, snapshots of the simulated instantaneous particle positions are presented in Figure 2.4, to show the bed behaviour for different restitution coefficients for the three cases. Subsequently, the results of the bed height will be shown, followed by a presentation of the pressure drop and finally the particle velocity will be discussed.

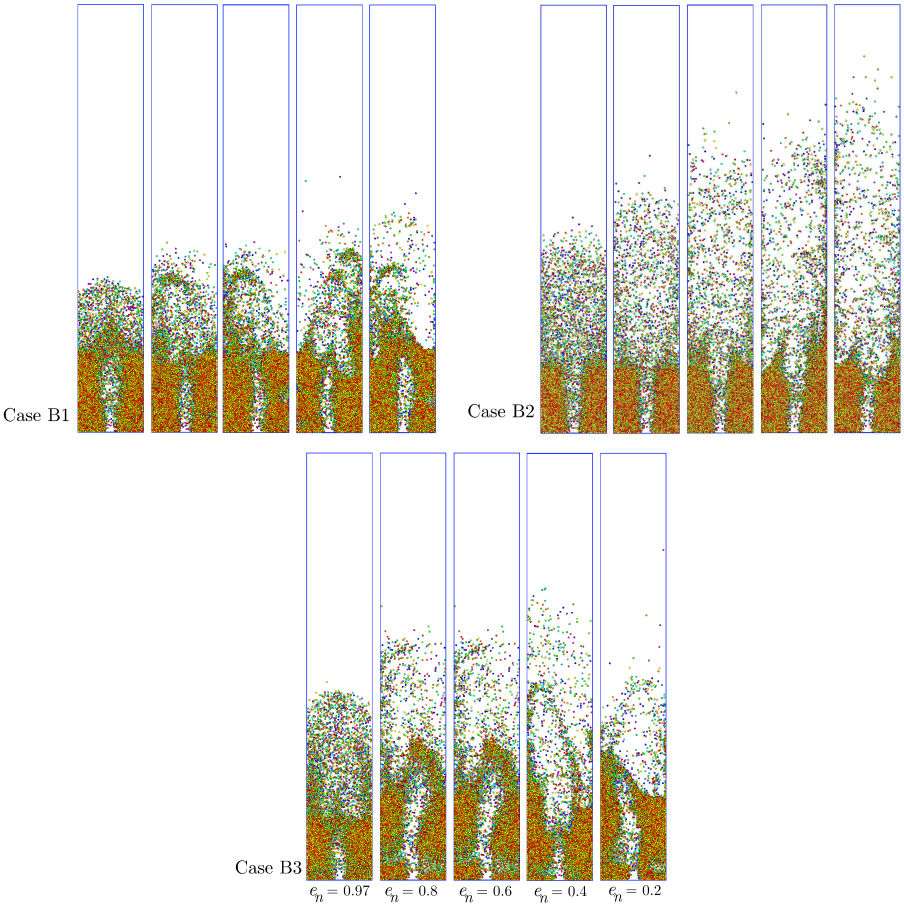

Figure 2.4: Snapshots of the simulated instantaneous particle positions for different restitution coefficients for case B1 (intermediate/spout-fluidization regime), B2 (spouting-with-aeration regime) and B3 (jet-in-fluidized-bed regime) at simulations time $t = 6.0$ s.

2.5.1 Bed Height

In Figure 2.5(a) the time-averaged bed height averaged over a period of 18 s is shown. The first 2 s of the simulations were excluded from the spectral analysis to prevent start-up effects from influencing the results. The simulated results were obtained at a frequency of 250 Hz. It is found that the average bed height decreases with increasing restitution coefficient. This is due to decreasing bubble hold-up. Particles with low restitution coefficient tend to promote the formation of dense regions and passage of gas through the bed mainly in the form of bubbles. It appears that the restitution coefficient influences the bed height most for case B2, the spouting-with-aeration regime. The gas velocity in the spout is quite large in this regime and consequently the particle clusters are dragged higher in the bed. As a result, the bed height increases more with decreasing restitution coefficient in the spouting-with-aeration regime. In Figure 2.5(b) the root mean square (RMS) of the bed height is displayed, which is a measure for the amplitude of the fluctuations of the bed height indicating the extent of bubble formation.

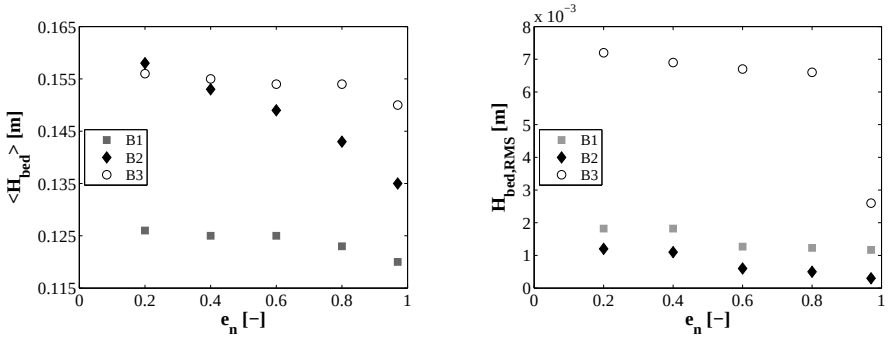

(a) (b)

Figure 2.5: Time-averaged bed height (a) and RMS (b) for different restitution coefficients for case B1 (intermediate/spout-fluidization regime), B2 (spouting-with-aeration regime) and B3 (jet-in-fluidized-bed regime).

It can be seen that the RMS for case B3, the jet-in-fluidized-bed regime is much larger than the RMS for the other flow regimes. This is due to the fact that the jet-in-fluidized-bed regime is less stable, caused by the interaction between bubbles and the spout channel. The RMS of the bed height of simulations at $e_n = 0.97$ is lower for all three flow regime cases, which is most pronounced for the B3 case.

The particles behave more ideally, leading to fewer bubbles in the bed and thus smaller fluctuations in the bed height.

2.5.2 Pressure Drop Fluctuations

The measured pressure drop fluctuations, which reflect the dynamic behaviour of the bed, are used for model validation. During the experiments, the pressure drop was recorded at a frequency of 100 Hz. The NL-experiments were conducted for about one minute, while most of the UK-experiments lasted one hour. The simulated pressure drop fluctuations were averaged over a period of 18 s. The first 2 s of the simulations were excluded from the spectral analysis to prevent start-up effects from influencing the results. The simulated results were obtained at a frequency of 250 Hz. Note that in the experiments only a single particle was tracked, whereas in the simulations all particles were used to obtain time-averaged quantities. The amplitude of the pressure drop fluctuations is represented in terms of the root mean square and is listed in Table 2.5.

Table 2.5: RMS of the measured and simulated pressure drop fluctuations [Pa].

Case	B1	B2	B3
Experiment-NL $e_n = 0.97$	209	166	795
Experiment-UK $e_n = 0.97$	241	84	763
Simulation Link $e_n = 0.97$	226	34	463
Simulation $e_n = 0.97$	179	37	418
Simulation $e_n = 0.8$	229	139	461
Simulation $e_n = 0.6$	177	175	464
Simulation $e_n = 0.4$	243	180	495
Simulation $e_n = 0.2$	254	179	518

The simulated values with $e_n = 0.97$ show good agreement with the experimental data as reported in Link et al. (2007). In addition, the simulated results with $e_n = 0.97$ of Link et al. (2007) differ 10 % from the simulations with $e_n = 0.97$ conducted in this work. This may be due to differences in the mapping function that is used to map properties from Lagrangian coordinates to Eulerian grid cells and vice versa. Link et al. (2007) used a cubic mapping function and in our simulations a tri-angular mapping function has been used. The RMS of the pressure drop for case B3 is higher compared to the other flow regimes, because this regime

is less stable as mentioned earlier. The RMS values listed in Table 2.5 are also presented in Figure 2.6, where lines are added to indicate the trend of the effect of the restitution coefficient. It can be seen that the near-ideal case, with e_n = 0.97, gives a small RMS value, indicating small fluctuations in the pressure drop. In addition, a clear transition is noticeable from the near-ideal to non-ideal cases around $e_n = 0.8$, whereas at lower restitution no further increase of RMS is observed. This trend is also found in the averaged pressure drop. The influence of the restitution coefficient on the pressure drop exhibits a different trend than on the bed height. Apparently, contrary to conventional fluidized beds, for spout fluidized beds the pressure drop is not inversely proportional to the bed height. This may be due to the heterogeneity prevailing in spout fluidized beds, *i.e.* the presence of a core-annulus structure.

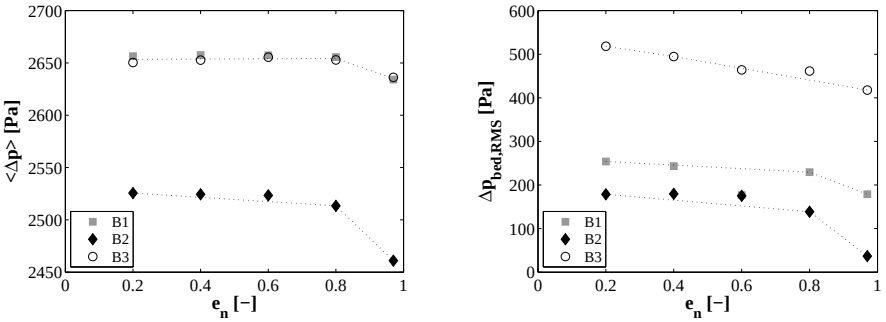

(a) (b)

Figure 2.6: Time-averaged pressure drop (a) and RMS (b) for different restitution coefficients for case B1 (intermediate/spout-fluidization regime), B2 (spouting-with-aeration regime) and B3 (jet-in-fluidized-bed regime).

2.5.3 Particle Velocity

The particle velocities resulting from the PEPT measurements are used to validate the simulation results in a more detailed manner. In the work of Link et al. (2007), the PEPT data consisted of particle trajectories from which a particle velocity history was retrieved. Consequently, for each time step the particle velocity was only known at a single location. To obtain a time-averaged velocity field the results from a measurement over a longer period of time were combined. In the simulations, the time-averaged velocities were calculated by averaging over all particles, employing the same numerical grid that is used to solve the gas phase flow field:

$$\langle \mathbf{v}_{i,j,k} \rangle = \frac{\sum_{t=t_0}^{t_{end}} \sum_{p=1}^{N_p} \mathbf{v}_p(t)\delta}{\sum_{t=t_0}^{t_{end}} \sum_{p=1}^{N_p} \delta} \quad \forall \begin{cases} \delta = 1 \ \forall p \in (i,j,k) \\ \delta = 0 \ \forall p \notin (i,j,k) \end{cases} \tag{2.36}$$

where p represents a particle in cell (i, j, k). N_p is the number of particles, t_0 initial time and t_{end} is the simulation time.

The particle velocity profiles in the central xz-plane are shown at a height $z = 0.15$ m to illustrate the particle velocities in the annulus and the spout channel. At this level a profile of the root mean square (RMS) of the particle velocity in the vertical direction and the horizontal x-direction is displayed, as well. The RMS of the velocity in the x-direction is presented to study the fluctuations of the lateral particle velocity which is caused by the presence of bubbles and periodic lateral movement of the spout channel.

Spout-Fluidization Regime

According to Link et al. (2007), a spout channel is present in the spout-fluidization regime which is periodically blocked by particles from the annulus. Figure 2.7(a) shows the time-averaged vertical particle velocity and the RMS of velocities for case B1, the spout-fluidization regime, obtained from both simulation and experiment. The simulation results with $e_n = 0.97$ (both velocity and RMS) show good resemblance with the experimental results compared to the results reported by Link et al. (2007). It is noted that the experimentally determined RMS of the velocities are obtained from a series of six particle positions, which has a smoothing effect, according to Link et al. (2007). When the restitution coefficient decreases, the

vertical velocity in the spout channel slightly increases and in the annulus more down-flow of the particles is observed. The RMS of the vertical velocity increases with decreasing restitution coefficient, caused by the more frequently opening and closing of the spout channel. As a result, particles are moved upwards in the bed in clusters, by which a higher vertical velocity is reached. The stability of the spout is also influenced by the restitution coefficient, shown by the altered shape of the RMS profile of the vertical velocity. The RMS of both the vertical and lateral velocity in the annulus increases as the restitution coefficient is decreasing, which is attributed to the presence of more bubbles in the annulus.

Spouting-with-Aeration Regime

In the spouting-with-aeration regime, the spout channel is stable and continuously penetrates the entire bed, due to the relatively high gas velocity in the spout. Figure 2.7(b) shows the time-averaged vertical particle velocity and the RMS of velocities for case B2, the spouting-with-aeration regime, obtained from both simulation and experiment. The simulation results with $e_n = 0.97$ show good resemblance with the experimental results. In Figure 2.7(b) it is shown that the vertical particle velocity in the spout channel increases with decreasing restitution coefficient. The difference in downwards velocity in the annulus is less pronounced compared to case B1. In this case, the RMS of the vertical velocity in the spout channel also increases as the restitution decreases. This is attributed to the more frequently opening and closing of the spout channel. In addition, the flow regime turns from spouting-with-aeration into intermediate/spout-fluidization regime at $e_n \approx 0.4$. This is consistent with the flow regime maps of particles with different restitution coefficient, presented in the work of Link (2006). The RMS of the vertical and lateral velocity in the annulus increases with decreasing restitution, indicating that more bubbles are present in the annulus at low restitution coefficient. The shape of the RMS of the vertical and lateral velocity presented in Figure 2.7(b) shows a regular profile. Apparently, the restitution coefficient does not influence the stability of the spout in this flow regime. This may be due to the sufficiently high gas velocity in the spout, which transports all particles in the spout, independent of the state the particles are in (*i.e.* having high or low restitution coefficient).

Jet-in-Fluidized-Bed Regime

In the jet-in-fluidized-bed regime, the bed contains both a spout channel and bubbles in the annulus with mutual interaction, which causes either stable or unstable behaviour. The stable behaviour has been indicated as the single frequency mode and the unstable behaviour as the multiple frequency mode by Link et al. (2005). In the single frequency mode the bubbles leave the bed through the spout channel and in the multiple frequency mode the bubbles and the spout influence each other. Figure 2.8 shows the time-averaged vertical particle velocity and its RMS of vertical and lateral particle velocity for case B3, the jet-in-fluidized-bed regime, obtained from both simulation and experiment. The simulation results of the vertical particle velocity at $e_n = 0.97$ show corresponding resemblance with the experimental data compared to the results reported by Link et al. (2007). The vertical velocity is barely affected by the restitution coefficient. However, the RMS in the vertical velocity does significantly change with varying restitution coefficient, implying that the spout channel becomes unstable. It is very likely that a transition from the single frequency to the multiple frequency mode occurs at lower restitution coefficient.

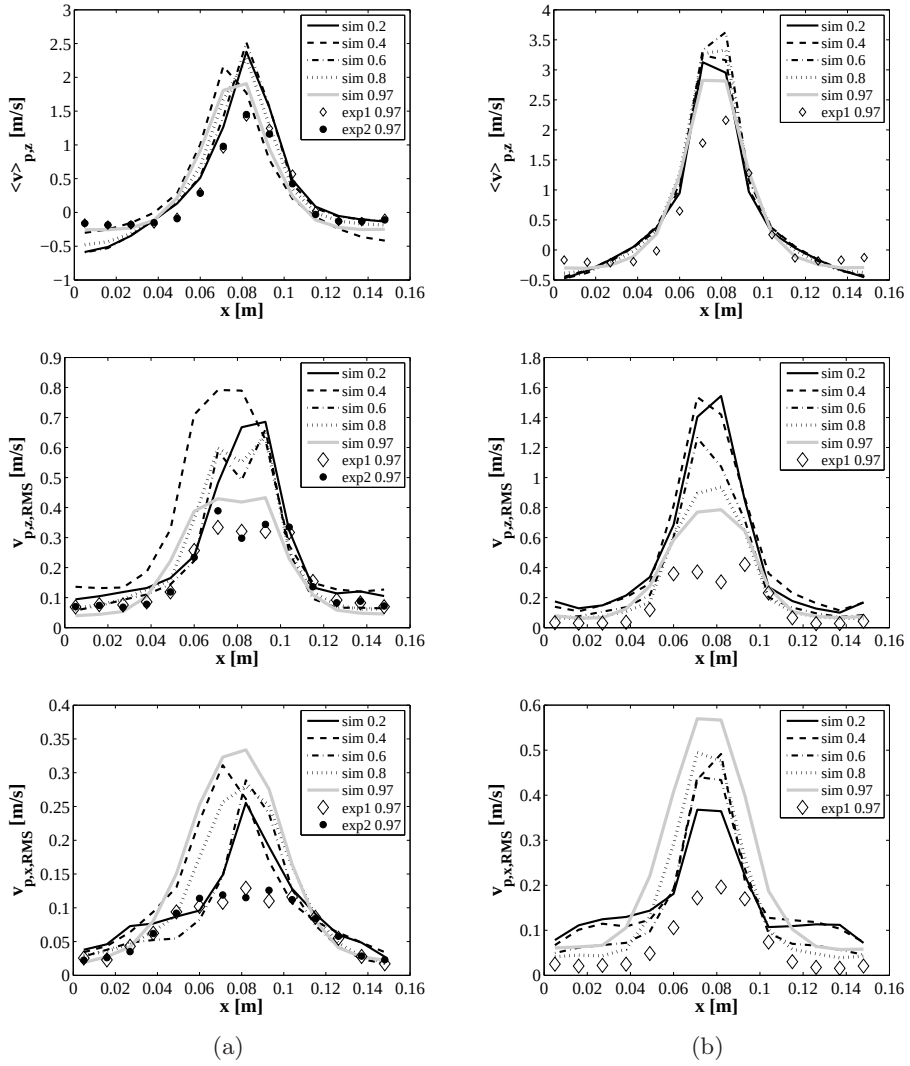

Figure 2.7: Profiles of the time-averaged vertical particle velocity (top), the RMS of the vertical particle velocity (middle) and the RMS of the velocity in the x-direction (bottom) in the central xz-plane at $z = 0.15$ m for (a) case B1 (intermediat/spout-fluidization regime) and (b) B2 (spouting-with-aeration regime)

.

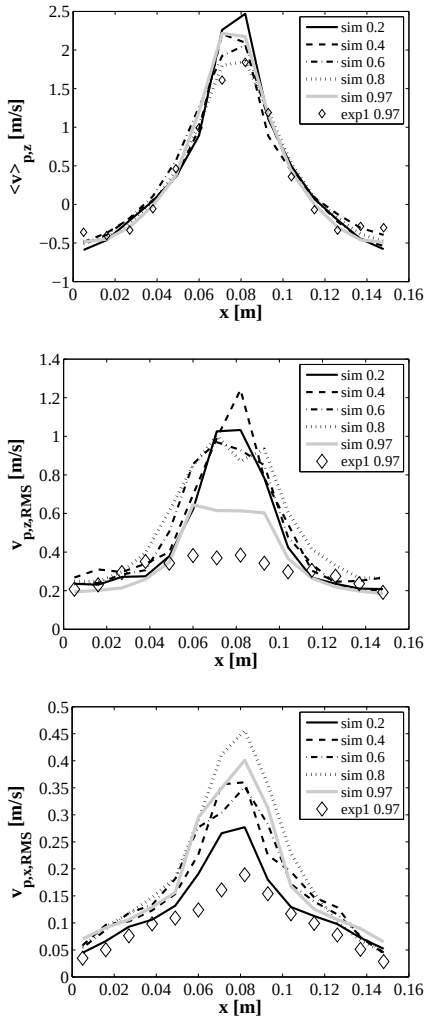

Figure 2.8: Profiles of the time-averaged vertical particle velocity (top), the RMS of the vertical particle velocity (middle) and the RMS of the velocity in the x-direction (bottom) in the central xz-plane at $z = 0.15$ m for case B3 (jet-in-fluidized-bed regime)

.

2.6 Conclusions

The influence of the restitution coefficient on the bed dynamics is studied using the discrete element model (DEM). The fluctuations in the bed height, bed pressure drop, and the time-averaged vertical particle velocity were determined. Additionally, the amplitude of the fluctuations was studied in terms of the root mean square (RMS). For our study three flow regimes were investigated: the intermediate / spout-fluidization regime (B1), spouting-with-aeration regime (B2) and the jet-in-fluidized-bed regime (B3). The pressure drop and the vertical particle velocity were compared to the experimental data reported by Link et al. (2007) to validate the DEM model. The computed results with $e_n = 0.97$ showed good resemblance with the experiments as well as the simulations reported by Link et al. (2007). Furthermore, it was found that with decreasing restitution coefficient, the average bed height increased for all flow regime cases. The averaged pressure drop was lowest at $e_n = 0.97$ for all three regime cases, showing the near-ideal mutual interaction of the particles. A transition from near-ideal to non-ideal behaviour is observed around $e_n = 0.8$. This was confirmed with the trend of the RMS of the pressure drop. Thus, as the restitution coefficient decreases, the dynamic behaviour of the bed becomes more pronounced, with an extent depending on the flow regime. The particle velocity and RMS profiles confirmed the effect on the dynamics of the bed and revealed that the spout channel for cases B1 (intermediate/spout-fluidization regime) and B3 (jet-in-fluidized-bed regime) becomes unstable when the restitution coefficient decreases. For case B2, a transition occurs from the spouting-with-aeration to the intermediate/spout-fluidization regime at low restitution coefficient. These findings reveal the significant impact of the influence of the restitution coefficient on the dynamics of the bed. During the granulation process, when the particles contain different loadings of moisture, regions in the bed exist that contain particles with different restitution coefficient. These regions thus display distinctly different bed dynamics. It is therefore desirable to further improve the discrete element model, by giving each particle its own restitution coefficient dependent on its moisture content, which is the subject of Chapter 4.

Nomenclature

Roman letters		
D	[m]	Diameter
D	[-]	Distribution function
e_n	[-]	Coefficient of normal restitution
e_t	[-]	Coefficient of tangential restitution
$\mathbf{F}_{ab}$	[N]	Contact force
$\mathbf{g}$	[m/s^2]	Gravitational acceleration
$\mathbf{H}$	[-]	Rotation matrix
$< H_{bed} >$	[m]	Time-averaged bed height
$\mathbf{I}$	[-]	Unit vector
k_n	[N/m]	Spring stiffness
m_{ab}	[kg]	Effective particles mass
m_p	[kg]	Particle mass
$\mathbf{n}_{ab}$	[-]	Normal unit vector
N_p	[-]	Number of particles
N_t	[-]	Number of time steps
N_x	[-]	Number of grid cells x-direction
N_y	[-]	Number of grid cells y-direction
N_z	[-]	Number of grid cells z-direction
N_w	[-]	Number of system walls
p	[Pa]	Pressure
$<\mathbf{p}>$	[Pa]	Time-averaged pressure drop
$\mathbf{r}$	[m]	Position
Re_p	[-]	Particle Reynolds number
$\mathbf{S}_p$	[-]	Particle drag sink term
t	[s]	Time
$\mathbf{T}$	[Nm]	Torque
$\mathbf{t}_{ab}$	[-]	Tangential unit vector
Δt	[s]	Time step in simulation
$\mathbf{u}_f$	[m/s]	Gas velocity
$\mathbf{v}_p$	[m/s]	Particle velocity
$<\mathbf{v}_p>$	[m/s]	Time-averaged particle velocity
V	[m^3]	Volume

Greek symbols

β	[kg/(m^3 s)]	Inter-phase momentum transfer coefficient
$\boldsymbol{\delta}$	[m]	Overlap
ε	[-]	Volume fraction
λ_f	[kg/(m s)]	Gas phase bulk viscosity
μ	[-]	Dynamic friction coefficient
μ_f	[kg/(m s)]	Gas phase shear viscosity
$\boldsymbol{\eta}$	[Ns/m]	Damping coefficient
ρ	[kg/m^3]	Density
$\boldsymbol{\tau}_f$	[Pa]	Gas phase stress tensor
$\boldsymbol{\omega}$	[1/s]	Angular velocity

Subscripts

bg	Background fluidization
coll	Collisions
end	End of simulation
exp	Experimental
f	Fluid phase
flow	Flowsolver
mf	Minimum fluidization
n	Normal direction
p	Particle
pdf	Pressure drop fluctuations
sim	Simulation
sp	Spout
sup	Superficial
t	Tangential direction
w	Wall
x	Horizontal direction
z	Vertical direction
0	Initial

Abbreviations

3D	Three-dimensional
DEM	Discrete element model
PEPT	Positron emission particle tracking
RMS	Root mean square

3

Experimental Study on the Effect of Dry Particle-Particle Interactions

This chapter is based on:
M.S. van Buijtenen, M. Börner, N.G. Deen, S. Heinrich, S. Antonyuk and J.A.M. Kuipers: An experimental study of the effect of collision properties on spout fluidized bed dynamics, *Powder Technology* **2011**, *206 (1-2)*, 139.

Abstract

In this chapter we experimentally study the effect of collision properties of different particle systems on the bed dynamics of a spout fluidized bed. This is done for different flow regimes: the spout-fluidization regime (case B1), the spouting-with-aeration regime (case B2) and the jet-in-fluidized-bed regime (case B3). The considered particle systems comprise glass beads, γ-alumina oxide and zeolite 4A particles, which are all classified as Geldart D. A non-intrusive measurement technique is used, *viz.* particle image velocimetry (PIV) to measure the particle flow field in a pseudo two-dimensional (2D) spout fluidized bed. Additionally, digital images are analyzed using a newly developed digital image analysis (DIA) algorithm to evaluate the particle volume fraction. It is demonstrated that the new proposed DIA algorithm provides reliable information on the particle volume fraction distribution, showing that it is a powerful tool when combined with PIV. The added value of DIA is confirmed by comparing the particle velocity fields and volumetric particle fluxes. The particle flux obtained with the combined PIV/DIA technique is used to validate simulation results of the jet-in-fluidized-bed regime (case B3) for all three particle systems. It is shown that the vertical particle fluxes obtained from the simulations are slightly overpredicted higher up in the bed and in the annulus region, which might be due to the larger wall effect in pseudo-2D beds. Simulations with a larger friction coefficient for particle-wall interactions with glass beads showed (for this examined system) a better resemblence of the computed downward flux in the annulus compared to the experimental results. The effect of the collision properties for glass beads, γ-alumina oxide and zeolite 4A particles has been studied in three flow regimes, *i.e.* the intermediate/spout-fluidization regime (case B1), the jet-in-fluidized-bed regime (case B3) and the spouting-with-aeration regime (case B2). For each flow regime, the particle volume fraction shows small differences between the different particle systems. For the γ-alumina oxide and zeolite 4A particles, the spout channel is less stable for the cases B1 and B2. The particle fluxes display also small differences between the particle systems for each flow regime.

3.1 Introduction

In the previous numerical study (Chapter 2) the effect of the collision properties, *i.e.* the restitution coefficient, on the bed dynamics was investigated. It was found that the influence of the restitution coefficient on the bed dynamics is very important. To verify if the same trend is found experimentally, an experimental study is conducted to examine different particle systems with different collision properties in a spout fluidized bed. Particle Image Velocimetry (PIV) is used to non-intrusively measure the particle flow field in a pseudo two-dimensional (2D) spout fluidized bed and a newly developed Digital Image Analysis algorithm (DIA) is applied to determine the local particle volume fraction. Several workers applied PIV to study 2D granular flows, such as gas-fluidized beds (Bokkers et al. (2004)-Dijkhuizen et al. (2007)), spout fluidized beds (Link et al. 2004), spouted beds (Liu et al. 2008), but also vibrated granular beds (Zeilstra et al. (2008) and Deng and Wang (2003)), rotating drums (Jain et al. 2002) and silos or hoppers (Medina et al. (1998) and Steingart and Evans (2005)). Through these applications, PIV has proven to be a powerful tool for 2D granular flow field measurement. However, PIV is generally used to determine velocity profiles of the solids phase rather than individual particle velocities. This means that information about the distribution of the particles inside the bed is lacking. Consequently, Laverman et al. (2008) and Link et al. (2004) were the first to combine digital image analysis (DIA) with PIV. Laverman et al. (2008) used PIV/DIA to correct for the large velocities associated with particle raining through the roofs of the larger bubbles in bubbling fluidized beds. Link et al. (2004) used PIV/DIA to determine the particle flux in spout fluidized beds by combining the particle velocity data obtained from PIV with the particle volume fraction gained from DIA. Hence, these workers show that the combination of DIA with PIV provides much more detailed information about the dynamics of granular systems.

The objective is to study the effect of the collision properties of various particle systems on the bed dynamics in different flow regimes, by employing PIV/DIA to a pseudo-2D spout fluidized bed. The organization of this chapter is as follows: first the experimental set-up is briefly discussed. Then, the experimental techniques are described including the newly proposed DIA algorithm, followed by a detailed description of the procedures to obtain the particle volume fraction from DIA. The particle velocity obtained from PIV and the particle flux obtained from PIV/DIA are mutually compared, and finally the particle flux is compared with DEM simulations for one flow regime.

3.2 Experimental Set-up

The pseudo-2D spout fluidized bed used in this work is schematically presented in Figure 3.1(a). The depth of the bed is assumed to be sufficiently small to display pseudo-2D behaviour and is large enough to avoid extreme particle-wall interaction.

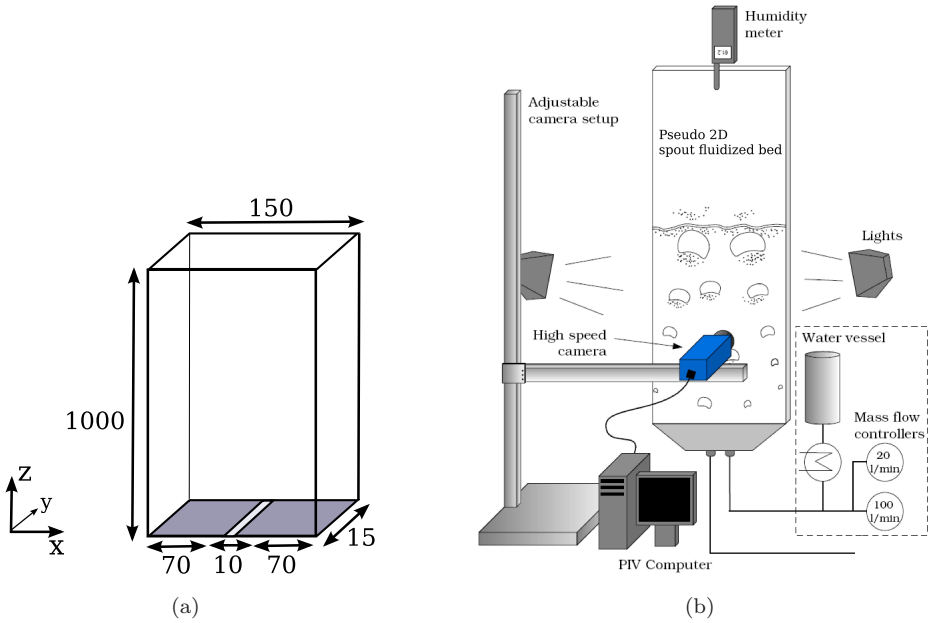

Figure 3.1: Schematic overview of pseudo-2D spout fluidized bed, with dimensions in mm (a) and experimental set-up including equipment (b).

The front wall of the bed consists of a glass plate to enable visual detection of the particle motion. The side walls of the bed are made of aluminium strips and the back wall is made of polycarbonate. Pressurized air is fed to the bed through three separate sections. The spout section is located in the middle and is surrounded by two sections that provide the background fluidization air. The spout section is covered with a 0.5 mm gauze and the fluidization section is covered with a 3 mm thick porous plate with an average pore size of 10 microns. The flow rate of the gas in each section is controlled by mass flow controllers and rapidly responding magnetic valves. The air in the fluidization sections was humidified till $\sim$ 50%

relative humidity to prevent electrostatic charging. Digital images are recorded with a 625 Hz high speed camera (LaVision Imager Pro) equipped with a 50 mm lens. The aperture of the camera is set to f6 and the exposure time is fixed at 0.4 ms. The recorded images consist of 312 x 1280 pixels and are stored in the memory of the camera. After all the images for one experiment have been recorded, the 12-bit images are transferred to the hard disk of the PC.

3.3 Experimental Techniques

3.3.1 Particle Image Velocimetry

Particle image velocimetry (PIV) is an optical, non-intrusive measurement technique that produces instantaneous 2D velocity data for a whole plane in a 3D flow field. It was originally developed in the field of experimental fluid dynamics to study the flow of single phase fluids (Westerweel (1997)). In this work, PIV has been applied to study the particle flow in a pseudo-2D spout fluidized bed. The front view of the bed is recorded using the equipment shown in Figure 3.1(b). Two subsequent images of the flow, separated by a short time delay, Δt, are divided into small interrogation areas. Cross-correlation analysis is used to determine the volume-averaged displacement, $\mathbf{s}_p(\mathbf{x}, t)$, of the particle images between the interrogation areas in the first and second image. The velocity within the interrogation area is then easily determined by dividing the measured displacement by image magnification, M, and the time delay:

$$\mathbf{v}_p(\mathbf{x}, t) = \frac{\mathbf{s}_p(\mathbf{x}, t)}{M \Delta t} \tag{3.1}$$

provided that Δt is sufficiently small. For further details of this technique, the interested reader is referred to the work of Westerweel (1997). A multi-pass correlation algorithm with a final interrogation size of 32 px was used to obtain the final velocity field. Outliers were removed with a standard median filter.

3.3.2 Digital Image Analysis

Digital image analysis (DIA) finds its origin in the work of Agarwal et al. (1997), where bubbles were detected. Goldschmidt et al. (2003) used this technique to detect particles and Link et al. (2004) successfully applied DIA to study spout-fluidized beds. In this work, the particles are detected with the use of DIA, and additionally, a new algorithm is proposed to determine the volume fraction of particles in each interrogation area. The digital image consists of pixels with different intensities, distinguishing the particles from the gas phase. Particles in front of the bed experience the highest intensity and the particles near the back wall have a lower intensity. The lowest intensity is assigned to the gas phase. Due to the fact that homogeneous illumination is difficult to accomplish in practice, the digital image is corrected for inhomogeneities and subsequently the intensities are normalized producing a range between 0 and 1. The value of 1 represents the brightest particle and 0 the gas phase. Furthermore, the intensities are averaged over interrogation areas with the same size as used for PIV. The averaged intensity represents the apparent 2D volume fraction of the particles. In Figure 3.2, the original intensity, corrected and normalized intensity and the resulting 2D particle volume fraction are shown.

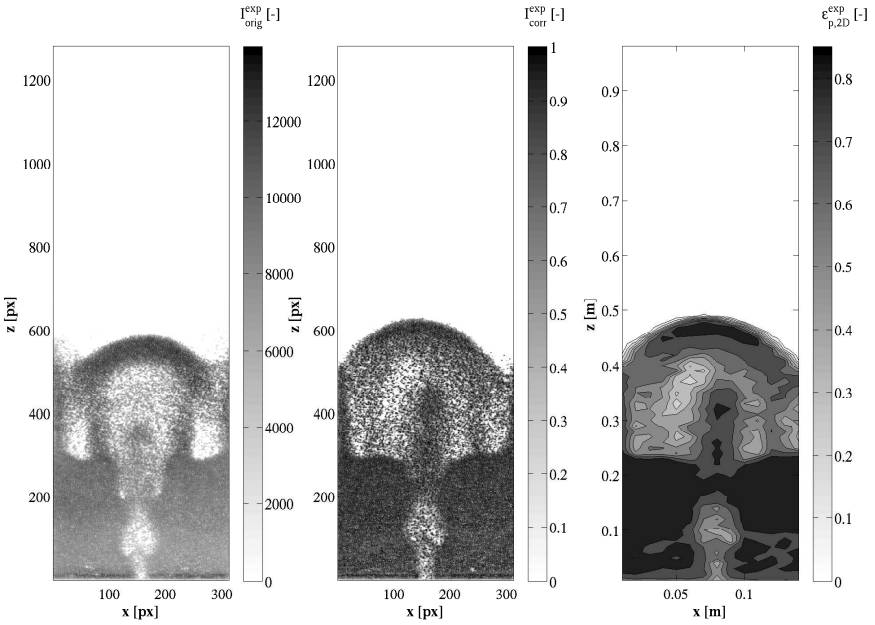

Figure 3.2: Original intensity, corrected and normalized intensity and resulting 2D particle volume fraction obtained from digital analysis on experimental image.

In order to translate the apparent 2D particle volume fraction to the true 3D particle volume fraction, a relationship between these two parameters is required. To this end, spout fluidized bed simulation data of a discrete element model (DEM) is used, in which both parameters can be obtained. The 3D particle volume fraction was obtained by applying the Euler-Lagrange coupling as described in Chapter 2. The apparent 2D particle volume fraction was determined from synthetic particle images generated from the particle position data in the DEM simulations. The intensity distribution over a single particle is described by a Gaussian function and the intensity across the depth of the bed decreases linearly. As a result, each particle obtains the highest intensity in the centre of the particle, and particles in the front of the bed obtain a higher intensity than particles in the back of the bed. Since both the 2D and 3D particle volume fraction are known in the simulation, a relationship is found which is shown in Figure 3.3.

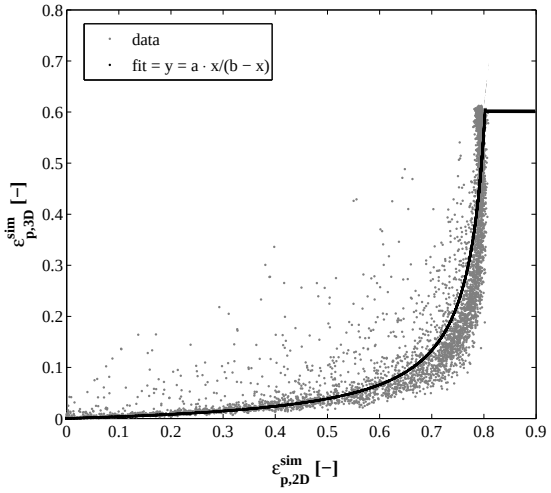

Figure 3.3: Simulation data of 3D and 2D particle volume fraction including the proposed fit.

It can be seen that at low particle volume fractions the relationship between $\varepsilon_{p,2D}$ and $\varepsilon_{p,3D}$ is approximately linear, whereas at $\varepsilon_{p,2D} \approx 0.8$ the relationship displays asymptotic behaviour. Both limits are described quite well with the following function:

$$\varepsilon_{p,3D}(\mathbf{x},t) = A \cdot \frac{\varepsilon_{p,2D}(\mathbf{x},t)}{B - \varepsilon_{p,2D}(\mathbf{x},t)} \tag{3.2}$$

This function yields unrealistic values of $\varepsilon_{p,3D}$ for values of $\varepsilon_{p,2D}$ close to B. To prevent this from happening the function is bounded by the maximum packing fraction $\varepsilon_{p,3D} = 0.6$, or the corresponding 2D volume fraction $\varepsilon_{p,2D} = \frac{0.6B}{A+0.6}$:

$$\varepsilon_{p,3D}(\mathbf{x},t) = \begin{cases} A \cdot \frac{\varepsilon_{p,2D}(\mathbf{x},t)}{B-\varepsilon_{p,2D}(\mathbf{x},t)} & \text{if } \varepsilon_{p,2D}(\mathbf{x},t) < \frac{0.6B}{A+0.6} \\ 0.6 & \text{if } \varepsilon_{p,2D}(\mathbf{x},t) \geq \frac{0.6B}{A+0.6} \end{cases} \tag{3.3}$$

Equation 3.3 contains two fit parameters that were fitted by minimizing the summed square of residuals using the synthetic images. In the experimentally recorded images, the obtained fit gave rise to deviated values for the overall bed mass. This is caused by the small differences in illumination, by which for each experiment the asymptotic value B slightly shifts. Therefore, the value of B was

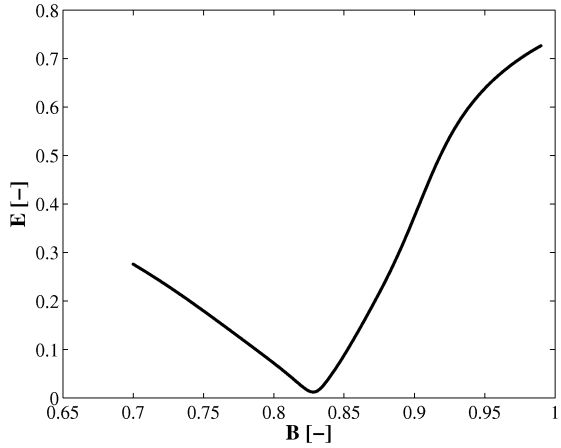

Figure 3.4: Error in bed mass as function of fit parameter B.

altered in such a way that a minimum error in the bed mass is obtained. To this end, equation 3.3 is used to compute the values of $\varepsilon_{p,3D}(\mathbf{x}, t)$, which are subsequently averaged in space and time to obtain the bed mass using:

$$m_{bed,calc} = \rho_p V_{bed} \langle \varepsilon_{p,3D} \rangle \tag{3.4}$$

The value of B is now obtained by determining the minimum error in the time averaged bed mass E, not exceeding a value of approximately 4%, and is defined as:

$$E = \left| \frac{m_{bed,real} - m_{bed,calc}}{m_{bed,real}} \right| \tag{3.5}$$

In Figure 3.4 the error in bed mass is plotted against the fitting parameter B. The optimal value for B corresponds to the smallest bed mass error E.

In Figure 3.5, synthetic particle images, 2D and 3D particle volume fraction and the calculated 3D particle volume fraction of the simulations are displayed. The value of the 2D particle volume fraction in the dense regions is difficult to relate to the 3D particle volume fraction. This is because loosely packed bed regions and densely packed bed regions are difficult to distinguish from each other.

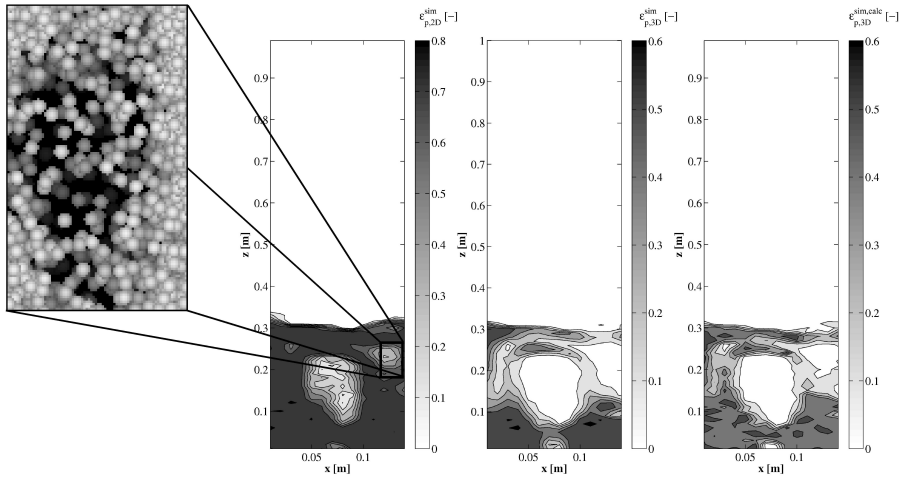

Figure 3.5: Synthetic generated particle image, 2D particle volume fraction, true 3D particle volume fraction and calculated 3D particle volume fraction obtained from digital image analysis on simulated image.

3.4 Test Cases

Three different particle systems, i.e. glass beads, γ-alumina oxide and zeolite 4A particles are considered. The diameter of the particle systems is chosen such that the particle to bed depth ratio is at least six, to prevent the formation of stable particle structures extending from wall to wall. Each particle system is studied in three different flow regimes: the spout-fluidization regime (case B1), the spouting-with-aeration regime (case B2) and the jet-in-fluidized-bed regime (case B3). The flow regimes are scaled by the minimum fluidization velocity, to exclude the effect of the particle diameter and density on the bed dynamics. In this way, the collision properties are the only influencing parameters. Tables 3.1 and 3.2 respectively summarize the properties of the particle systems and the flow regimes. In comparison with experiments, DEM simulations were performed for all three particle systems for the jet-in-fluidized-bed regime. The dimensions in the simulations are the same as in the experiments (see Figure 3.1(a)), as well as the particle properties and gas velocities. The numerical settings are listed in Table 3.3. For glass beads two simulations were run with different coefficients of friction with the wall, to examine the influence of the particle-wall interaction on the particle flux patterns.

Table 3.1: Properties of particles systems.

Property	Glass beads	γ-alumina oxide	Zeolite 4A	Unit
d_p	1.5	1.8	1.9 - 2.3	mm
ρ_p	2526	1040	1140	kg/m^3
e_n	0.87	0.74	0.65	-
u_{mf}	0.93	0.62	0.82	m/s

Table 3.2: Flow regimes.

Case	Flow regime	u_{bg}/u_{mf} [-]	u_{sp}/u_{mf} [-]
B1	Spout-fluidization	1.2	23
B2	Spouting-with-aeration	1.2	45
B3	Jet-in-fluidized bed	2.3	16

Table 3.3: Numerical settings.

Property	Value	Unit
N_x	30	-
N_y	2	-
N_z	100	-
Δt	10^{-4}	s
t_{end}	20	s
$N_{p,Glass}$	$11.5 \cdot 10^4$	-
$N_{p,AlO}$	$6.6 \cdot 10^4$	-
$N_{p,Zeo}$	$4.2 \cdot 10^4$	-
k_n	10^4	N/m
$\mu_{p\leftrightarrow p}$	0.10	-
$\mu_{p\leftrightarrow w}$	0.10	-
$\mu_{p\leftrightarrow w,Glass}$	0.10 & 0.30	-

3.5 Results and Discussion

Firstly, the time-averaged 3D particle volume fractions resulting from the proposed DIA algorithm will be discussed. Subsequently, the velocity fields are discussed and compared to the resulting volumetric particle fluxes, followed by comparison with DEM simulations.

3.5.1 Time-averaged 3D Particle Volume Fraction

Figure 3.6(a) shows the different contour plots of the 3D volume fraction obtained for the different flow regimes. Cases B1 and B2 show the typical dense packed annulus region and the diluted spout channel, which is characteristic for spout fluidized beds. For these cases, $\langle \varepsilon_{p,3D} \rangle$ in the annulus approaches 0.6, since the background velocity is close to the minimum fluidization velocity. The small differences in $\langle \varepsilon_{p,3D} \rangle$ in the annulus are difficult to observe, which is caused by the uncertainty in the calibration curve for the dense regions. For case B3, the variations in $\langle \varepsilon_{p,3D} \rangle$ in the spout and annulus region are very clear. For this flow regime, the typical dense packed annulus is not present. As a result the $\langle \varepsilon_{p,3D} \rangle$ is determined more accurately. For case B1 (spout fluidization regime) the background velocity is around the minimum fluidization velocity and the spout velocity is high enough to enable the spout channel to form, but not to break through continuously. As a result, the spout channel is periodically blocked causing pressure build up. When the pressure is sufficiently high, the spout gas breaks through and launches a cluster of particles into the freeboard region of the bed. This is clearly depicted in Figure 3.6(a) with a large value of $\langle \varepsilon_{p,3D} \rangle$ above the spout channel. Figure 3.6(b) shows that the characteristic fountain is less obviously present for the γ-alumina oxide and zeolite 4A particles, which can also be seen in Figure 3.6(a) having a smaller value of $\langle \varepsilon_{p,3D} \rangle$ above the spouts.

For case B (jet-in-fluidized-bed regime), the background velocity is rather high and the spout velocity is moderate. Due to bubble formation in the annulus region, the stability of the spout channel is fully disrupted. Consequently, the typical shape/configuration of a denser packed annulus with a dilute packed spout channel breaks down, as shown in Figure 3.6(b). The contour plots of $\langle \varepsilon_{p,3D} \rangle$ for the different particle types are very similar.

For case B2 (spouting-with-aeration regime), the spout velocity is very high causing a permanent break through of the spout gas. The spout channel is continuously open and the particles are dragged up high in the bed and subsequently

rain down in the annulus region. As shown in Figure 3.6(b), the spout channel for γ-alumina oxide and zeolite 4A particles is disturbed by the lateral motion of the particles in the annulus, hindering permanent breakthrough, disturbing the regular pattern of the spouting-with-aeration regime. As a result, the large value of $\langle \varepsilon_{p,3D} \rangle$ that is present higher up in the bed for glass beads in Figure 3.6(a) is smeared out for γ-alumina oxide and zeolite 4A particles.

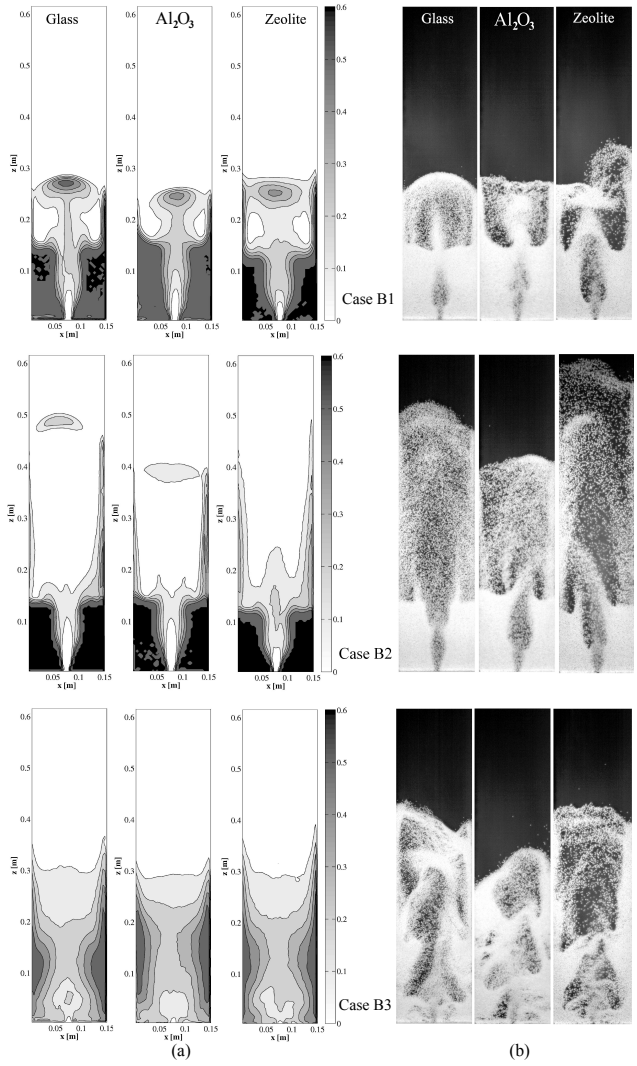

Figure 3.6: Time-averaged 3D particle volume fraction (a) and instantaneous image (b) for spout-fluidization regime (case B1), spouting-with-aeration regime (Case B2) and jet-in-fluidized-bed regime (case B3).

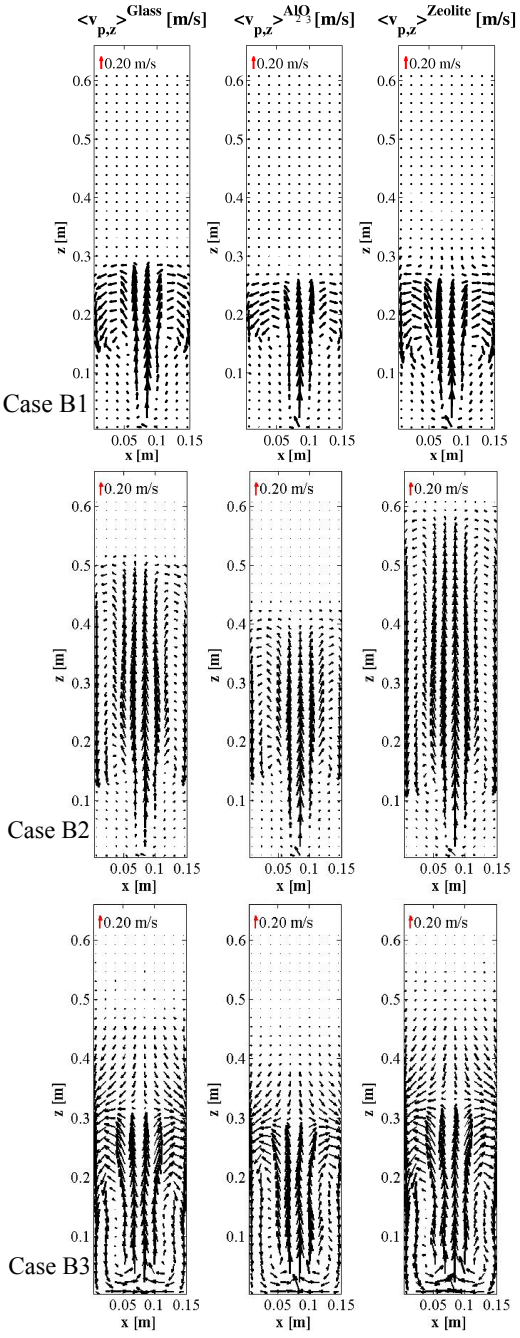

Figure 3.7: Time-averaged particle velocity for spout-fluidization regime (case B1), spouting-with-aeration regime (Case B2) and jet-in-fluidized-bed regime (Case B3). Note that only every second vector in each direction is shown for the sake of clarity.

3.5.2 Time-averaged Particle Velocity and Volumetric Particle Flux

In Figure 3.7 the vector fields of the time-averaged particle velocity and time-averaged volumetric particle flux are displayed. The vector field of the time-averaged particle velocity shows the measured velocity of the particles. These graphs, however, give no information about the number of particles that possess that velocity. *Viz.* the velocity in the spout region is very high, which is only the case for very few particles. This cannot directly be inferred from Figure 3.7. In Figure 3.8(a) an example is shown where the velocity is displayed for interrogation areas containing different amount of particles.

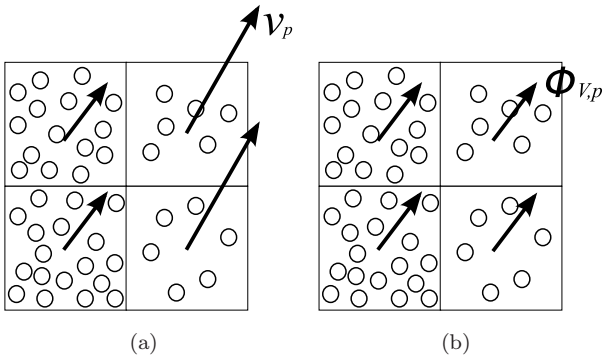

Figure 3.8: Schematic drawing of the particle velocity (a) and volume flux (b) in interrogation areas with different amount of particles

The particle velocity in the interrogation area with many particles is much lower than in the area with few particles. As a result, the dynamics of the particles can be misinterpreted when the information of the amount of particles is not accounted for. This is shown in Figure 3.8(b) displaying a different vector field, due to the presence of the particles. Therefore, the instantaneous particle velocity is multiplied with the instantaneous particle volume fraction, followed by averaging over time to obtain the time-averaged volumetric particle flux:

$$\langle \mathbf{\Phi}_{V,p}(\mathbf{x}) \rangle = \frac{1}{N_t} \sum_{t}^{N_t} (\mathbf{v}_p(\mathbf{x}, t) \cdot \varepsilon_p(\mathbf{x}, t)) \tag{3.6}$$

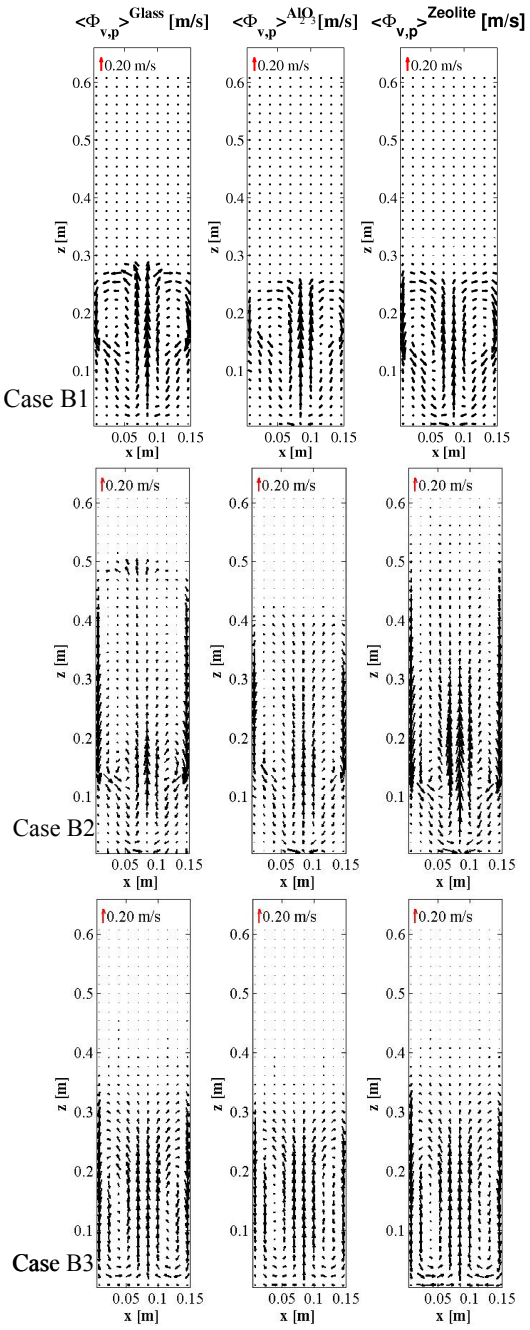

Figure 3.9: Time-averaged volumetric particle flux $[m^3/(m^2 \cdot s)]$ for spout-fluidization regime (case B1), spouting-with-aeration regime (Case B2) and jet-in-fluidized-bed regime (Case B3). Note that only every second vector in each direction is shown for the sake of clarity.

In Figure 3.9, the time-averaged volumetric particle flux is presented, revealing a clear picture of the motion of the particles. For cases B1 and B2, the motion of the particles in the annulus region follows the expected behaviour. Although the velocity is very low in the annulus region, the particle flux is comparable to that in the spout channel, because of the high particle volume fraction.

For case B1, the flux in the spout channel seems to be a bit larger for the glass beads and the downward flux of the glass beads is also slightly larger.

For case B2, the patterns depict large similarity for all the particle systems. However, for zeolite 4A the particle flux in the spout is larger and the particles are more scattered in the upper half of the bed. This is due to the lateral disturbance of the spout channel and a higher pressure build up. Furthermore, the glass beads reach a higher bed height compared to the γ-alumina oxide particles. This may be due to the difficulty of the spout gas to break through the bed with γ-alumina oxide particles.

For case B3, the flux vector field displays large resemblance with that of an ordinary fluidized bed, where the characteristic vortices in the annulus regions are more vertically stretched for the γ-alumina oxide and zeolite 4A particles. This is due to the fact that for zeolite 4A particles, large bubbles are directly formed, disrupting the spout channel to such an extent that it looses its influence.

3.5.3 Volumetric Particle Flux: Experiment and Simulation

In Figure 3.10 the time-averaged vertical particle flux obtained from the PIV/DIA experiments and DEM simulations is presented. The same trends are observed, however, it is shown that the particle flux in the simulations is larger higher up in the bed compared to the experimental results. This could be due to wall effects that are more dominant in pseudo-2D beds than in 3D systems. The profiles in Figure 3.11 in the central xz-plane at $z = 0.15$ m comply well in the spout region and deviate in the annulus region which can be attributed to the treatment of the particle-wall friction. Therefore, a second simulation is run with glass beads having a friction coefficient of $\mu_{p\leftrightarrow w} = 0.3$ instead of 0.1, showing in Figure 3.11(a) that the simulation results in the annulus region correspond better to the experiments. Hence, a friction coefficient of $\mu_{p\leftrightarrow w} = 0.3$ is a more realistic value in simulations of pseudo-2D beds.

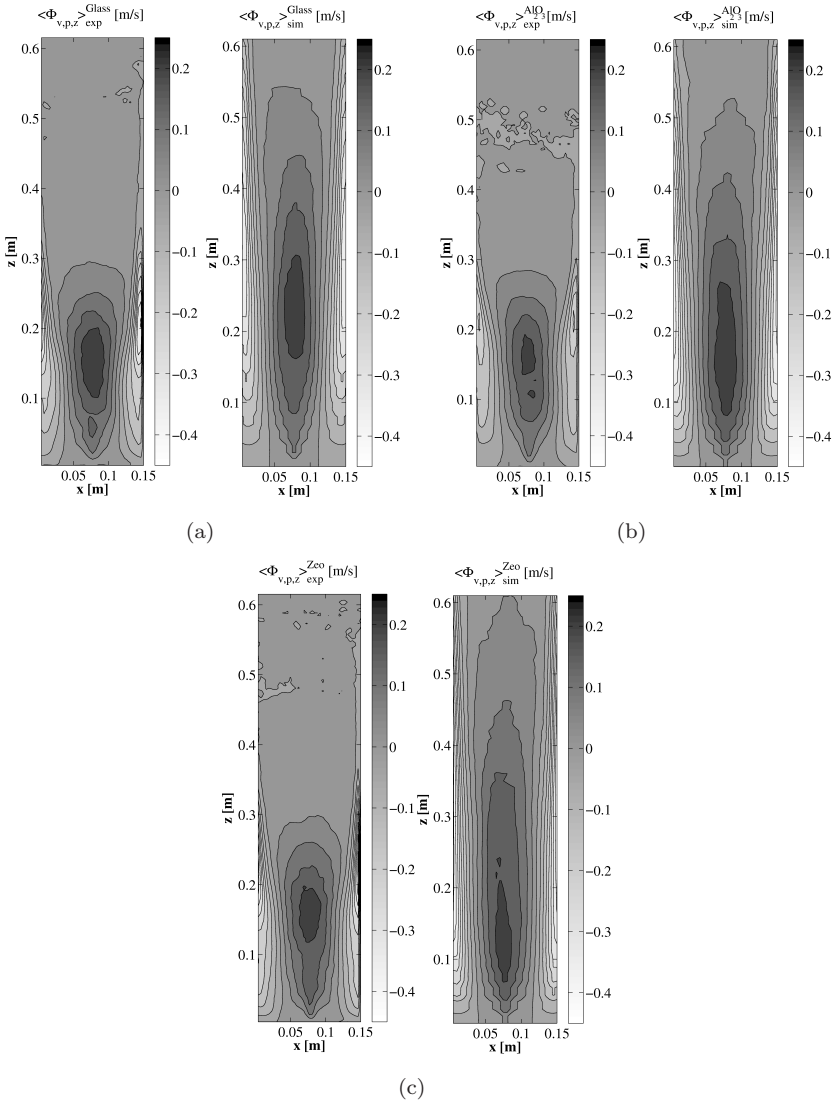

Figure 3.10: Contour plot of time-averaged vertical volumetric particle flux $[m^3/(m^2 \cdot s)]$ from PIV/DIA experiments (left) and DEM simulations (right) for case B3, the jet-in-fluidized-bed regime, for (a) Glass beads, (b) γ-alumina oxide and (c) zeolite particles.

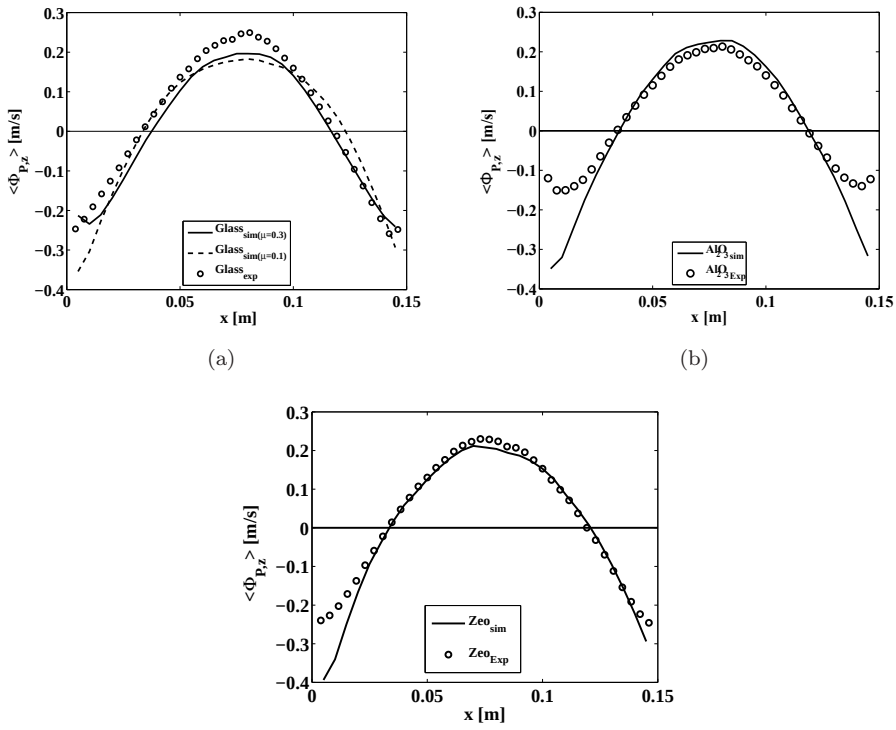

Figure 3.11: Profiles of time-averaged vertical volumetric particle flux $[\mathrm{m}^3/(\mathrm{m}^2 \cdot \mathrm{s})]$ from PIV/DIA experiments and DEM simulations for glass beads (a), γ-alumina oxide (b) and zeolite (c) particles, in the central xz-plane at $z = 0.15$ m for case B3, the jet-in-fluidized-bed regime.

3.6 Conclusions

The effect of the collision properties of different particle systems on the bed dynamics has been experimentally investigated. Particle Image Velocimetry (PIV) and Digital Image Analysis (DIA) were applied to a pseudo-2D spout fluidized bed, to obtain particle velocity fields and the particle volume fraction, non-intrusively. To this end, a new DIA algorithm has been proposed, which successfully translates the apparent 2D particle volume fraction to the real 3D particle volume fraction. By employing this DIA algorithm, a more detailed picture of the complex solids motion in spout-fluidized beds can be obtained.

Additionally, the particle flux obtained with the combined PIV/DIA technique was compared with simulation results of the jet-in-fluidized-bed regime (case B3) for all three particle systems. It is shown that the vertical particle fluxes obtained from the simulations are larger higher up in the bed than in the experiments, and secondly, that the downward flux is larger in the annulus region in the simulations. This might be due to the larger wall effect in pseudo-2D beds, and simulations with a larger friction coefficient for particle-wall interactions with glass beads showed indeed a better resemblence of the downward flux in the annulus with the experiments.

The effect of the collision properties for glass beads, γ-alumina oxide and zeolite 4A particles has been studied in three flow regimes, *i.e.* the intermediate/spout-fluidization regime (case B1), the spouting-with-aeration regime (case B2) and the jet-in-fluidized-bed regime (case B3). For each flow regime, the particle volume fraction shows small differences between the different particle systems, contrary to the simulation results of previous studies. For the γ-alumina oxide and zeolite 4A particles, the spout channel is more disturbed for the cases B1 and B2 which leads to different dynamics above the spout channel. The particle fluxes display only small differences between the particle systems for each flow regime. This may be due to the high spout gas velocity providing large momentum exchange between the gas phase and particles. In our case, the competition between particle-particle and gas-particle interaction might be dominated by the latter.

Summarizing, since small differences of the flow behaviour are observed between the particles with different collision properties, it can be concluded that the collision properties of dry particles only have a small influence on the average bed dynamics of spout fluidized beds.

Nomenclature

Roman letters

A	[-]	Fitting parameter
B	[-]	Fitting parameter
d	[m]	Diameter
e_n	[-]	Coefficient of normal restitution
E	[-]	Relative error in bed mass
I	[-]	Intensity of a pixel
k_n	[N/m]	Spring stiffness
m	[kg]	Mass
M	[-]	Image magnification
N_t	[-]	Number of timesteps
N_p	[-]	Number of particles
N_x	[-]	Number of grid cells in simulation x-direction
N_y	[-]	Number of grid cells in simulation y-direction
N_z	[-]	Number of grid cells in simulation z-direction
s	[m]	Volume-averaged displacement vector
t	[s]	Time
Δt	[s]	Time delay / time step in simulation
$\mathbf{v}$	[m/s]	Velocity
V	[m^3]	Volume
$\mathbf{x}$	[m]	Coordinate vector

Greek symbols

ε	[-]	Volume fraction
μ	[-]	Dynamic friction coefficient
ρ	[kg/m^3]	Density
Φ	[m^3/(m^2s)]	Flux

Subscripts

Al_2O_3	γ-alumina oxide particles
bg	Background fluidization
end	End of simulation
exp	Experimental
f	Fluid phase

Glass	Glass beads
mf	Minimum fluidization
n	Normal direction
p	Particle
sim	Simulation
sp	Spout
sup	Superficial
t	Tangential direction
w	Wall
x	Horizontal direction
z	Vertical direction
Zeo	Zeolite 4A particles
0	Initial

4

Discrete Simulation Study on the Effect of Wet Particle-Particle Interactions

This chapter is based on:
M.S. van Buijtenen, N.G. Deen, S. Heinrich, S. Antonyuk and J.A.M. Kuipers: A discrete element study of wet particle-particle interaction during granulation in a spout fluidized bed, *The Canadian Journal of Chemical Engineering* **2009**, *87*, 308.

Abstract

In this chapter, the effect of the inter-particle interaction on the bed dynamics is studied, by considering a variable restitution coefficient. The restitution coefficient is varied in time and space depending on the moisture content due to the particle-droplet interaction and evaporation. This study is done computationally, by using an extended discrete element model (DEM). The examined flow regimes comprise the intermediate/spout fluidization regime (B1), spouting-with-aeration regime (B2) and the jet-in-fluidized-bed regime (B3). For all flow regimes, the averaged bed height increases with decreasing restitution coefficient. Moreover, the averaged bed height for a variable restitution coefficient is larger for all flow regimes compared to a case with a constant restitution coefficient, indicating that the spatial distribution of the restitution coefficient influences the bed dynamics. The effect of evaporation on the distribution of the restitution coefficient is only observed for the jet-in-fluidized-bed regime (B3), where the background velocity is relatively high leading to enhanced evaporation from the particles in the annulus region. This is reflected in the averaged bed height for the evaporation test case, which is larger compared to a test case without evaporation. A larger bed height for cases with variable restitution coefficient is due to the pressure build up in the spout region caused by the longer closing period of the spout channel. This is confirmed by the recorded pressure fluctuation signal and its root mean square which are larger for the cases with the variable restitution coefficient.

4.1 Introduction

In granulation processes particles get wetted due to interactions with droplets. As described in Chapter 2, the restitution coefficient significantly influences the spout fluidized bed dynamics. Since the restitution coefficient changes in space and time due to particle-droplet interaction during the granulation process, in this chapter the effect of the moisture content on the restitution coefficient is considered.

It has been shown in literature that as wet particles collide, energy dissipates not only due to deformation of the particle, but also due to viscous dissipation in the liquid layer. Moreover, according to Ennis et al. (1991) this energy dissipation can also be caused by capillary forces. Depending on how much kinetic energy is left, the particles will stick or rebound. Ennis et al. (1991) used the dimensionless liquid binder Stokes number St_v, which is a measure for the ratio of granule collisional kinetic energy to the viscous dissipation brought about by the interstitial binder. Below a critical value of the Stokes number the particles stick to each other and above, the particles rebound. This effect was simulated by Talu et al. (2000). They found that the liquid binder between particles indeed dissipates viscous energy and keeps particles together due to capillary effects.

Research has thus shown that the moisture content in spout fluidized beds has a significant influence on the inter-particle collision properties and hence on the flow behaviour. Consequently, the DEM is further developed by improving the description of both the particle-droplet and particle-particle interactions. The effect of the moisture content on the particle-particle interaction is studied, by defining an empirical based relation between the restitution coefficient and moisture content. The influence of the impact velocity is excluded in this work, to first study solely the effect of the moisture dependent restitution coefficient on the bed dynamics. However, in practice, the impact velocity does influence the restitution coefficient as well, which should be the subject of a subsequent study of this work. Besides the addition of droplets, the moisture content is also affected by the removal of moisture due to evaporation. The objective is to gain insight in the influence of the restitution coefficient on the flow behaviour of spout fluidized beds at different flow regimes using the further developed DEM. The organization of this chapter is as follows: first, the DEM, including the improvement is briefly discussed. Then, the studied test cases are described and finally, the simulation results are discussed and compared.

4.2 Numerical Model

The simulations were conducted with a discrete element model that describes the dynamics of the continuous gas-phase and the discrete particles and droplets. For each element force balances are solved and the momentum transfer among each of the phases is described in detail at the level of individual elements. The DEM was further developed to describe the motion of the droplets in more detail and the inter-particle collisions being affected by the particle state (*i.e.* particle wetness).

4.2.1 Gas Phase

In Chapter 2 the equations for the description of the dynamics of the continuous (gas) phase are explained. A major difference is that the porosity in this case is dependent on both particles and droplets, that is:

$$\varepsilon_f + \varepsilon_p + \varepsilon_d = 1 \tag{4.1}$$

4.2.2 Particle Motion

The motion of each individual particle present in the system is calculated from the Newtonian equation of motion:

$$m_p \frac{d\mathbf{v}_\mathrm{p}}{dt} = -V_p \nabla p + \frac{V_p \beta}{(1-\varepsilon_f)}(\mathbf{u}_f - \mathbf{v}_p) + m_p \mathbf{g} + \sum_{N_p} \mathbf{F}_{p \leftrightarrow p} + \sum_{N_w} \mathbf{F}_{p \leftrightarrow w} + \sum_{N_d} \mathbf{F}_{p \leftrightarrow d} \tag{4.2}$$

4.2.3 Droplet Motion

The DEM extended by Link et al. (2007) contains a simplified description of the phenomena in which the droplets are involved. In this work the DEM is extended by incorporating the full equation of motion of the droplets and two-way coupling of the drag between the droplets and the gas phase. The equation of motion of the droplets resembles that of the particles, although it is assumed that the droplets do not collide with each other, because of their small size and low volume fraction:

$$m_d \frac{d\mathbf{v}_\mathrm{d}}{dt} = -V_d \nabla p + \frac{V_d \beta}{(1-\varepsilon_f)}(\mathbf{u}_f - \mathbf{v}_d) + m_d \mathbf{g} \tag{4.3}$$

The inter-phase momentum transfer coefficient due to drag is calculated in the same way as for the particles (equation 2.5), using the Reynolds number for the relative velocity of the droplets and the droplet size.

4.2.4 Particle State

Due to the addition of droplets and subsequent impact on the particle surface, the particle is moisturized and subsequently, evaporation occurs. As a result, the state of the particle changes which is expressed through a (coupled) mass and energy balance over each particle. The mass balance is formulated as:

$$\frac{dm_p}{dt} = \dot{m}_d - \Phi_{m,evap} \tag{4.4}$$

The accumulation of droplets due to particle-droplet collisions is given by:

$$\dot{m}_d = \sum_{i=0}^{i-N_{coll}} m_d \tag{4.5}$$

where N_{coll} is the number of particle-droplet encounters. The mass transfer due to evaporation is described as:

$$\Phi_{m,evap} = k(w^*_{d,g} - w_{d,g})A_p \tag{4.6}$$

in which $w^*_{d,g}$ represents the saturated mass concentration of moisture in the gas film layer at the surface of the particle (calculated using the Clausius-Clapeyron relationship) and $w_{d,g}$ the mass concentration of moisture in the bulk of the gas phase. As a first approximation, it is assumed that $w_{d,g} = 0$ kg/m^3. The mass transfer coefficient k is determined using the Sherwood correlation proposed by Gunn (1978). Due to the mass transfer into the bulk, moisture on the particle will evaporate resulting in heat transfer, described by the energy balance on each particle:

$$\frac{dE_p}{dt} = m_p C_p \frac{dm_p}{dt} = \Phi_{h,conv} - \Phi_{h,evap} + \dot{q}_d \tag{4.7}$$

where the heat flow due to evaporation is formulated by:

$$\Phi_{h,evap} = \Phi_{m,evap} \cdot \Delta H_{evap} \tag{4.8}$$

It is assumed that the heat flow necessary for evaporation, fully originates from the gas phase via convection and the heat conduction from the inner centre of the particle is thus ignored:

$$\Phi_{h,conv} = \alpha(T_g - T_p)A_p \tag{4.9}$$

The temperatures of the particle and the gas phase are assumed to be uniform. The heat transport coefficient is also determined using the Nusselt relationship

proposed by Gunn (1978), using the Chilton-Colburn analogy. The heat brought along by the colliding droplets is formulated by:

$$\dot{q}_d = \dot{m}_d C_{p,d}(T_d - T_p) \tag{4.10}$$

The particle growth is defined by the change in volume due to addition of droplets and evaporation of moisture:

$$\frac{dV_p}{dt} = \frac{\dot{m}_d - \Phi_{m,evap}}{\rho_d} \tag{4.11}$$

4.2.5 Particle-Droplet Interaction

The encounter between a droplet and a particle is described differently compared to particle-particle collisions, because of the very small size of an individual droplet. When the droplet meets a particle, it is assumed that it always transfers its mass and momentum to the particle and is removed from the simulation. Droplet-droplet interaction is ignored, because of the small size of the droplets and their low volume fraction. The velocity of the particle is affected by momentum transfer of the droplet:

$$\mathbf{v}'_p = \frac{\mathbf{v}_p m_p + \mathbf{v}_d m_d}{m'_p} \tag{4.12}$$

where m'_p is the new mass of the particle which results from the mass balance. Furthermore, it is assumed that the angular velocity is unaffected by the particle-droplet interaction:

$$\boldsymbol{\omega}'_p = \boldsymbol{\omega}_p \tag{4.13}$$

When a droplet hits a particle, it is assumed that the droplet forms a uniform film on the surface of the particle. Hence, the resulting particle remains spherical and the position of the particle is not altered:

$$\mathbf{r}'_p = \mathbf{r}_p \tag{4.14}$$

The volume of the particle varies in time caused by the change in amount of moisture:

$$V'_p = V_p + V_d \tag{4.15}$$

Due to the droplet-particle interactions, a particle consists of an amount of moisture, which is defined as the moisture content:

$$X_w = \frac{m_{moist}}{m_{p,0} + m_{moist}} \tag{4.16}$$

The mass of moisture is formulated as the summation of the mass of each droplet hitting particle p minus the amount of moisture that is evaporated.

4.2.6 Particle-Particle Interaction

The inter-particle collisions are described using a soft sphere approach and is described in Chapter 2. Due to the moisture content on each particle the mutual interaction varies, since the particles collide less ideal with increasing moisture load. This is approximated with the following relation:

$$e_{n,p} = (e_{n,p_0} - e_{n,p_{sat}}) \cdot 10^{-5X_w} + e_{n,p_{sat}} \tag{4.17}$$

where e_{n,p_0} is the normal restitution coefficient of the dry particle, that is, $X_w = 0$, and $e_{n,p_{sat}}$ is the normal restitution coefficient of a saturated particle. This relation is based on detailed impact measurements of dry particles on a flat plate with a thin liquid layer (Vorhauer 2007). It is assumed here that the restitution coefficient does not depend on the relative velocity of the colliding particles. There is ample room for improvement of equation 4.17. However, in this work it is used as a first attempt to model the effect of moisture on the restitution.When two particles (a and b) with different restitution coefficients collide, an overall restitution coefficient is determined using harmonic averaging:

$$e^{-1}_{n,p,ab} = \frac{1}{2}(e^{-1}_{n,p,a} + e^{-1}_{n,p,b}) \tag{4.18}$$

Harmonic averaging was used to ensure that the moisture on either particle involved in the collision really determines the effective restitution coefficient.

4.2.7 Euler-Lagrange Coupling

To solve the force balance on a single droplet, gas phase properties are needed on the Lagrangian coordinates, and thus these properties are mapped in analogy with the Euler-Lagrange coupling for particles. However, since the droplets are quite small compared to the Eulerian grid mesh, the size of the cube is in the order of one grid cell, *i.e.* $n = \Delta X$, making the mapping computational less expensive.

4.3 Test Cases

The objective is to study the bed dynamics as a function of the restitution coefficient, which varies in time and space due to the particle-droplet interaction and evaporation. To enable the study of a variable restitution coefficient, several test cases were chosen which are listed in Table 4.1.

Table 4.1: Test cases.

Case	e_n	Mass	Evaporation	T [^{o} C]
Constant e_n	Constant	Constant	No	25
Variable e_n	Variable	Constant	No	25
Wetting	Variable	Variable	No	25
Evaporation	Variable	Variable	Yes	25
Extended evaporation	Variable	Variable	Yes	60

The cases with constant and variable restitution coefficient are clarified in Figure 4.1. Firstly, the effect of the distribution of the restitution coefficient on the bed dynamics is studied by comparing the results of the constant e_n and variable e_n test cases. For the constant e_n test case, several simulations were conducted

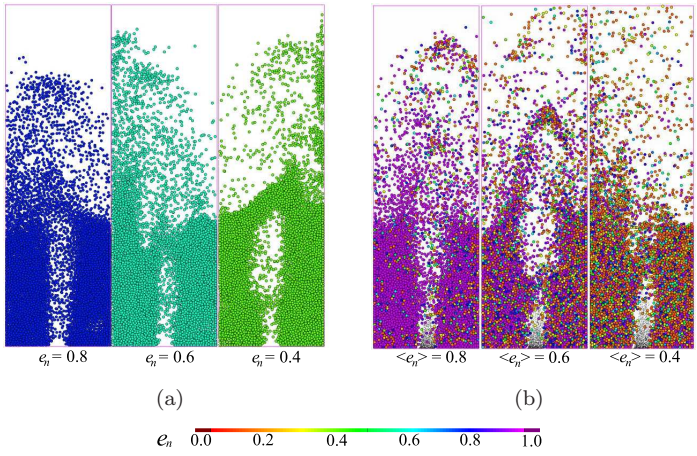

Figure 4.1: Test cases with constant and variable restitution coefficient.

where the restitution coefficient equals successively 0.8, 0.6, and 0.4 being constant in time and space across the bed. For the variable e_n, the restitution coefficient changes with varying moisture content, while the particle mass and volume remain constant. Secondly, the results of the wetting and evaporation test cases are considered to investigate the effect of evaporation on the distribution of the restitution coefficient. In these cases, the particle mass and volume do change. The effect on the bed dynamics is studied for different flow regimes, which are shown in Table 2.2. The properties of the particles and droplets are listed in Table 4.2 and the numerical settings are listed in Table 4.3 (for further details of the numerical procedure, the interested reader is referred to Hoomans et al. (1996)). A schematic representation of the geometry of the 3D spout fluidized bed is displayed in Figure 2.3.

Table 4.2: Particle and droplet properties.

Property	Value	Unit
d_p	4.0	mm
ρ_p	2526	kg/m^3
$e_{n,p\leftrightarrow p}$	0.97	-
$e_{n,p\leftrightarrow w}$	0.97	-
$e_{n,p\leftrightarrow p,sat}$	0.10	-
$e_{n,p\leftrightarrow w,sat}$	0.10	-
$e_{t,p\leftrightarrow p}$	0.33	-
$e_{t,p\leftrightarrow w}$	0.33	-
$\mu_{p\leftrightarrow p}$	0.10	-
$\mu_{p\leftrightarrow w}$	0.10	-
d_d	0.4	mm
ρ_d	998	kg/m^3
m_d	$3.344 \cdot 10^{-8}$	kg

Table 4.3: Numerical settings.

Property	Value	Unit
N_x	21	-
N_y	14	-
N_z	100	-
Δt	10^{-4}	s
t_{end}	40	s
N_p	$4.48 \cdot 10^4$	-
k_n	10^4	N/m
$\dot{N}_{drop}$	$8.5 \cdot 10^5$	drops/s

4.4 Results and Discussions

To study the effect of the variable restitution coefficient on the bed dynamics, the bed height and pressure drop fluctuations will be examined. Firstly the constant e_n and variable e_n test case will be considered, secondly the wetting and evaporation test case. The bed height is defined as the averaged z-location of the particles:

$$\langle r_z \rangle = \frac{1}{N_{part}} \sum_{N_{part}} r_z \tag{4.19}$$

In the simulations with constant restitution coefficient, the first 10 s were excluded from the spectral analysis to prevent start-up effects from influencing the results. The variable e_n, wetting and evaporation test cases were initiated at the end of the simulations with $e_n = 0.97$, injecting droplets in a spout-fluidized bed in which realistic bed dynamics prevails. The bed height for the constant e_n test case is time-averaged over 10 s, whereas the averaging period for the other test cases depends on the globally averaged restitution coefficient, which should comply with the constant restitution coefficient to enable a fair comparison. To this end, the instantaneous restitution coefficient for the variable e_n, wetting and evaporation test cases is averaged over all particles. The averaging periods are chosen such that the time-averaged restitution coefficient deviates ± 5 % around the constant values, distinguishing the different stages of the wetting process (Figure 4.2).

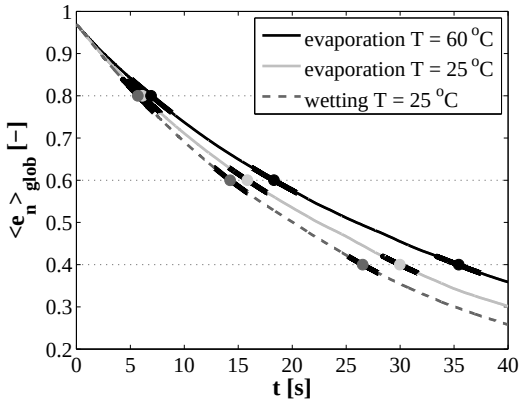

Figure 4.2: Globally averaged restitution coefficient versus time for the wetting, evaporation and extended evaporation test cases. The selected averaging periods per stage of the granulation or wetting process are visualized by the bold black lines.

Snapshots of the simulated instantaneous particle positions of both the constant e_n and variable e_n test case are presented in Figure 4.3, showing the bed behaviour for different restitution coefficients for the three flow regimes. The time-averaged distribution of the restitution coefficient is displayed in Figure 4.4 for every stage of the wetting test case. Below, the results of the bed height and the pressure drop fluctuations will be shown.

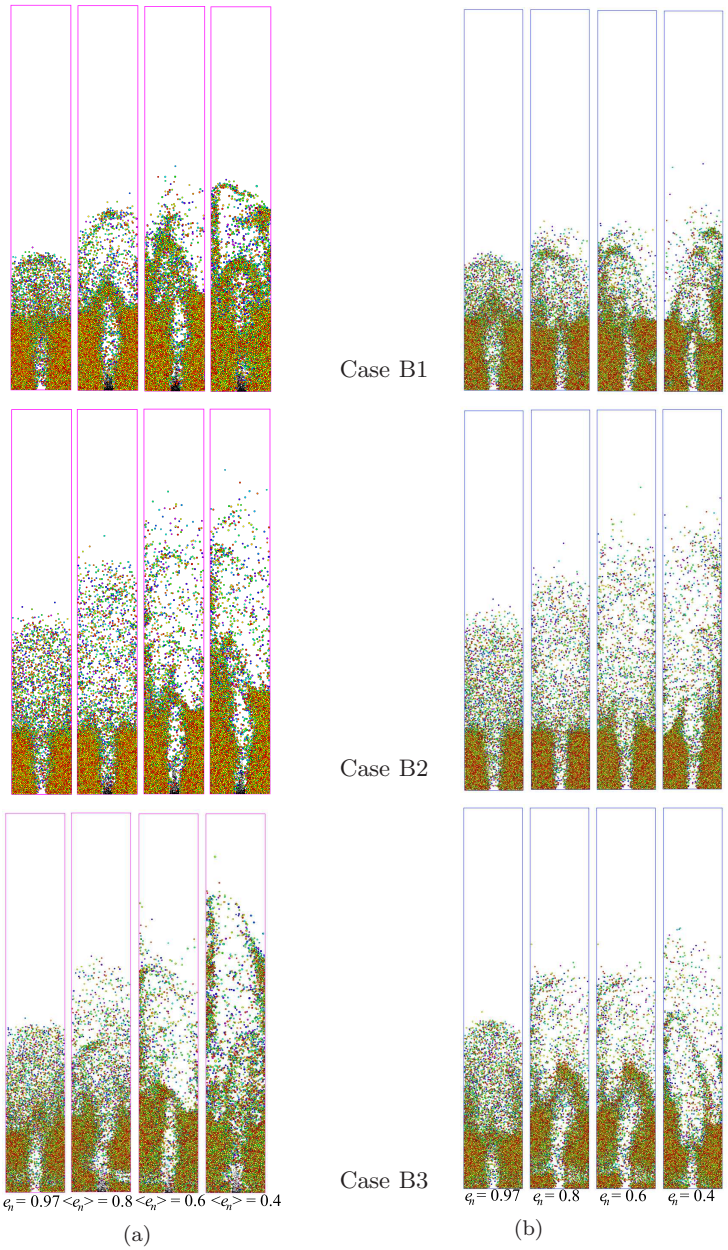

Figure 4.3: Snapshots of the simulated instantaneous particle positions for different variable restitution coefficients (a) and different constant restitution coefficients (b) for case B1 (intermediate/spout-fluidization regime), B2 (spouting-with-aeration regime) and B3 (jet-in-fluidized-bed regime).

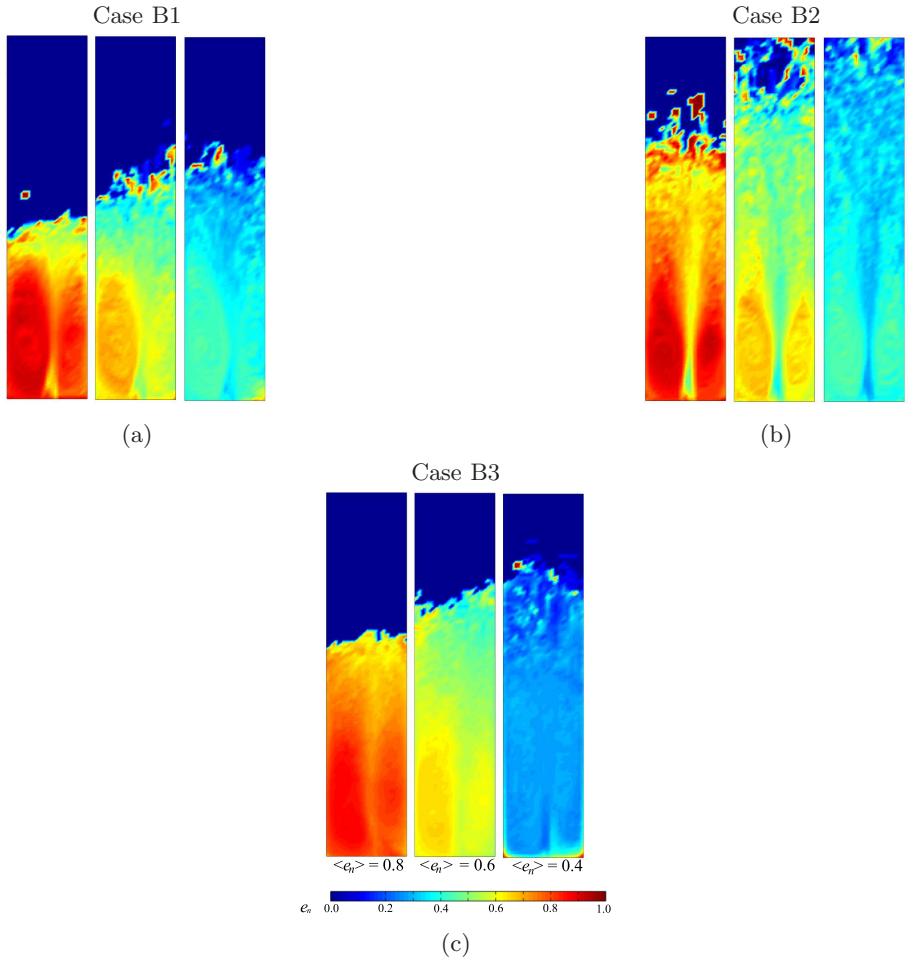

Figure 4.4: Spatial distribution of the locally time-averaged restitution coefficient for different variable restitution coefficients for (a) case B1 (intermediate/spout-fluidization regime), (b) B2 (spouting-with-aeration regime), and (c) B3 (jet-in-fluidized-bed regime) at different stages of the wetting process, distinguished by the globally averaged restitution coefficient $\langle e_n \rangle$.

4.4.1 Bed Height

In Figure 4.5(a) the time-averaged bed height of the simulation results for the test cases with constant e_n and variable e_n are shown, and in Figure 4.5(b) the results are displayed for the wetting and evaporation test case. Note that the bed height corresponding to the constant e_n was averaged over a period of 10 s, whereas the bed height of the other test cases was averaged over at least 4 s. This period is chosen to gain a time-averaged restitution coefficient which deviates $\pm 5\%$ around the constant value. As a result, the time-averaged bed height will have larger uncertainties due to the short period of averaging. The variable e_n, wetting and evaporation test cases were initiated at the end of the constant e_n test case with $e_n = 0.97$, injecting droplets in a spout-fluidized bed in which realistic bed dynamics prevails. In Figure 4.3 the instantaneous snapshots of the simulation with constant $e_n = 0.97$ are therefore displayed as a reference. It is found that the average bed height increases with decreasing restitution coefficient for both the constant and variable restitution coefficient. This is due to decreasing bubble hold-up. Particles with low restitution coefficient tend to promote the formation of dense regions and passage of gas through the bed mainly occurs in the form of bubbles.

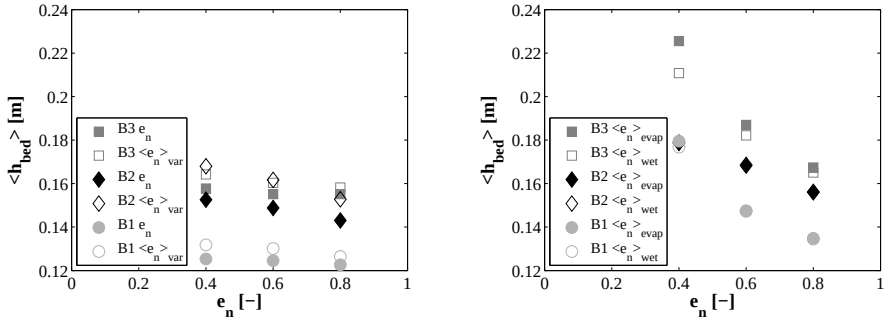

(a) (b)

Figure 4.5: Time-averaged bed height for different constant restitution coefficients and different variable restitution coefficients (a) and for for different variable restitution coefficients corresponding to the wetting and evaporation test cases (b), at different stages of the wetting process, distinguished by the overall restitution coefficient $\langle e_n \rangle$, for case B1 (intermediate/spout-fluidization regime), B2 (spouting-with-aeration regime), and B3 (jet-in-fluidized-bed regime).

Furthermore, for the variable restitution coefficient the elevated bed height is observed for every restitution coefficient and flow regime. This may be due to the fact that during the granulation process, the particles in the spout region contain the highest moisture content and thus the lowest restitution coefficient (see Figure 4.4). As a result, the spout channel is longer closed which causes a larger pressure build up and hence particles are pushed higher up in the bed. This effect is enhanced when the particle mass also varies with moisture content (wetting and evaporation test cases, shown in Figure 4.5(b)). In these cases, particles in the spout region are heavier enlarging the closure time of the spout channel. The effect of evaporation is minor for case B1 (intermediate/spout-fluidization regime) and B2 (spout-with-aeration regime), although for case B3 (jet-in-fluidized bed regime) evaporation does influence the bed height (Figure 4.5(b)). This is probably due to the fact that for case B3 the background gas velocity is relatively high, resulting in more evaporation in the annulus region which gives a larger difference in moisture content between particles in the annulus and spout region. Thus, the restitution coefficient in the spout region is smaller compared to the restitution coefficient of the particles in the annulus, causing a longer closing period of the spout and therefore a larger bed height.

4.4.2 Pressure Drop Fluctuations

As mentioned in the previous section, it is expected that the closing time of the spout channel increases with a larger distribution of the restitution coefficient of particles in the spout and annulus region. To confirm this hypothesis, the pressure fluctuation is plotted against time for the wetting and evaporation test case in the jet-in-fluidized-bed regime (B3), accompanied with instantaneous snapshots of the particle positions at moments that are marked in the pressure fluctuation graph (Figure 4.6(a)). The pressure fluctuations of the evaporation test case are larger than the pressure fluctuations of the wetting test case, indicating that the spout channel is indeed longer closed causing a larger pressure build up. The instantaneous snapshots of the particle positions of the evaporation test case (Figure 4.6(b)) show that the spout channel is closed by which the pressure increases, pushing up a cluster of particles (second picture). Then, if the pressure beneath the particle cluster is high enough to break through, the particle cluster is launched high in the bed. At last, as shown in the third picture, the particles rain down in the annulus and the spout channel is closed again, initiating a new pressure build up.

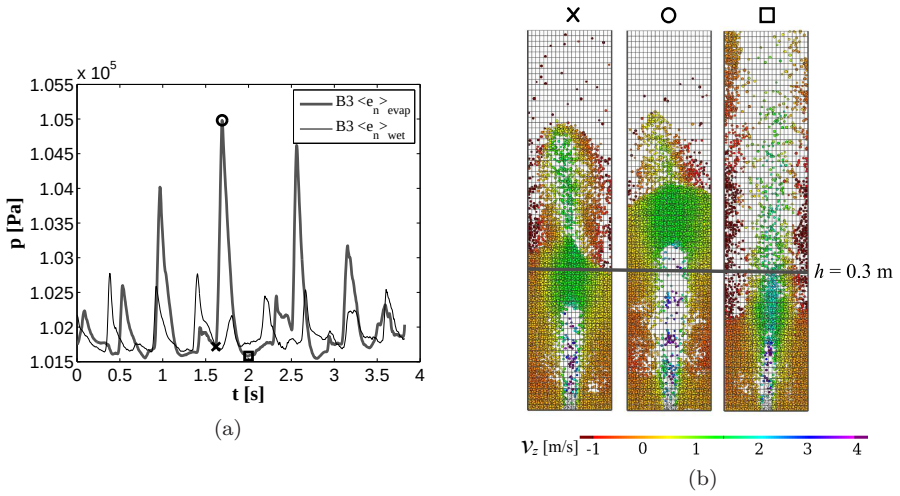

Figure 4.6: Pressure fluctuations versus time (a) of the wetting and evaporation test case in the jet-in-fluidized-bed regime (B3), at a bed height $h = 0.3$ m and instantaneous snapshots of the particle positions (b) of the evaporation test case corresponding to the specified times. The colour of the particles indicates the magnitude of the vertical particle velocity.

In Figure 4.7 the amplitude of the pressure fluctuations is displayed at different bed heights. The RMS for the evaporation test case is larger compared to the wetting test case at every bed height, showing that the observation depicted in Figure 4.6(a) is valid at every vertical location across the bed.

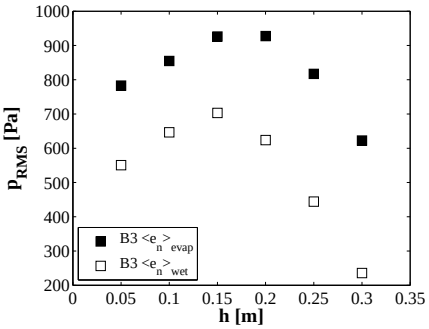

Figure 4.7: RMS of the pressure fluctuations of the wetting and evaporation test case in the jet-in-fluidized-bed regime (B3) at different heights in the bed.

4.5 Conclusions

The influence of the restitution coefficient on the bed dynamics is studied using the discrete element model (DEM), where the restitution coefficient is time and space dependent due to the particle-droplet interaction and evaporation. The time-averaged bed height, bed pressure fluctuations, and the magnitude of the corresponding amplitude (RMS) were determined. For our study four test cases were formulated: the constant e_n, variable e_n, wetting and evaporation test cases. Firstly, the effect of the distribution of the restitution coefficient on the bed dynamics (constant e_n *vs.* variable e_n) was investigated and secondly the influence of evaporation on the distribution of the restitution coefficient (wetting versus evaporation test case) was examined. This is done for three flow regimes, *viz.* the intermediate/spout-fluidization regime (B1), spouting-with-aeration regime (B2) and the jet-in-fluidized-bed regime (B3). For all test cases and flow regimes, the averaged bed height increases with decreasing restitution coefficient (Figure 4.5). Moreover, the averaged bed height for the variable restitution coefficient is larger for all flow regimes compared to the constant restitution coefficient, indicating that the distribution of the restitution coefficient, which provides regions in the bed with particles having different collision properties, indeed influences the bed dynamics. The effect of evaporation on the distribution of the restitution coefficient is only observed for the jet-in-fluidized-bed regime (B3), where the background velocity is relatively high leading to enhanced evaporation from the particles in the annulus region. This is reflected in the averaged bed height for the evaporation test case, which is larger only in flow regime B3 compared to the wetting test case. A larger bed height for cases with variable restitution coefficient is due to the pressure build up in the spout region caused by the closing of the spout channel. When the restitution coefficient of the particles in the spout region is smaller compared to the particles in the annulus, the spout channel is longer closed, building up more pressure until the cluster of particles is launched in the bed. Due to the larger pressure build up, the particle cluster is pushed higher in the bed resulting in an increased bed height. This is confirmed by the pressure fluctuations and its root mean square in Figures 4.6 and 4.7. Consequently, these findings reveal the significant impact of the influence of the variable restitution coefficient on the dynamics of the bed, which is clearly different compared to the constant restitution coefficient. This is due to the presence of distinctive regions with different restitution coefficient, which can only be simulated when the dependency of the moisture content and evaporation on the restitution coefficient is accounted for.

Currently, only the evaporation of moisture on the particles has been simulated without crystallization of the deposited granulate solution, which is very important in the granulation process. Furthermore, the change in moisture concentration and temperature in the gas phase is neglected, also influencing the bed dynamics. It is therefore desirable to further improve the discrete element model, by solving the mass and energy balances for the gas phase, as well.

Nomenclature

Roman letters

A	[m^2]	Surface area
C_p	[J/(kgK)]	Heat capacity of particle
$C_{p,d}$	[J/(kgK)]	Heat capacity of droplet
d	[m]	Diameter
D	[-]	Distribution function
e_n	[-]	Coefficient of normal restitution
$e_{n,p}$	[-]	Variable coefficient of normal restitution
e_{n,p_0}	[-]	Initial variable restitution coefficient
$e_{n,p_{sat}}$	[-]	Variable restitution coefficient of a saturated particle
$< e_n >$	[-]	Time-averaged restitution coefficient
$< e_n >_{glob}$	[-]	Globally averaged restitution coefficient over all particles
e_t	[-]	Coefficient of tangential restitution
E	[J]	Energy
$\mathbf{F}_{a\leftrightarrow b}$	[N]	Contact force
$\mathbf{g}$	[m/s^2]	Gravitational acceleration
h	[m]	Bed height
$< H_{bed} >$	[m]	Time-averaged bed height
ΔH_{evap}	[J/kg]	Enthalpy of evaporation
$\mathbf{I}$	[-]	Unit vector
k	[m/s]	Mass transfer coefficient
k_n	[N/m]	Spring stiffness
m_p	[kg]	Particle mass
m_d	[kg]	Droplet mass
$\dot{m}_d$	[kg/s]	Droplet mass flow on each particle
N_p	[-]	Number of particles
$\dot{N}_{drop}$	[drops/s]	Rate of injection of droplets
N_{coll}	[-]	Number of collisions
N_t	[-]	Number of time steps
N_x	[-]	Number of grid cells x-direction
N_y	[-]	Number of grid cells y-direction
N_z	[-]	Number of grid cells z-direction
N_w	[-]	Number of system walls
p	[Pa]	Pressure

$<\mathbf{p}>$	[Pa]	Time-averaged pressure drop
$\dot{q}_d$	[J/s]	Heat brought along by droplets
$\mathbf{r}$	[m]	Position
Re_p	[-]	Particle Reynolds number
$\mathbf{S}_p$	[-]	Particle drag sink term
t	[s]	Time
Δt	[s]	Time step in simulation
$\mathbf{u}_f$	[m/s]	Gas velocity
$\mathbf{v}_p$	[m/s]	Particle velocity
$<\mathbf{v}_p>$	[m/s]	Time-averaged particle velocity
V	[m^3]	Volume
$w*_{d,g}$	[kg/m^3]	Saturated mass concentration of moisture in gas film layer on the particle surface
$w_{d,g}$	[kg/m^3]	Mass concentration of moisture in gas film layer around particle
X_w	[-]	Moisture content
$< X_w >$	[-]	Averaged moisture load

Greek symbols

α	[$W/(m^2K)$]	Heat transfer coefficient
β	[$kg/(m^3\ s)$]	Inter-phase momentum transfer coefficient
ε	[-]	Volume fraction
λ_f	[kg/(m s)]	Gas phase bulk viscosity
μ_f	[kg/(m s)]	Gas phase shear viscosity
ρ	[kg/m^3]	Density
τ_f	[Pa]	Gas phase stress tensor
Φ	[kg/s] or [J/s]	Mass or heat transfer rate
ω	[1/s]	Angular velocity

Subscripts

bg	Background fluidization
coll	Collision
conv	Convective
d	Droplet
end	End of simulation
evap	Evaporation

exp	Experimental
f	Fluid phase
h	Heat
m	Mass
mf	Minimum fluidization
moist	Moisture
p	Particle
pdf	Pressure drop fluctuations
sim	Simulation
sp	Spout
sup	Superficial
w	Wall
x	Horizontal direction
z	Vertical direction
0	Initial

Abbreviations

3D	Three-dimensional
DEM	Discrete particle model
RMS	Root mean square

5

Discrete Simulation and Experimental Study on Multiple-Spout Fluidization

This chapter is based on:
M.S. van Buijtenen, W.J. van Dijk, N.G. Deen, J.A.M. Kuipers, T. Leadbeater and D.J. Parker: Numerical and experimental study on multiple-spout fluidized beds, *Chemical Engineering Science* **2011**, doi: 10.1016/j.ces.2011.02.055.

Abstract

In this chapter we study the effect of multiple spouts on the bed dynamics in a pseudo-2D triple-spout fluidized bed, employing the Discrete Element Model (DEM) and non-intrusive measurement techniques such as Particle Image Velocimetry (PIV) and Positron Emission Particle Tracking (PEPT). A flow regime map was constructed, revealing new regimes that were not reported so far. The multiple-interacting-spouts regime (C) has been studied in detail for a double- and triple-spout fluidized bed, where the corresponding fluidization regime for a single-spout fluidized bed has been studied as a reference case. The experimental results obtained with PIV and PEPT agree very well for all the three cases, showing the good performance of these techniques. The DEM simulation results slightly deviate from the experiments which is attributed to particle-wall effects that are more dominant in pseudo-2D beds than in 3D systems. The investigated multiple-interacting-spouts regime is a fully new flow regime that does not appear in single-spout fluidized beds. Two flow patterns have been observed, *viz.* particle circulation in between the spouts near the bottom of the bed, and an apparent single-spout fluidization motion at a higher location upwards in the bed. These findings show that the presence of multiple spouts in a spout fluidized bed highly affect the flow behaviour, which cannot be distinguished by solely investigating single-spout fluidized beds.

5.1 Introduction

The bed dynamics of a spout fluidized bed is influenced by the particle collision properties, as well as the bed geometry. On industrial scale, the dimensions of a spout fluidized bed are such that multiple spouts are necessary to induce the desired particle motion. However, research has so far mainly been focused on single-spout fluidized beds and hence, little is known about the effect of multiple spouts on the bed dynamics. Only a few workers studied the effect of multiple nozzles in spout fluidized and spouted beds. Guo et al. (2003) and Hong et al. (2003) studied the effect of two nozzles in a jetting fluidized bed with a V-type distributor. The formation mechanisms of jets and the interaction of the two vertical jets were analyzed. Three types of flow patterns were identified, *i.e.* isolated jets, transitional jets, and interacting jets. Guo et al. (2003) studied the jetting fluidized transition velocity as a function of nozzle distance, nozzle diameter, particle properties and static bed height.

Gong et al. (2006) and Hu et al. (2008) investigated the effect of multiple air nozzles in an annular spouted bed. In their work, each nozzle contained its own V-shaped guide plates, by which each bottom part individually exists. Three distinct flow patterns, such as internal jet, jet-spouting, and fully developed spouting, and two transitional flow patterns, *viz.* single internal jet, single jet-spouting, and bubbling or slugging were identified.

Although the examined beds differ, these studies show that the presence of two or more nozzles highly affect the flow patterns, and thus the bed dynamics. Therefore, the objective of this work is to study the effect of two and three spouts on the bed dynamics of a pseudo-2D spout fluidized bed, by applying Particle Image Velocimetry (PIV) and Positron Emission Particle Tracking (PEPT) techniques. Laverman (2010) was the first to compare PIV results with PEPT for a fluidized bed.

A flow regime map is constructed for triple-spout fluidization and one flow regime is examined in detail for double- and triple-spout fluidization. The corresponding spout-fluidized-bed regime for single-spout fluidization is studied as a well, to enable comparison between single-, double- and triple-spout fluidization. The experimental results obtained by PIV and PEPT are mutually compared and DEM simulations are validated with the experimental results.

The organization of this chapter is as follows: first the numerical model will be described, followed by the experimental set-up and the employed techniques. Subsequently, the experimentally obtained flow regime map will be presented,

from which one flow regime will be chosen to study in detail for single-, double and triple-spout fluidization.

5.2 Numerical Model

Multiple-spout fluidization is studied in this work for the dry case. Therefore, simulations were conducted with the discrete element model that describes the dynamics of the continuous gas-phase and the discrete particles, which is explained in paragraph 2.2.

5.3 Experimental Set-up

The pseudo-2D spout fluidized bed used in this work is schematically presented in Figure 5.1(a). The bed consisted of three spouts and can be viewed as a composition of three unit cells containing a single spout. This enables the set-up to be utilized also as a single-spout or double-spout fluidized bed by mounting baffles at locations of the dashed lines as depicted in Figure 5.1(a).

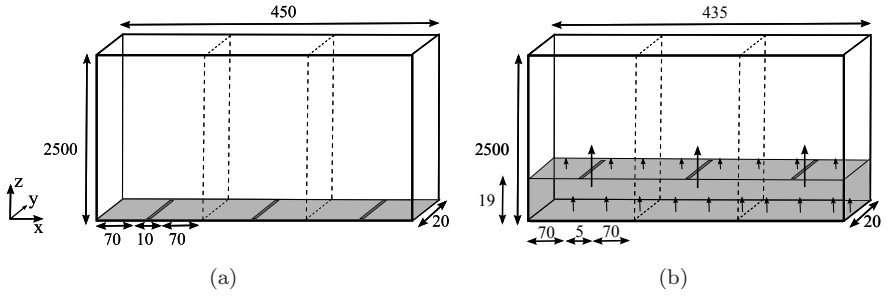

Figure 5.1: Schematic overview of experimental (a) and numerical (b) pseudo-2D spout fluidized bed, with dimensions in mm. The dashed lines display the borders of the three unit cells of which the triple-spout fluidized bed is composed. The grey arced part in (b) represents the windbox.

The depth of the bed was assumed to be sufficiently small to display pseudo-2D behaviour and large enough to avoid extreme particle-wall interaction. The front and back walls of the bed consisted of a Lexan plate to enable visual detection of the particle motion, whereas the side walls of the bed were made of aluminium strips.

Background fluidization air was supplied by a two-stage side channel blower, having a maximum capacity of 312 m^3/hr, a maximum pressure of 580 mbar, and a power of 7.5 kW. To prevent electrostatic charging of the particles, the background fluidization air was humidified till $\sim 50\%$ relative humidity with the aid of a spray tower. The spout air is supplied by a second two-stage side channel blower, with a maximum capacity of 205 m^3/hr, a maximum pressure of 500 mbar, and a power of 4.0 kW. The flow rates of both background and spout sections were controlled by two frequency controllers and were measured by two turbine flowmeters. The spout air was split into three parts, to provide the three spout channels with air. In case of single-spout or double-spout fluidization, the redundant spout channels were closed by a valve. The fluidization section was covered with a 3 mm thick porous plate with an average pore size of 100 microns whereas the spout sections were covered with a 2.0 mm gauze.

For the PEPT measurements the spout fluidized bed was positioned in between the two PEPT detectors, as shown in Figure 5.2. The detectors cover a measurement height of 0.50 m and width of 0.40 m.

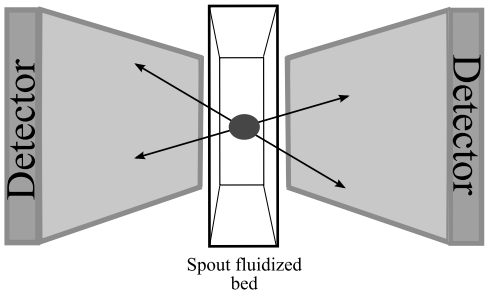

Figure 5.2: Experimental set-up of PEPT measurement technique including the radioactively labelled particle emitting back-to-back γ-rays (represented by $\leftrightarrow$).

For the PIV measurements, digital images were recorded with a high speed camera (LaVision Imager Pro) equipped with a 50 mm lens. The aperture of the camera was set to f6 and the exposure time was fixed at 0.4 ms. The recorded images consist of 608 x 1280 pixels and were stored in the memory of the camera. After all the images for one experiment were recorded, the 12-bit images were transferred to the hard disk of the PC. As shown in Figure 3.1(b), the pseudo-2D bed was illuminated by two 500 W halogen lamps, which were positioned in such a way that the bed was illuminated under a small angle ($< 45^o$), to prevent undesired reflections. The lamps were fed by a direct current supply to minimize

temporal variation in the illumination. The back wall was painted black to provide contrast between particles and background.

Pressure drop fluctuations were measured during all experiments with two high-frequency pressure sensors (Kulite XT-190M-0.35BAR VG) at a frequency of 100 Hz for 2 minutes. The sensors were mounted in the left and right side wall at 0.01 m above the distributor plate.

5.4 Experimental Techniques

In this chapter three different experimental techniques are used: Particle Image Velocimetry, spectral analysis of pressure drop fluctuations, and Positron Emission Particle Tracking. PIV non-invasively obtains instantaneous velocity data for the pseudo-2D bed. A detailed description of the PIV technique can be found in paragraph 3.3.

Pressure drop fluctuations were non-intrusively measured just above the distributor plate, to capture the characteristic flow behaviour of the entire bed. Spectral analysis of the pressure drop fluctuations was carried out with a Fourier transform following Link (2006), resulting in a frequency spectrum that characterizes the dynamic behaviour of the bed.

In PEPT, a radio-actively labelled particle is detected at high speed by a positron camera (Parker et al. 1997). The glass bead (used in this work) is labelled by direct irradiation with a ^{3}He beam, which is generated from a cyclotron, yielding a glass bead that contains the radionuclide ^{18}F with half-life of 110 min. The labelled particle decays with the emission of a positron, and each positron rapidly annihilates with an electron, resulting in an almost exactly back-to-back emisison of a pair of 511 keV γ-rays, which is non-intrusively detected by the two detectors. These detectors define a line of response (LOR) passing close to the active particle. The intersection of several LORs determines the location of the particle in three dimensions. In Figure 5.2, only two LORs are shown.

The position of the tracer particle was recorded over a period of 1.5 h at a frequency ranging from 100 to 300 Hz depending on the amount of radiation emitted by the single tracer particle and the location of the detectors. The instantaneous particle position is subject to a variable amount of noise, since the detectors are less accurate at the borders of the detectors, and in the horizontal plane the point of intersection is more difficult to determine due to the small differences in the slopes of the LORs. To obtain accurate results near the bottom of the bed, the spout

fluidized bed was placed at 0.10 m from the lowest border of the detectors. Noise suppression was achieved by applying a cubic spline to the PEPT output data, as proposed by Link et al. (2008). Due to the (limited) dimensions of the PEPT detectors, the tracer particle occasionally moved out of the detectable area, which was accounted for by leaving out the readings just before exit and after return of the particle in the measurement area. The remaining noise on the time-averaged velocities could be limited by calculating the velocity over six subsequent particle positions, and by subsequent assignment to the cell containing the average over six particle locations. The particle velocity is determined with linear regression where the least squares method is used to minimize the deviation of the fit to the measurement data:

$$\mathbf{v}_p(\mathbf{x},t) = \frac{n\sum_{i=1}^{n}(t\mathbf{x}) - \sum_{i=1}^{n} t \sum_{i=1}^{n} \mathbf{x}}{n\sum_{i=1}^{n}\mathbf{x}^2 - \left(\sum_{i=1}^{n}\mathbf{x}\right)^2} \tag{5.1}$$

5.5 Test Cases

The objective of this work is to study the effect of multiple spouts on the spout fluidized bed dynamics, both numerically and experimentally. A flow regime map for triple-spout fluidization was constructed in accordance with Link et al. (2005), from which a flow regime was selected to study single-, double- and triple-spout fluidization in detail. In the experimental set-up, the gas flow through the three spouts was supplied by a single blower. If one spout experiences a larger pressure drop for intance due to particles blocking the spout channel the gas will have a preference to flow through the other spouts causing variation in the gas velocities of the spout channels. In other words, the spout channels communicate with each other via the pressure drop they experience. To capture this effect in the DEM simulations, the windbox that is situated below the bottom plate was incorporated in the simulation domain. The windbox supplies the spout velocity through the three spouts whereas on the internal bottomplate the background velocity is prescribed, which is shown Figure 5.1(b). The inner dimensions of the spouts in the experimental set-up are 7×17 mm, and therefore the dimensions of the spouts in DPM are chosen to be 5×20 mm. In this way the surface areas are matched as good as practically possible. In Table 5.1 and 5.2 the particle properties and numerical settings are listed.

Table 5.1: Particle properties.

Property	Value	Unit
Material	Glass	-
d_p	3.0	mm
ρ_p	2505	kg/m^3
$e_{n,p\leftrightarrow p}$	0.97	-
$e_{n,p\leftrightarrow w}$	0.97	-
$e_{t,p\leftrightarrow p}$	0.33	-
$e_{t,p\leftrightarrow w}$	0.33	-
$\mu_{p\leftrightarrow p}$	0.10	-
$\mu_{p\leftrightarrow w}$	0.30	-
u_{mf}	1.90	m/s

Table 5.2: Numerical settings.

Property	Single-spout	Double-spout	Triple-spout	Unit
N_x	29	58	87	-
N_y	2	2	2	-
N_z	250	250	250	-
$N_{z,windbox}$	19	19	19	-
t_{end}	20	20	20	s
N_p	$1.2 \cdot 10^4$	$4.8 \cdot 10^4$	$10.7 \cdot 10^4$	-
k_n	10^4	10^4	10^4	N/m

5.6 Results and Discussion

5.6.1 Flow Regime Map

Different flow characterics were experimentally determined and identified as distinctive flow regimes, as shown in Figure 5.3. The flow regimes were distinguished both by visual observation and pressure drop fluctuation measurements, conducted at different operating conditions. The background velocity was varied from 0 to 4.6 m/s with increments of $0.4 \cdot u_{mf}$, and the spout velocity ranged from 0 to 95 m/s with increments of $5 \cdot u_{mf}$. Compared to the flow regime map of a single-spout fluidized bed (Link et al. 2005), similarities are found for high background (u_{bg}) and low spout (u_{sp}) velocities, where in both cases a fluidized bed arises with a single or multiple penetrating jets, and for $u_{sp}/u_{mf} = 30$ and $u_{bg} < u_{mf}$ blocking of the spout channel occurs in both a single- and triple-spout fluidized bed. Despite these similarities, large differences were observed due to the interaction and contraction of the three spouts. The three spouts always interact to a certain extent, depending on u_{bg}. The higher u_{bg} the more often the spouts interact, and the bed dynamics are more influenced. The *degree* of contraction depends on u_{sp}. The higher u_{sp}, the more stable the contraction of the spouts is, eventually resulting in one spout channel. Pressure drop fluctuation measurements were conducted to support the visual observations. For each of the investigated flow conditions the Fast Fourier Transformation (FFT) frequency spectrum of the pressure signal was computed, where the power of the highest peak in the frequency spectrum is a measure for the periodicity and amplitude of the pressure fluctuations. These powers are shown in Figure 5.4, displaying similarity with the constructed flow regime map in Figure 5.3. The flow regime map for triple-spout fluidization reveals different flow behaviour compared to single-spout fluidization, and therefore it is important to study a flow regime in detail. The multiple-interacting-spouts regime (C) will be discussed for double- and triple-spout fluidization and compared to the corresponding spout-fluidization regime for a single-spout fluidized bed.

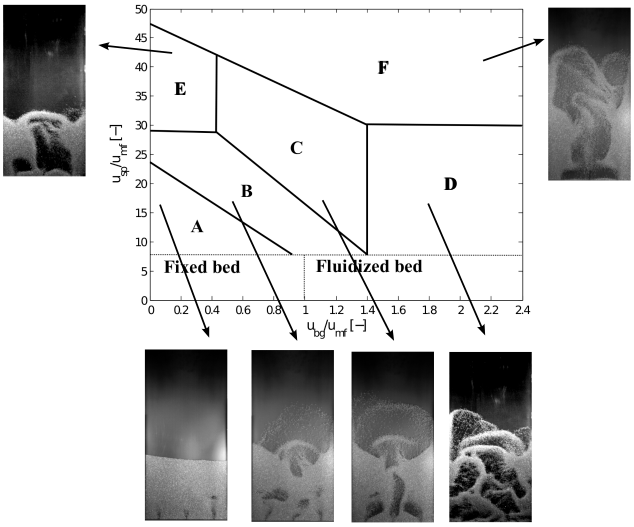

Figure 5.3: Regime map with example snapshots of the pseudo-2D bed. All gas velocities were normalized using the minimum fluidization velocity (u_{mf}) The distinguished flow regimes are the multiple-internal-spouts (A), multiple-spouts (B), multiple-interacting-spouts (C), multiple-jets-in-fluidized-bed (D), alternating-two-spout-contraction (E) and contracted-spouts-with-periodic-channel-blocking (F) regime.

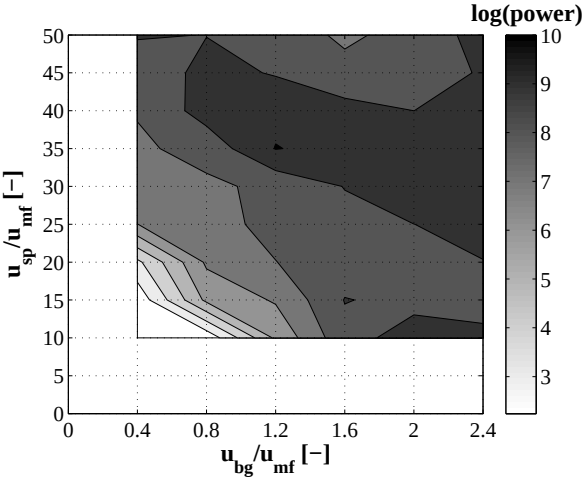

Figure 5.4: Contour plot of the maximum value of the log(power) obtained with Fast Fourier Transformation (FFT) of the pressure drop fluctuation results.

5.6.2 Single-Spout Fluidization

The spout-fluidization regime for a single-spout fluidized bed is presented to show the particle behaviour in a spout fluidized bed with the same spout and background gas velocities as in the multiple-interacting-spouts regime (C) for double- or triple-spout fluidized beds. The experimental results obtained by PIV and PEPT are mutually compared, and secondly, the DEM simulations are validated with the experimental results. In Figure 5.5 the time-averaged particle velocity obtained from PIV shows very good resemblance with the results from the PEPT measurements. The spout channel in the vector field from PIV is slightly slanted. The reason for this is, that in single-spout fluidization both side walls are made up of baffles that are mounted inside the bed. Apparently, the right wall is less well fixed during PIV measurements, causing a small slip stream along the right wall that results in attraction of the spout channel to the right. Nevertheless, both experimental results comply.

The velocity vector field obtained with DEM agrees with the experiments, however at higher locations in the bed, DEM calculates larger particle velocities. In Figure 5.6 the velocity profiles are shown in the central xz-plane at $z = 0.05$ m and $z = 0.10$ m, respectively. At these heights, the simulated particle velocities in the spout channel comply with experiments, but in the annulus the particle velocity is overpredicted by DEM. This could be due to wall effects that are more pronounced in pseudo-2D beds than in 3D systems, which are not accounted for with sufficient accuracy in DEM. In conclusion, the DEM simulates single-spout fluidization quite well and the PIV technique measures similar particle velocities as the PEPT technique.

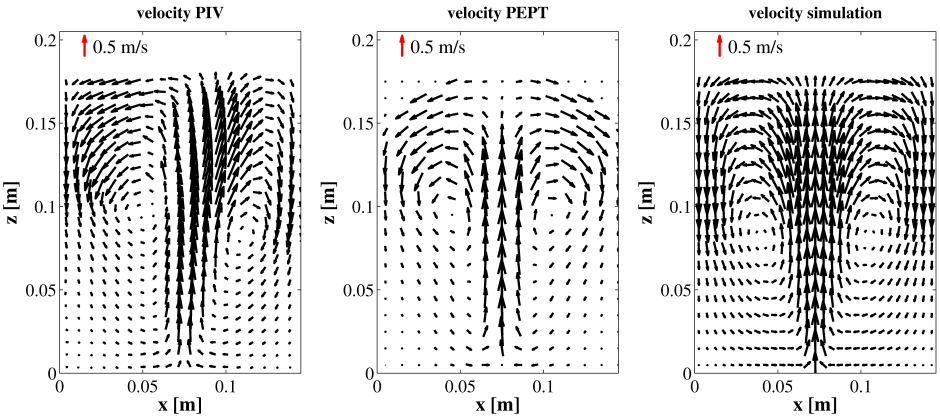

Figure 5.5: Time-averaged particle velocity fields for the spout-fluidization regime (u_{bg} = 2.4 m/s, u_{sp} = 43.5 m/s) in a single-spout fluidized bed, obtained by Particle Image Velocimetry (left), Positron Emission Particle Tracking (centre) and DEM simulations (right).

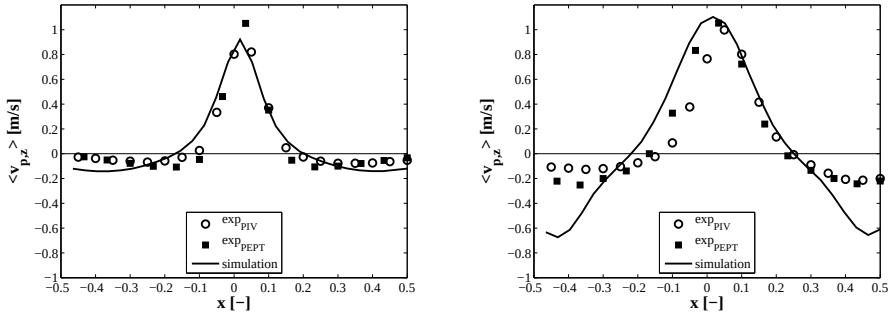

(a) (b)

Figure 5.6: Profiles of time-averaged vertical particle velocity for the spout-fluidization regime (u_{bg} = 2.4 m/s, u_{sp} = 43.5 m/s) in a single-spout fluidized bed obtained from PIV and PEPT measurements and from DEM simulations in the central xz-plane at z = 0.05 m (a) and z = 0.10 m (b).

5.6.3 Double-Spout Fluidization

Figure 5.7 shows that the time-averaged particle velocity for a system with two spouts displays a different pattern compared to single-spout fluidization, due to the interaction of the spout channels. Circulation of particles occurs in between the spouts as well as on top of the spouts followed by acceleration in the centre of the bed. Hence the characteristic flow pattern of a spout fluidized bed is identified at a higher location upwards in the bed.

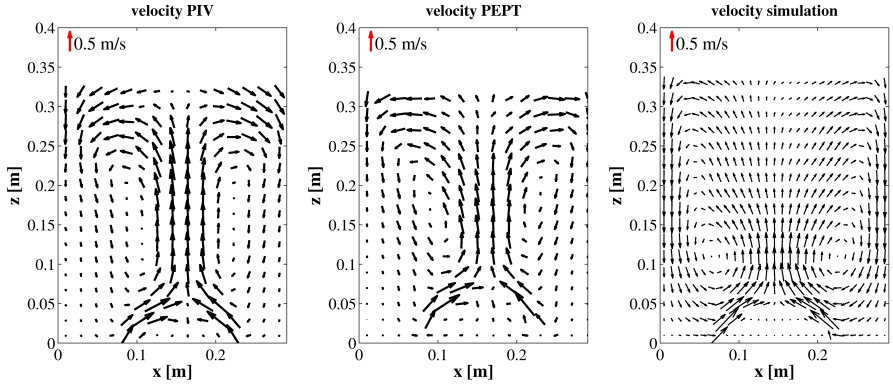

Figure 5.7: Time-averaged particle velocity for the multiple-interacting-spouts regime ($u_{bg} = 2.4$ m/s, $u_{sp} = 40.5$ m/s) in a double-spout fluidized bed, obtained by Particle Image Velocimetry (left), Positron Emission Particle Tracking (centre) and DEM simulations (right).

The additional circulation pattern in between the spouts is also seen in Figure 5.8, depicting profiles of the time-averaged vertical particle velocity in the central xz-plane, where the vertical particle velocity is negative at $z = 0.05$ m for the experimental results.

Comparison of the experimental results from PIV and PEPT show large similarities between the time-averaged particle velocities. However, the time-averaged particle velocity calculated with DEM deviates more from the experiments compared to the single-spout fluidization case. In DEM, the spout channels contract more and the downward velocity in the annulus is larger compared to the experimental results. In Figure 5.8(a) the profiles of the time-averaged vertical particle velocity at $z = 0.02$ m show that the particle velocity in the spout channel is larger in DEM (although the spout *gas* velocity is the same), which could cause

the larger degree of contraction of the spouts. This is depicted in Figure 5.8(b) where the velocity in between the spouts is upwards in DEM instead of downwards as in the experiments.

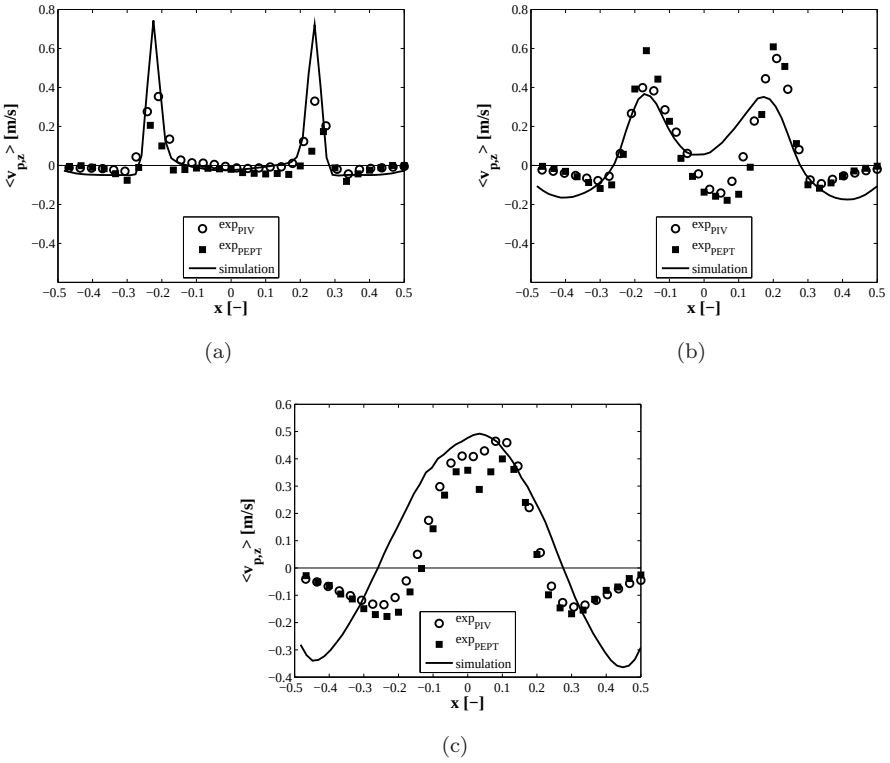

Figure 5.8: Profiles of time-averaged vertical particle velocity fields for the multiple-interacting-spouts regime (u_{bg} = 2.4 m/s, u_{sp} = 40.5 m/s) in a double-spout fluidized bed obtained from PIV and PEPT measurements and DEM simulations in the central xz-plane at $z = 0.02$ m (a), $z = 0.05$ m (b) and $z = 0.10$ m (c).

At $z = 0.10$ m the particle velocity in the spout channel and the particle velocity in the annulus is overpredicted by DEM, and this difference is larger than in the single-spout fluidization. This is attributed to the larger contraction of the spout channels in DEM, enhancing the gas velocity and thus the particle velocity. Similar to single-spout fluidization, the downward velocities for DEM and the

experiments comply quite well in the annulus region near the bottom and differ higher up in the bed. PIV and PEPT display large resemblance, showing that the experimental techniques produce the correct particle velocity in double-spout fluidization. Although DEM slightly differs from the experiments, the same trends are observed, which indicates that DEM can also simulate multiple-spout fluidized beds.

5.6.4 Triple-Spout Fluidization

For triple-spout fluidization the PEPT detectors could only partly cover the width of the bed, resulting in a partial vector field that is shown in Figure 5.9. Nevertheless, the interaction of the left and centre spouts are observable, which still enables comparison with PIV and DEM simulations. It shows that again PIV and PEPT comply very well, and that DEM slightly overestimates the particle velocity in the spout and in the annulus regions, confirmed by Figure 5.10. Furthermore, the additional circulation pattern near the bottom of the bed and the typical spout fluidization profile at a higher location in the bed is present in triple-spout fluidization, as well.

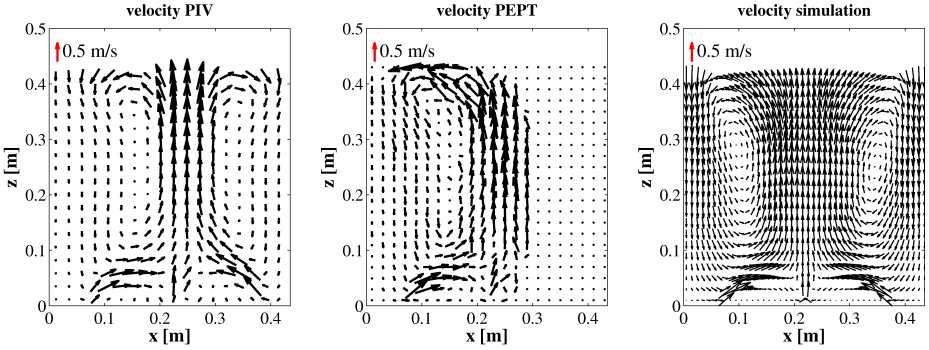

Figure 5.9: Time-averaged particle velocity fields for the multiple-interacting-spouts regime (u_{bg} = 2.3 m/s, u_{sp} = 43.8 m/s) in a triple-spout fluidized bed, obtained by Particle Image Velocimetry (left), Positron Emission Particle Tracking (centre) and DEM simulations (right).

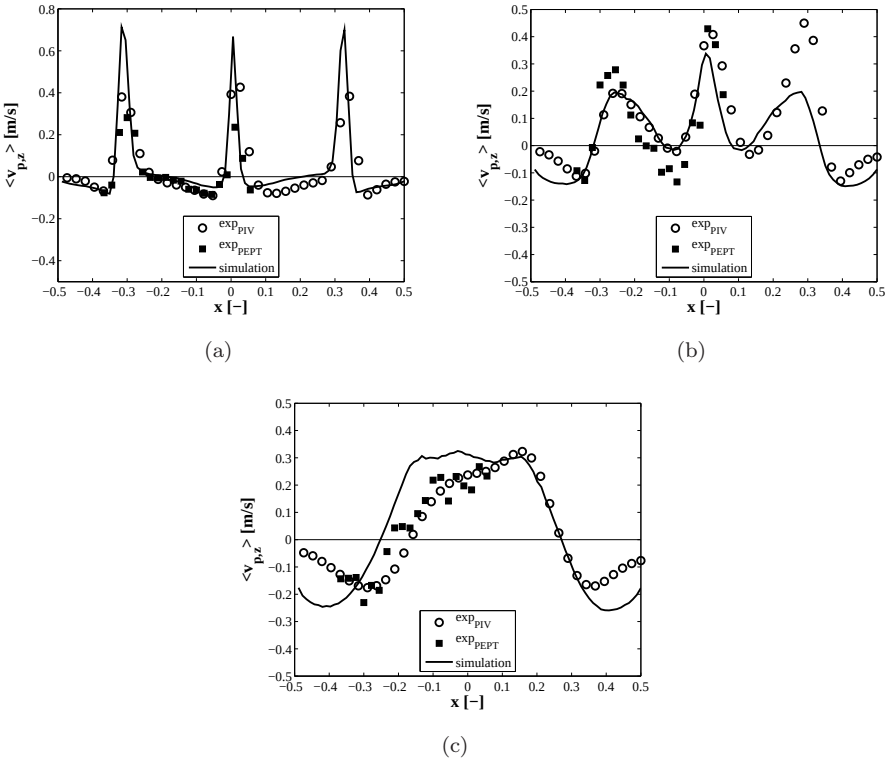

Figure 5.10: Profiles of time-averaged vertical particle velocity for the multiple-interacting-spouts regime ($u_{bg} = 2.3$ m/s, $u_{sp} = 43.8$ m/s) in a triple-spout fluidized bed obtained from PIV and PEPT measurements and DEM simulations in the central xz-plane at $z = 0.02$ m (a), $z = 0.05$ m (b) and $z = 0.10$ m (c).

5.7 Conclusions

In this chapter, the effect of two and three spouts on the spout fluidized bed dynamics has been investigated numerically and experimentally. A flow regime map has been constructed for a triple-spout fluidized bed, which is quite different compared to the flow regime map for a single-spout fluidized bed. It appeared that the background velocity influences the mutual interaction of the spouts, and the spout velocity affects the stability of contraction into a single spout channel. The multiple-interacting-spouts regime (C) has been studied in detail for a double- and triple-spout fluidized bed, both numerically and experimentally, and the corresponding spout-fluidization regime for a single-spout fluidized bed has been studied as a reference case. Particle Image Velocimetry (PIV) and Positron Emission Particle Tracking (PEPT) were used as experimental techniques, and simulations were run with the Discrete Element Model (DEM). The experimental results obtained with PIV and PEPT comply very well for all the three cases, showing the good performance of these techniques. The DEM simulations slightly deviate from the experiments, which could be due to the particle-wall effects that are more pronounced in pseudo-2D beds than in 3D systems. The investigated multiple-interacting-spouts regime is a fully new flow regime that does not appear in single-spout fluidized beds. Two flow patterns have been observed, *viz.* particle circulation in between the spouts near the bottom of the bed, and the typical spout fluidization motion at a higher location upwards in the bed. Hence, the presence of multiple spouts in a spout fluidized bed highly affects the flow behaviour, which cannot be distinguished by solely investigating single-spout fluidized beds. During granulation processes in industry, the wet particles sometimes deposit and stick to the bottom of the bed. This could be caused by the observed additional circulation pattern in between the spouts, since the particles remain longer near the bottom of the bed than would be expected from study on single-spout fluidization. The effect of multiple spouts is thus very important, and should therefore be further investigated in three dimensional systems in future work.

Nomenclature

Roman letters		
D	[m]	Diameter
e_n	[-]	Coefficient of normal restitution
e_t	[-]	Coefficient of tangential restitution
k_n	[N/m]	Spring stiffness
N_{cell}	[-]	Number of grid cells
N_p	[-]	Number of particles
N_x	[-]	Number of grid cells x-direction
N_y	[-]	Number of grid cells y-direction
N_z	[-]	Number of grid cells z-direction
n	[-]	Number of particle locations
p	[Pa]	Pressure
$\mathbf{r}$	[m]	Position
t	[s]	Time
Δt	[s]	Time delay / time step in simulation
$\mathbf{u}_f$	[m/s]	Gas velocity
$\mathbf{v}_p$	[m/s]	Particle velocity
V	[m^3]	Volume
$\mathbf{x}$	[m]	Coordinate vector
Greek symbols		
ε	[-]	Volume fraction
μ	[-]	Dynamic friction coefficient
ρ	[kg/m^3]	Density
Subscripts		
bg		Background fluidization
end		End of simulation
exp		Experimental
f		Fluid phase
mf		Minimum fluidization
n		Normal direction / Normalized
p		Particle

sim	Simulation
sp	Spout
x	Horizontal direction
z	Vertical direction

Abbreviations

2D	Two-dimensional
3D	Three-dimensional
DPM	Discrete Particle Model
FFT	Fast Fourier Transformation
LOR	Line Of Response
PEPT	Positron Emission Particle Tracking
PIV	Particle Image Velocimetry
RMS	Root Mean Square

6

Discrete Simulation and Experimental Study on Elevated Spout Fluidization

This chapter is based on:
M.S. van Buijtenen, K.A. Buist, N.G. Deen, J.A.M. Kuipers, T. Leadbeater and D.J. Parker: Numerical and experimental study on elevation in spout fluidized beds, *AIChE Journal*, submitted.

Abstract

In this chapter we study the effect of elevating the spout on the dynamics of a spout fluidized bed, both numerically and experimentally. The experiments were conducted in a pseudo-2D and a cylindrical 3D spout fluidized bed, where Positron Emission Particle Tracking (PEPT) and Particle Image Velocimetry (PIV) were applied to the pseudo-2D bed, and PEPT and Electrical Capacitance Tomography (ECT) to the cylindrical 3D bed. A discrete particle model (DPM) was used to perform full 3D simulations of the bed dynamics. Several cases were studied, *i.e.* beds with spout heights of 0, 2 and 4 cm. In the pseudo-2D bed the spout-fluidization and jet-in-fluidized-bed regime were considered first, and it was shown that in the spout-fluidization regime the expected dead zones appear in the annulus near the bottom of the bed as the spout is elevated. However, in the jet-in-fluidized-bed regime the circulation pattern of the particles is affected, without the development of stagnant zones. The jet-in-fluidized-bed regime was further investigated, and additionally the experimental results obtained with PIV and PEPT were compared with the DPM simulation results. The experimental results obtained with PIV and PEPT agreed mutually very well, and in addition agreed well wtih the DPM results, although the velocities in the annulus region were slightly over predicted. The latter is probably due to the particle-wall effects that are more dominant in pseudo-2D systems compared to 3D systems. In the jet-in-fluidized-bed regime the background gas velocity is relatively high, producing bubbles in the annulus that interact with the spout channel. In case of a non-elevated spout, this interaction occurs near the bottom of the bed. As the spout is elevated, this interaction is shifted upwards in the bed, which allows the bubbles to remain undisturbed providing the motion of the particles in the annulus near the bottom of the bed. As a result, no dead zones are created and additionally, circulation patterns are vertically stretched. These findings were also obtained for the cylindrical 3D bed, though, the effects were less pronounced. In the cylindrical 3D bed the PEPT results show that the effect on the bed dynamics starts at $h_{spout} = 4$ cm, which is confirmed by the ECT results. Additionally, ECT measurements were conducted for $h_{spout} = 6$ cm to verify if indeed the effect happens at larger spout heights. The root mean square of the particle volume fraction slightly increased at $h_{spout} = 2$ cm, while a larger increase is found at $h_{spout} = 4$ and 6 cm, showing that indeed more bubbles are formed. The presented results have not been reported so far and form valuable input information for improving industrial granulators.

6.1 Introduction

Spout fluidized beds combine the favourable properties of both spouted and fluidized beds and in industry, the spout is slightly elevated from the bottom of the bed to enable efficient spraying of liquid. However, research has so far mainly been focused on non-elevated spouts. Related research has been done on spouted beds with draft or Wurster tubes, showing that the degree of mixing is influenced by the dimensions and position of the draft tube (f.i. Kalwar et al. (1993) and da Cunha et al. (2009)). In these types of beds the effect of the spout channel is physically imposed by a draft tube, whereas in spout fluidized beds the spout channel arises from the ratio of the spout gas and background fluidization gas velocity. Although it has been demonstrated that draft tubes highly influence the circulation patterns inside spouted beds, the effect of an elevated spout in spout fluidized beds is not known, and is therefore the topic of this work. Both experiments and simulations were conducted. The experiments were carried out on a pseudo-2D and a cylindrical 3D bed, where Positron Emission Particle Tracking (PEPT) and Particle Image Velocimetry (PIV) were applied to the pseudo-2D bed, and PEPT and Electrical Capacitance Tomography (ECT) to the cylindrical 3D bed. The simulations were conducted with a full 3D Discrete Element Model (DEM), originally developed by Hoomans et al. (1996) and further developed by Link et al. (2007).

With particle image velocimetry (PIV) the particle flow field in a pseudo two-dimensional (2D) spout fluidized bed can be obtained. Several workers applied PIV to study 2D granular flows, such as gas-fluidized beds (Bokkers et al. (2004)-Dijkhuizen et al. (2007)), spout fluidized beds (Link et al. 2004), spouted beds (Liu et al. 2008), but also vibrated granular beds (Zeilstra et al. (2008) and Deng and Wang (2003)), rotating drums (Jain et al. 2002) and silos or hoppers (Medina et al. (1998) and Steingart and Evans (2005)). Through these applications, PIV has become a powerful tool for flow field measurements in granular media. Positron Emission Particle Tracking (PEPT) finds its origin in the commonly-used medical diagnostic technique of positron emission tomography (PET) and was developed at the University of Birmingham. A single active particle is tracked, making it a non-intrusive measurement technique with the additional advantage that it can be applied to 3D systems which are not optically accessible. Since a single particle is tracked, the disadvantage is however, that long measurement times are necessary to obtain statistically reliable results. Nevertheless, PEPT has proven to be a rather precise technique, and several workers have used it for various applications. Seville et al. (2005) summarized examples of such applications in several types of

solids processing equipment. Top spray fluidization was investigated by Depypere et al. (2009) and circulating fluidized beds were studied using PEPT by Chian et al. (2009) and Van de Velden et al. (2008). Hoomans et al. (2001), Fan et al. (2008), Stein et al. (2000) and Laverman (2010) applied PEPT to fluidized beds, where Laverman (2010) was the first who compared experimental PIV results with PEPT. Link et al. (2008) used PEPT to study spout fluidized beds, and compared their results with DPM simulations. In this work, PEPT is applied to a pseudo-2D and a cylindrical 3D bed, where for the pseudo-2D bed the PEPT results will be compared to results obtained with PIV and DPM simulations.

Electrical Capacitance Tomography (ECT) is based on the difference in permittivity of two non-conductive materials inside a system, which has been compared to other advanced measurement techniques by Mudde (2010). An image is obtained that represents the particle volume fraction in a 2D slice of the cross-sectional area of the bed. It is a low cost technique, with high temporal but low spatial resolution. The measurement rate is up to 100 Hz, which makes it suitable for online monitoring and control. However, the image quality depends on the interaction of the probing field and the materials present in the measurement volume (*i.e.* soft field effects) and on the image reconstruction that is used (Tapp et al. 2003). As a result, the development and improvement of reconstruction techniques are often topic of research. Isaksen (1996) outlines and Yang and Peng (2003) assesses various algorithms for the reconstruction, and Li and Yang (2008) improved the conventional Landweber algorithm, while Lei et al. (2009) improved the Tikhonov algorithm. Several workers applied ECT to study gas-solid flows, such as circulating fluidized beds (Du et al. (2004) and Liu et al. (2005)) and fluidized beds (Makkawi and Wright (2002), Du et al. (2005) and Godlieb (2010)). In this work, ECT is applied to a cylindrical 3D spout fluidized bed yielding valuable results (despite its low spatial resolution) in particular in combination with the PEPT technique.

The objective of this work is to both experimentally and numerically study the effect of an elevated spout on the bed dynamics in a pseudo-2D and cylindrical 3D spout fluidized bed. The organization of this chapter is as follows: first the numerical model is described. Then, the experimental set-ups and the experimental techniques are explained. Two flow regimes in the pseudo-2D bed will be studied using PIV, which will be shown first, followed by one flow regime that is compared to PEPT and DPM results. Finally, the experimental results obtained by PEPT and ECT of the same flow regime in the cylindrical 3D bed is shown.

The objective of this work is to both experimentally and numerically study the effect of an elevated spout on the bed dynamics in a pseudo-2D and cylindrical 3D spout fluidized bed. The organization of this chapter is as follows: first the numerical model is described. Then, the experimental set-ups and the experimental techniques are explained. Two flow regimes in the pseudo-2D bed are measured with PIV, which will be shown first, followed by one flow regime that is compared to PEPT and DPM results. Finally, the experimental results obtained by PEPT and ECT of the same flow regime in the cylindrical 3D bed is shown.

6.2 Numerical Model

This study on spout elevation is carried out for the dry case. Therefore, simulations were conducted with the discrete element model that describes the dynamics of the continuous gas-phase and the discrete particles as explained in paragraph 2.2.

6.3 Experimental Set-up

The pseudo 2D and cylindrical 3D bed used in this work are schematically presented in Figure 6.1. Background fluidization air was supplied by a two-stage side channel blower, having a maximum capacity of 312 m^3/hr, a maximum supply pressure of 580 mbar, and a power of 7.5 kW.

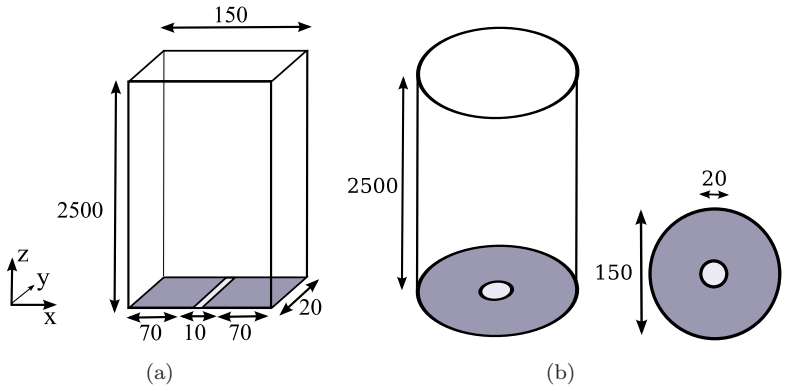

Figure 6.1: Schematic overview of the experimental pseudo-2D (a) and cylindrical 3D (b) spout fluidized bed, with dimensions in mm.

To prevent electrostatic charging of the particles, the background fluidization air was humidified till $\sim 50\%$ relative humidity with the aid of a spray tower. The spout air was supplied by a second two-stage side channel blower, with a maximum capacity of 205 m^3/hr, a maximum supply pressure of 500 mbar, and a power of 4.0 kW. The flow rates of both background and spout sections were controlled by two frequency controllers and were measured by two turbine flowmeters.

The depth of the pseudo-2D bed was assumed to be sufficiently small to display pseudo-2D behaviour and large enough to avoid extreme particle-wall interaction. The front and back walls of the bed consisted of a Lexan plate to enable visual detection of the particle motion. The side walls of the bed were made up of baffles that were mounted inside the bed, to enable single-spout fluidization. The fluidization section was covered with a 3 mm thick porous plate with an average pore size of 100 microns and the spout section was covered with a 2.0 mm gauze.

The column of the cylindrical 3D bed consisted of a PVC tube, whereas the bottom section wass made of either metal for the PEPT measurements or plastic for the ECT measurements. The latter is done to avoid problems with the ECT measurements. The distributor plate of the fluidization section contained 1.0 mm holes to limit the pressure drop. However, due to this low pressure drop the distribution of the background fluidization air was slightly non-uniform. The spout tube was covered with a 2.0 mm gauze for the metal section and in the ECT measurements the plastic spout tube was covered with the same distributor plate as the plastic fluidization section.

For the PIV measurements on the pseudo-2D bed, digital images were recorded with a high speed camera (LaVision Imager Pro) equipped with a 50 mm lens. The aperture of the camera was set to f6 and the exposure time was fixed at 0.4 ms. The recorded images consisted of 608 x 1280 pixels and were stored in the memory of the camera. After all the images for one experiment were recorded, the 12-bit images were transferred to the hard disk of the PC. As shown in Figure 3.1(b), the pseudo-2D bed was illuminated by two 500W halogen lamps, which were positioned in such a way that the bed was illuminated under a small angle ($< 45^o$), preventing undesired reflections. The lamps were fed by a direct current supply to minimize temporal variation in the illumination. The back wall was painted black to provide better contrast between particles and gas.

To carry out PEPT measurements, the spout fluidized bed (either pseudo-2D or cylindrical 3D) was positioned in between the two PEPT detectors, as shown in Figure 5.2. The detectors covered a measurement height of 0.50 m and a width of 0.40 m.

In Figure 6.2 a schematic illustration of the ECT set-up is presented. The ECT measurements were conducted in a cylindrical 3D bed, for which a special column was prepared containing the ECT sensor that was mounted around the column circumference. An earthed screen was mounted around the sensor and shielded cables were used to connect the sensor to the data acquisition unit (Figure 6.2).

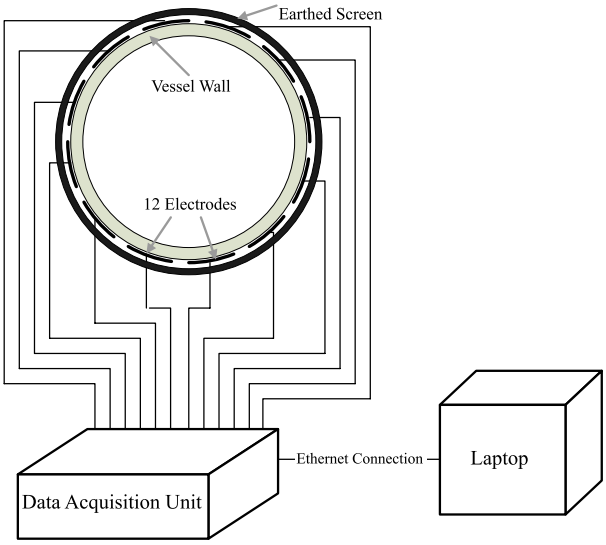

Figure 6.2: Experimental set-up of ECT measurement on the cylindrical 3D spout fluidized bed.

The ECT sensor was self-designed and constructed whereas commercial ECT computer hard- and software were supplied by Process Tomography Limited. It consisted of 2 measurement planes, each with 12 measurement electrodes. To prevent the electrical field from being diverted to earth at the ends of the measurement electrodes, guard electrodes surround the measurement electrodes as shown in Figure 6.3. The first and second measurement planes were located 5 and 15 cm above the bottom plate, respectively. The measurements lasted 5 minutes, using a frequency of 100 Hz and a pixel resolution of 32×32 to represent the sensor cross-sectional area, which makes a total of 1024 permittivity values per image

(pixel area: 0.18 cm^2). The sensor was calibrated before each measurement and to assure that the capacitances remained constant during a measurement, the capacitance of a static bed were measured before and after each measurement. If the measured volume fraction of the static bed remained constant, no shift in capacitance occurred during the fluidization measurement. The Landweber iteration method was used for the image reconstruction, for which the number of iterations and a relaxation parameter were set to respectively 110 and 0.01.

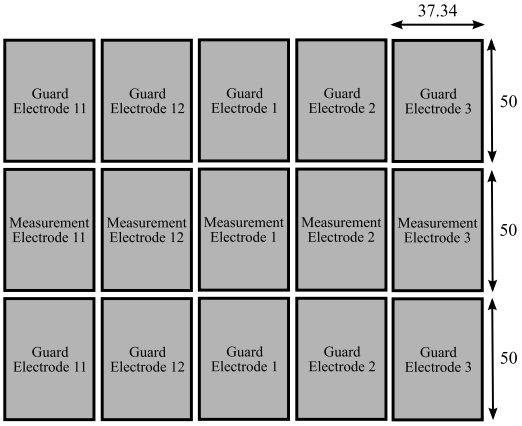

Figure 6.3: Schematic drawing of 5 (out of 12) measurement electrodes and guard electrodes for 1 measurement plane, with dimensions in mm.

6.4 Experimental Techniques

In this chapter three different experimental techniques are used: Particle Image Velocimetry (PIV), Positron Emission Particle Tracking (PEPT), and Electrical Capacitance Tomography (ECT).

Particle Image Velocimetry (PIV) non-invasively obtains instantaneous velocity data for the pseudo-2D bed. A detailed description of the PIV technique can be found in paragraph 3.3.

In Positron Emission Particle Tracking (PEPT) a single particle is non-intrusively tracked, resulting in an instanteneous location of the particle in three dimensions, from which particle the velocity is determined. In paragraph 5.4 the details of this technique are described.

Electrical Capacitance Tomography is based on the measurement of the permittivity distribution (using several electrodes) of two non-conductive materials (in this work air and glass beads), to determine the particle volume fraction. Each electrode is subsequently charged and the capacitance is measured between each electrode pair. The medium (air or glass beads) in between the electrode pairs influences the value of the capacitance, from which the permittivity and thus the particle distribution is reconstructed. The particle distribution in the sensor cross-sectional area is presented on a 32×32 px square grid. The sensor is calibrated by measuring the capacitances of an empty bed (lower permittivity material) and of a bed filled with particles (higher permittivity material). Additionally, these values are used to normalize the measured capacitances. The capacitance measurement between the electrode pairs depends on the electrical field lines that appear when one electrode is charged. Due to the varying distances of one electrode to the others, different field lines are present, which result in different capacitance values. This means that the detection of an object depends on its location, *i.e.* the capacitance measured of an object in the centre of the bed is different compared to the capacitance of an object near the wall. To account for this variation, the sensitivity at every (pixel) location in the cross-sectional area is determined for each electrode pair and stored in a sensitivity matrix. The sensitivity matrix and the measured capacitance values determine the permittivity at every (pixel) location in the cross-sectional area:

$$C_n = S \cdot K \tag{6.1}$$

C_n is a vector containing 66 measured inter-electrode pair capacitances, K is a vector with permittivity values at the 1024 pixels and S is the sensitivity matrix

with dimensions of 66×1024. The permittivity distribution K can be obtained from:

$$K = S^{-1} \cdot C_n \tag{6.2}$$

where S^{-1} is the inverse of matrix S. However, since S is a non-square matrix its inverse matrix does not exist, which is the mathematical consequence of trying to obtain permittivity values for 1024 pixels from 66 capacitance measurements. Due to the limited number of electrode-pair capacitance measurements, insufficient information is available to accurately calculate the permittitivity at every pixel location. Therefore, the best possible approximate solution to the problem (*i.e.* S^{-1}) should be found. This so-called inverse problem can be solved with different reconstruction techniques, such as the Linear Back-Projection (LBP), Iterative LBP, Tikhonov regularization and the Landweber iteration method, as described by Yang and Peng (2003). In this work the Landweber iteration method is used. The particle volume fraction is calculated using the Inverted Maxwell concentration model, as used by Godlieb (2010):

$$\varepsilon_p = \frac{2K_{EN} \cdot K_{perm} + K_{EN}}{3K_{perm} + K_{EN} - K_{EN} \cdot K_{perm}} \tag{6.3}$$

with $K_{perm} = \frac{K_H}{K_L}$ as the permittivity ratio, where K_L is the permittivity of air, whereas K_H is the permittivity of the bed filled with particles, defined as:

$$K_H = \epsilon_{packed} = \epsilon_{glass} \cdot \alpha + \epsilon_{air} \cdot (1 - \alpha) \tag{6.4}$$

where ϵ_{glass} is the relative permittivity of glass, ϵ_{air} the relative permittivity of air and α the volume fraction of a packed bed (≈ 0.6). Equation 6.4 shows that the high permittivity value is a mixture of particles and air, and thus depends on the packing fraction.
K_{EN} is the normalized permittivity value, given by:

$$K_{EN} = \frac{K_H \cdot \varepsilon_p + K_L(1 - \varepsilon_p) - K_L}{K_H - K_L} \tag{6.5}$$

The number of iterations and the relaxation parameter for the Landweber reconstruction technique are chosen by finding the smallest capacitance residual as proposed by Yang and Peng (2003):

$$C_{res} = \frac{C_n - K_{recon} \cdot S}{C_n} \times 100\% \tag{6.6}$$

where C_{res} is the capacitance residual, C_n the normalized measured capacitance, S the sensitivity matrix and K_{recon} is the reconstructed permittivity. $K_{recon} \cdot S$ is the capacitance that appears from the reconstructed permittivity and sensitivity matrix, and the capacitance residual is thus a measure for the performance of the reconstruction. By minimizing this value, the optimal reconstruction is obtained. It should be kept in mind that the resulting particle volume fraction satisfies $0 \leq \varepsilon_p \leq 0.6$. Therefore, the choice of the number of iterations and the relaxation parameter is a compromise of achieving the lowest capacitance residual and obtaining realistic values of ε_p.

6.5 Test Cases

In this work, three spout heights were used, *i.e.* 0 cm, 2 cm and 4 cm above the bottom plate. Additionally, for the cylindrical 3D bed, a spout height of 6 cm was studied as well using ECT. The static bed height was kept constant at 10 cm above the spout by increasing the amount of particles, as the spout height increases. In this way, the spout air faces similar resistance to break through the bed for each spout height. The spout gas velocity for ECT measurements in the cylindrical 3D bed could not be set equal to the spout gas velocity used for the PEPT measurements, due to pressure drop limitations for the plastic bottom section. Nevertheless, the bed dynamics still displayed characteristics of the jet-in-fluidized bed regime, enabling comparison with the PEPT measurements. The minimum fluidization velocity was determined experimentally for both the pseudo-2D and the cylindrical 3D bed. It appears that the value in the pseudo-2D bed is higher than in the cylindrical 3D bed, which is most probable due to the more pronounced particle-wall effect in pseudo-2D systems. In Tables 6.1 - 6.3 the particle properties, applied gas velocities, and the settings for the numerical simulations are listed.

Table 6.1: Particle properties.

Property	Value	Unit
Material	Glass	-
d_p	3.0	mm
ρ_p	2505	kg/m^3
$e_{n,p\leftrightarrow p}$	0.97	-
$e_{n,p\leftrightarrow w}$	0.97	-
$e_{t,p\leftrightarrow p}$	0.33	-
$e_{t,p\leftrightarrow w}$	0.33	-
$\mu_{p\leftrightarrow p}$	0.10	-
$\mu_{p\leftrightarrow w}$	0.30	-
u_{mf}	1.90[a] ; 1.76[b]	m/s

[a] in pseudo-2D bed

[b] in cylindrical 3D bed

Table 6.2: Gas velocities.

System	Flow regime	u_{bg} [m/s]	u_{sp} [m/s]
Pseudo-2D	Spout-fluidization[a]	2.20	43.40 ± 0.50
	Jet-in-fluidized-bed[b]	4.15 ± 0.15	37.25 ± 0.25
Cylindrical 3D	Jet-in-fluidized-bed[c]	3.80 ± 0.10	67.15 ± 1.5
	Jet-in-fluidized-bed[d]	3.60	48.80 ± 0.4

[a] PIV

[b] PIV & PEPT & DPM

[c] PEPT

[d] ECT

Table 6.3: Numerical settings for pseudo-2D spout fluidized bed simulation.

Property	Value	Unit
N_x	29	-
N_y	2	-
N_z	250	-
Δt	10^{-4}	s
t_{end}	20	s
N_p	$1.2 \cdot 10^4$; $1.4 \cdot 10^4$; $1.7 \cdot 10^4$[a]	-
k_n	10^4	N/m

[a] $h_{spout} = 0; 2; 4$ cm

6.6 Results and Discussion

6.6.1 Pseudo-2D bed

Jet-in-Fluidized-Bed and Spout-Fluidization Regime

Particle Image Velocity (PIV) measurements were conducted for the jet-in-fluidized-bed and spout-fluidization regime, the results of which are shown in Figure 6.4. For the spout-fluidization regime, elevation of the spout leads to dead zones in the annulus, but for the Jet-in-Fluidized bed regime particles in the annulus still move and the vortices are vertically more stretched. In the spout-fluidization regime, the spout gas provides motion of particles by dragging the particles into the spout channel, supported by the background gas. However, in case of an elevated spout, the spout gas influences the particles near the bottom of the bed to a lesser extent and the background velocity is not large enough to compensate for that, causing dead zones in the annulus region. In the jet-in-fluidized bed regime, the background velocity supplies enough air to move the particles in the annulus as the spout height is increased, leading to unexpected particle behaviour. Therefore, this regime is further investigated.

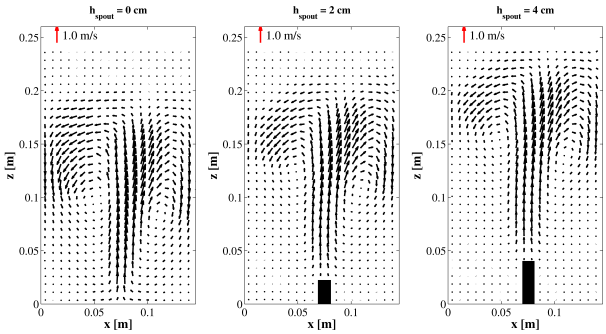

(a)

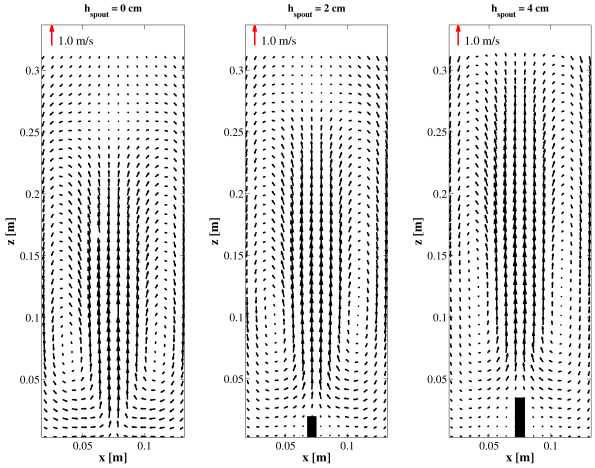

(b)

Figure 6.4: Time-averaged particle velocity fields in the pseudo-2D bed for $h_{spout} = 0$ cm (left), $h_{spout} = 2$ cm (centre) and $h_{spout} = 4$ cm (right) obtained from PIV measurements for the spout-fluidization regime ($u_{bg} = 2.2$ m/s and $u_{sp} = 43.8$ m/s) (a) and jet-in-fluidized-bed regime ($u_{bg} = 4.0$ m/s and $u_{sp} = 37.0$ m/s) (b).

Jet-in-Fluidized-Bed Regime

Besides PIV measurements, also PEPT measurements and DPM simulations have been conducted for the pseudo-2D spout fluidized bed for the jet-in-fluidized-bed regime. As shown in Figure 6.5, both experimental techniques and the DPM simulations display the same effect of the spout height. The velocity profiles in the central xz-plane at $z = 0.10$ m above the spout, as plotted in Figure 6.6, reveal that the velocity profiles obtained from PIV and PEPT agree very well. Moreover, the DPM simulation results agree well with the experimental data in the spout channel. However, in the annulus region, the DPM slightly overpredicts the downward velocity. In pseudo-2D beds the particle-wall effect is more dominant compared to 3D beds, causing a stronger (but yet small) overprediction in the annulus region. Nevertheless, the overall velocity field is quite well predicted and therefore the DPM simulations are used to study the bed behavior in more detail.

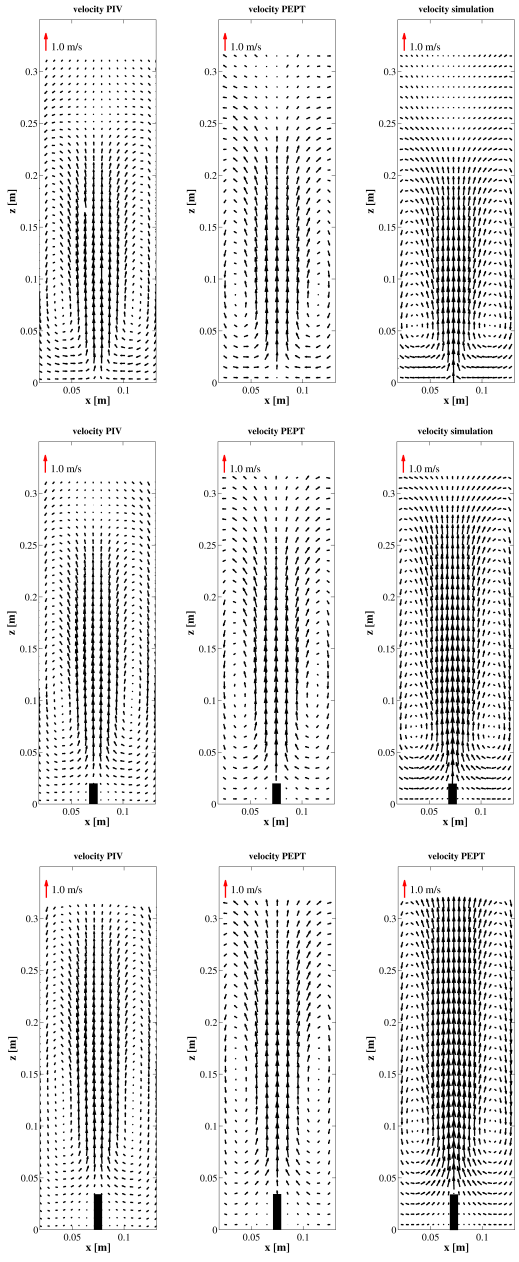

Figure 6.5: Time-averaged particle velocity field in the pseudo-2D bed for jet-in-fluidized-bed regime for $h_{spout} = 0$ cm (top), $h_{spout} = 2$ cm (centre) and $h_{spout} = 4$ cm (bottom) obtained with PIV (left), PEPT (centre) experiments and DPM simulations (right).

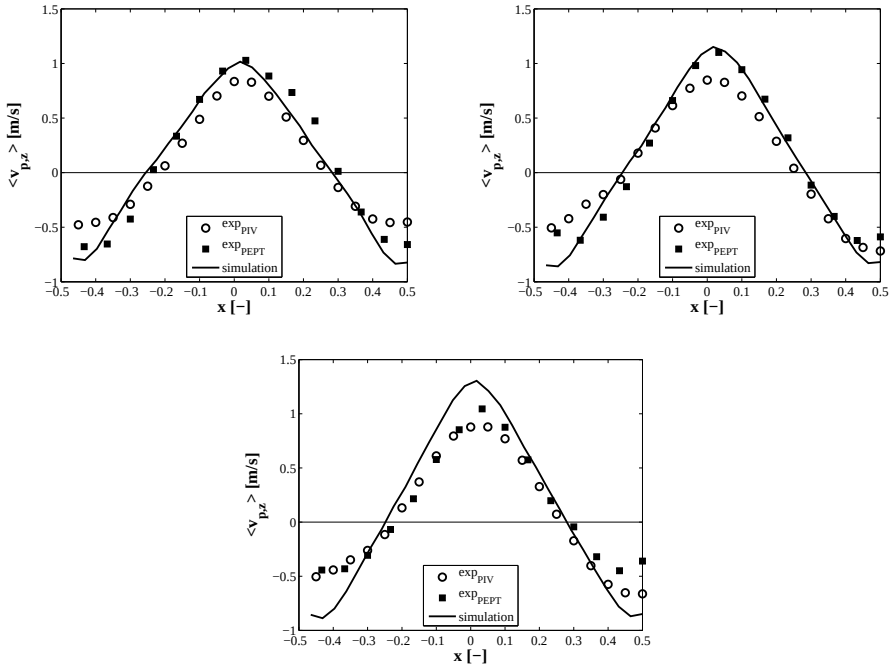

Figure 6.6: Profiles of the time-averaged vertical particle velocity for the jet-in-fluidized-bed regime in the pseudo-2D bed obtained from PIV and PEPT measurements and from DPM simulations, in the central xz-plane at $z = 0.10$ m above the spout. This is done to compare the velocity in the same region inside the bed.

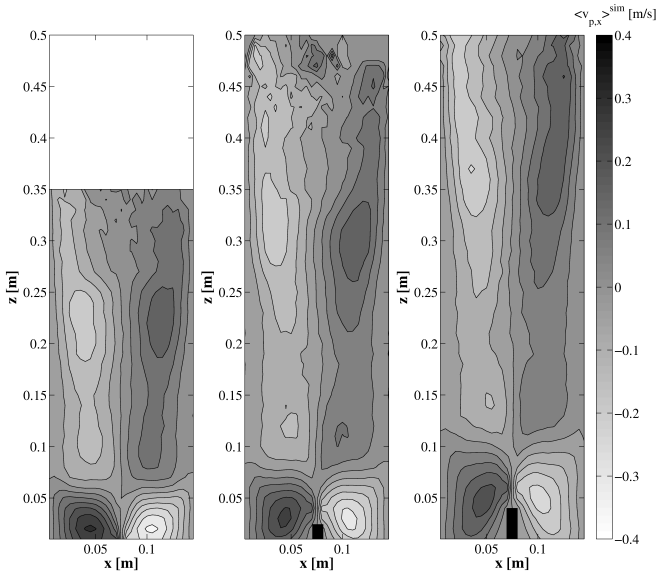

Figure 6.7: Contour plot of the time-averaged horizontal particle velocity for the jet-in-fluidized-bed regime in the pseudo-2D bed for $h_{spout} = 0$ cm (left), $h_{spout} = 2$ cm (centre) and $h_{spout} = 4$ cm (right), obtained from DPM simulations.

In Figure 6.7 the contour plot of the time-averaged horizontal particle velocity obtained from DPM simulations is shown. As the spout height increases, the profiles of the horizontal particle velocity stretch vertically in the bed whereas the horizontal particle velocity near the bottom boundary slightly decreases. For $h_{spout} = 2$ cm the velocity profile shifts accordingly, but for $h_{spout} = 4$ cm the velocity profile shifts higher up in the bed than the spout elevation. This is most likely due to the bubbles in the annulus region that remain undisturbed near the bottom, since the interaction with the spout occurs at a higher location in the bed. As a result, the particles in the annulus near the bottom of the bed are still able to move and are dragged higher up in the bed. The bubble formation with increasing spout height is also shown in Figure 6.8, where the particle volume fraction near the bottom of the bed decreases and the more dense region is located higher up in the bed. Near the spout tube, the particle volume fraction is slightly higher.

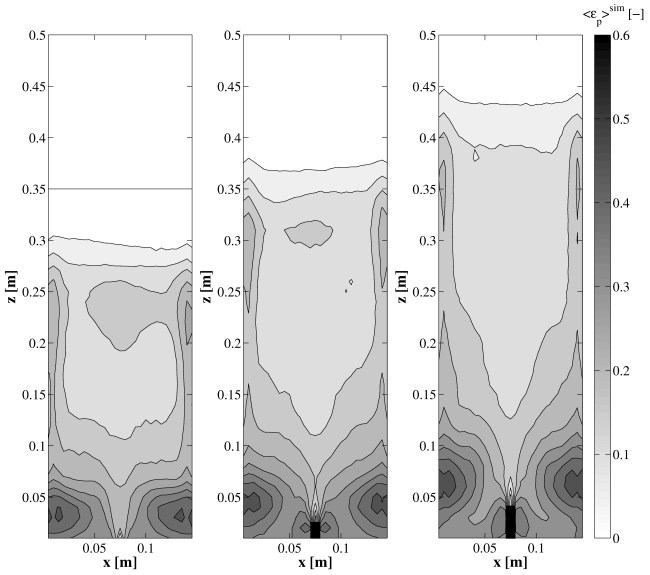

Figure 6.8: Contour plot of the time-averaged particle volume fraction for the jet-in-fluidized-bed regime in the pseudo-2D bed for $h_{spout} = 0$ cm (left), $h_{spout} = 2$ cm (centre) and $h_{spout} = 4$ cm (right), obtained from DPM simulations.

6.6.2 Cylindrical 3D Bed: Jet-in-Fluidized-Bed Regime

PEPT and ECT were used to study the cylindrical 3D spout fluidized bed. For the PEPT measurements, the particle velocity is determined in axi-symmetrical coordinates. Consequently, the velocity data are mirrored to visualize the full picture in the vector velocity field, as shown in Figure 6.9.

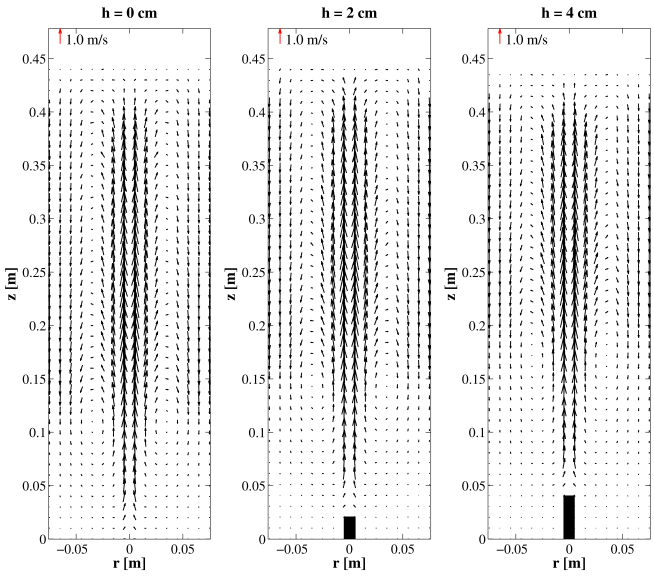

Figure 6.9: Time-averaged particle velocity field in the cylindrical 3D bed for $h_{spout} = 0$ cm (left), $h_{spout} = 2$ cm (centre) and $h_{spout} = 4$ cm (right) obtained with PEPT measurements for the jet-in-fluidized-bed regime. Note that only every second vector in each direction is shown for the sake of clarity.

It seems that the effect of spout elevation in the cylindrical 3D bed is smaller compared to the pseudo-2D bed, which is due to the less dominant particle-wall effect in 3D systems. The bubbles in the annulus region are less affected as the spout elevates, causing the vortices in the annulus being less vertically stretched. This is also shown in Figure 6.10, where the time-averaged radial particle velocity is shown in a contour plot. In this plot, the profiles also stretch vertically as the spout height increases, but to lesser extent compared to the pseudo-2D bed. Both figures display that the particle velocity near the bottom of the bed is much smaller.

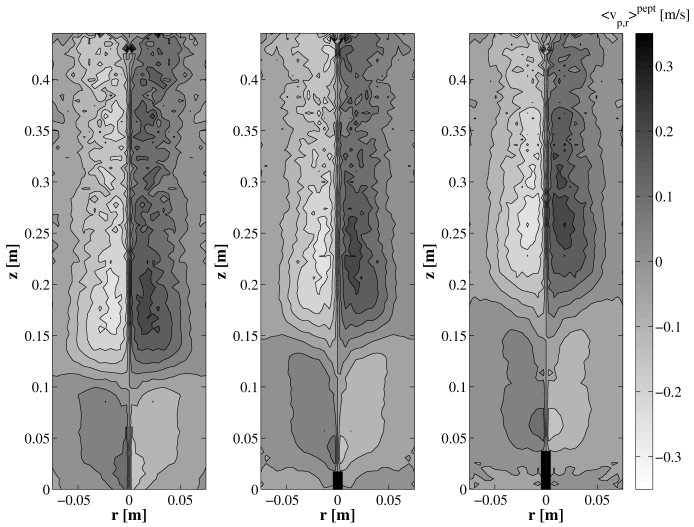

Figure 6.10: Contour plot of the time-averaged radial particle velocity for the jet-in-fluidized-bed regime in the cylindrical 3D bed for $h_{spout} = 0$ cm (left), $h_{spout} = 2$ cm (centre) and $h_{spout} = 4$ cm (right), obtained with PEPT measurements.

Since a single particle is tracked in the PEPT technique, the occupancy, *i.e.* the time that a particle spends in a grid cell, can be determined using equation 6.7. The time a particle is in the cell depends on the total number of cells that is employed. The larger the number of cells, the smaller the occupancy in each cell. Therefore, the occupancy is normalized to the number of cells (N_{cell}). A value of 1 for the occupancy thus implies that the time a particle spends in each cell is equal.

$$\sigma(\mathbf{x}) = \frac{\sum_{N_t} \Delta t \; \forall \; \mathbf{r}_p \cap \mathbf{x}}{\sum_{N_t} \Delta t} \cdot N_{cell} \tag{6.7}$$

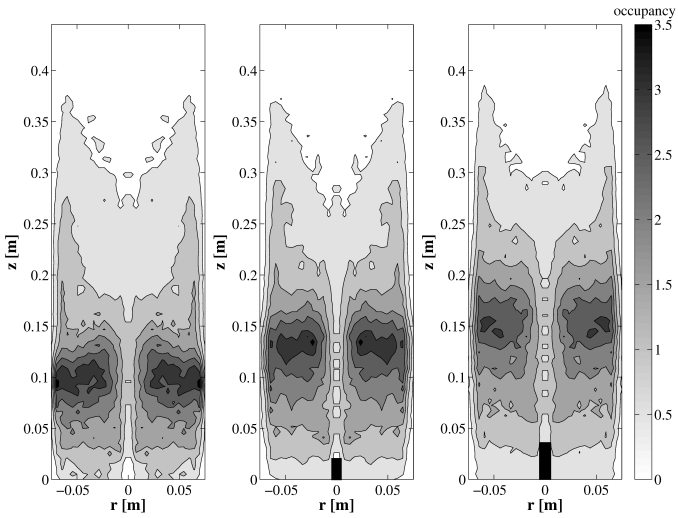

Figure 6.11: Contour plot of the time-averaged occupancy for the jet-in-fluidized-bed regime in the cylindrical 3D bed $h_{spout} = 0$ cm (left), $h_{spout} = 2$ cm (centre) and $h_{spout} = 4$ cm (right), obtained with PEPT measurements.

As shown in Figure 6.11, the occupancy near the bottom is quite low implying that the particle does not reach the bottom often, which is in accordance with the low velocity shown in Figures 6.9 and 6.10. The area where the particle is most, is located in the upper region in the annulus, where the particle apparently is dragged into the spout channel and arrives after raining down. This location with the maximum occupancy shifts linearly with the spout elevation. The maximum occupancy at $h_{spout} = 4$ cm has decreased, which means that the time the particle is in that region had decreased. This could be due to the presence of more bubbles, causing more mixing and thus more motion of the particles in the annulus region. It seems that at this spout height the bubbles originating from the background gas still exist and are (just as in pseudo-2D) affected by the spout gas at a higher location in the bed. Consequently, the effect of spout elevation in the cylindrical 3D bed starts at $h_{spout} = 4$ cm instead of 2 cm, and therefore, complementary ECT measurements were conducted at spout heights of $h_{spout} = 0$, 2, 4, and also 6 cm, to verify if indeed more bubbles are present in the annulus as the spout is elevated further.

The presence of bubbles causes fluctuations in the bed and hence in the particle volume fraction, which is shown in terms of the root mean square in Figure 6.12. As evident from Figures 6.12(a) and 6.12(b), the RMS of the volume fraction does

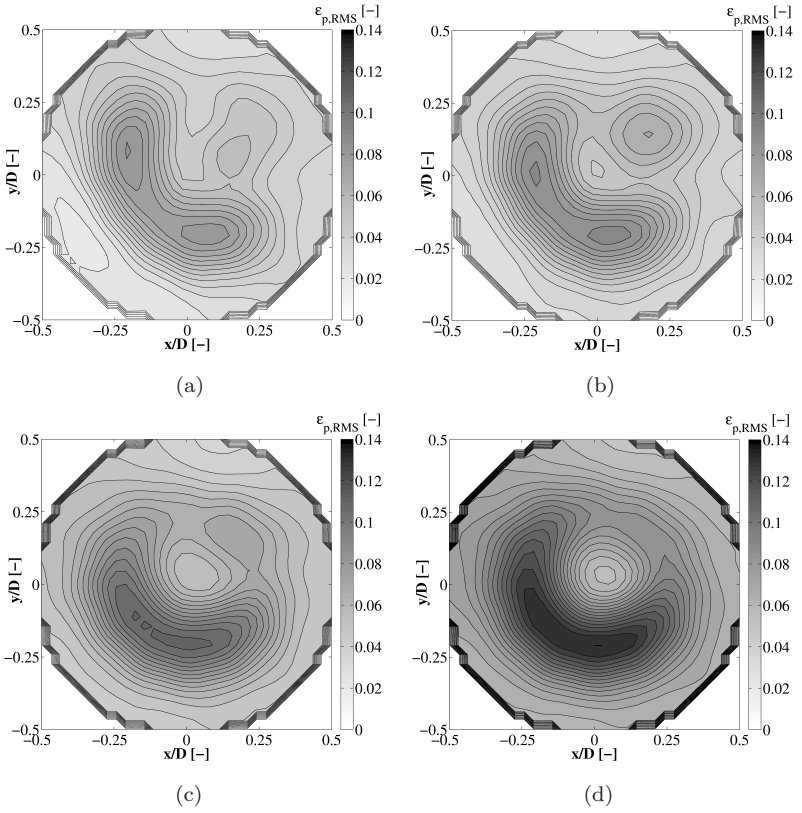

Figure 6.12: Contour plot of the xy-plane of the root mean square (RMS) of the particle volume fraction for $h_{spout} = 0$ cm with $C_{res} = 10.8\%$ (a), $h_{spout} = 2$ cm with $C_{res} = 9.9\%$ (b), $h_{spout} = 4$ with $C_{res} = 10.0\%$ cm (c) and $h_{spout} = 6$ cm with $C_{res} = 10.4\%$ (d), obtained with ECT measurements.

not change much with a spout elevation from 0 to 2 cm. However, the RMS of the volume fraction at $h_{spout} = 4$ and 6 cm increases in the annulus region, which is clearly seen in the central profile that is shown in Figure 6.13. Elevation of the spout at 2 cm does not influence the bubble formation much, while the elevations at 4 and 6 cm clearly have an effect. These ECT results thus confirm that an elevated spout also influences the dynamics in a cylindrical 3D bed, which occurs at a higher spout height than in the pseudo-2D bed.

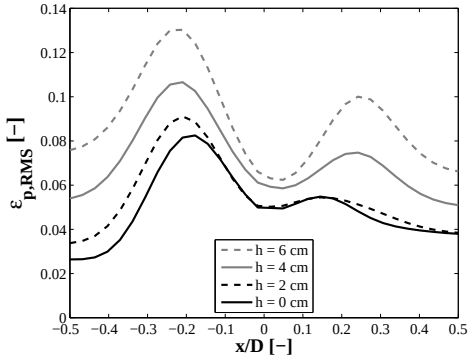

Figure 6.13: Profile of the root mean square of the particle volume fraction at the central row of the xy-plane.

6.7 Conclusions

In this chapter, the effect of spout elevation on the bed dynamics has been investigated experimentally and computationally using respectively non-invasive monitoring techniques and full 3D Euler-Lagrange simulations. In our study in both a pseudo-2D and a cylindrical 3D spout fluidizad bed, with spout heights of 0, 2 and 4 cm has been used. First, two flow regimes have been investigated in the pseudo-2D bed, from which it was concluded that the spout-fluidization regime did not show any dependency on spout height in the sense that increasing the spout height leads to the creation of dead zones up to the entrance of the spout, yielding a similar situation as a spout fluidized bed where the spout is not elevated. The jet-in-fluidized-bed regime, however, displayed unexpected particle behaviour. Therefore, the jet-in-fluidized-bed regime was investigated further in both the pseudo-2D and cylindrical 3D bed. The experimental techniques PIV and PEPT were applied to the pseudo-2D bed, showing very good quantitative agreement in the particle velocity implying that both techniques perform correctly. DPM simulations were also conducted and the results compared quite well with the experimental data. The downward velocity in the annulus region, however, was slightly overpredicted by DPM. The experimental and simulation results show that due to the elevation of the spout, the bubbles in the annulus remain undisturbed near the bottom of the bed and interact with the spout channel at a higher lo-

cation depending on the spout height. As a result, the particles still move in the annulus in contrary to the spout-fluidization regime where the particles become stagnant. The high background velocity in the jet-in-fluidized-bed accounts for the enhanced particle motion. To verify if these phenonema also occur in the cylindrical 3D spout fluidized bed, PEPT and ECT measurements were carried out for the jet-in-fluidized-bed regime. The particle velocity profiles obtained by PEPT show that the elevation of the spout influences the bed dynamics to a lesser extent, which was confirmed by the ECT results. ECT measurements were conducted for spout heights up to 6 cm, and it was shown that the effect was observable for $h_{spout} = 4$ and 6 cm. At these spout heights, the fluctuations in the bed (in terms of the root mean square of the particle volume fraction) increased obviously, indicating that more bubbles are present in the annulus. Summarizing, it is showed that the particle behaviour near the bottom of the bed is affected differently by the spout elevation for the jet-in-fluidized-bed regime. Instead of creating more dead zones in the annulus region, particles are fluidized by the bubbles. This has not been reported so far, and these findings are of great importance for industry where the spout is often elevated. This is particularly the case in granulation processes to enable liquid spray through the spout.

Nomenclature

Roman letters

C	[F]	Capacitance
D	[m]	Diameter
e_n	[-]	Coefficient of normal restitution
e_t	[-]	Coefficient of tangential restitution
h_{spout}	[m]	Spout height
$\mathbf{I}$	[-]	Unit vector
K	[-]	Permittivity distribution
k_n	[N/m]	Spring stiffness
m_p	[kg]	Particle mass
N_{cell}	[-]	Number of grid cells
N_p	[-]	Number of particles
N_t	[-]	Number of timesteps
N_x	[-]	Number of grid cells x-direction
N_y	[-]	Number of grid cells y-direction
N_z	[-]	Number of grid cells z-direction
n	[-]	Number of particle locations
p	[Pa]	Pressure
$\mathbf{r}$	[m]	Position
S	[-]	Sensitivity matrix
t	[s]	Time
Δt	[s]	Time delay / time step in simulation
$\mathbf{u}_f$	[m/s]	Gas velocity
$\mathbf{v}_p$	[m/s]	Particle velocity
V	[m^3]	Volume
$\mathbf{x}$	[m]	Coordinate vector

Greek symbols

α	[-]	Particle volume fraction of packed bed
ε	[-]	Volume fraction
ϵ	[-]	Relative permittivity
μ	[-]	Dynamic friction coefficient
ρ	[kg/m^3]	Density

σ	[-]	Occupancy

Subscripts

bg	Background fluidization
EN	Normalized
end	End of simulation
exp	Experimental
f	Fluid phase
H	High permittivity material
L	Low permittivity material
mf	Minimum fluidization
n	Normal direction / Normalized
p	Particle
perm	Permittivity ratio
r	Radial direction
recon	Reconstructed
res	Residual
sim	Simulation
sp	Spout
t	tangential direction
w	Wall
x	Horizontal direction
z	Vertical direction

Abbreviations

2D	Two-dimensional
3D	Three-dimensional
DPM	Discrete Particle Model
ECT	Electrical Capacitance Tomography
LOR	Line of response
PEPT	Positron Emission Particle Tracking
PIV	Particle Image Velocimetry
RMS	Root mean square

Epilogue

In this thesis, the effect on the spout fluidized bed dynamics of the particle collision properties on the one hand and the geometry of the granulator on the other hand was investigated. The effect of particle-particle interactions were investigated for dry and wet systems. For the dry system, several systems were studied where the particles possess a restitution coefficient mimicking systems with different wetting degrees. In this 3D system, it became clear that a decreasing restitution coefficient leads to more pronounced heterogeneity. To verify if the same trends are observed in experiments, different particle systems with *a.o.* different restitution coefficients were investigated in a pseudo-2D spout fluidized bed. The considered particle systems comprise glass beads, γ-alumina oxide and zeolite 4A particles, which are all classified as Geldart D. PIV combined with DIA resulted in data for volumetric particle fluxes, which were compared to simulation results for this system and showed good agreement. The particle fluxes display only small differences among the particle systems. This is contrary to the simulation results presented in chapter 2, where the restitution coefficient for each case differs more and thus more extreme situations were simulated. The restitution coefficient of the different particle systems in the experiments (chapter 3) differs less, resulting in smaller differences in the degree of non-ideality particle-particle interactions. Due to the high gas velocity in the spout that provides large momentum exchange between the gas phase and the particles, the gas-particle interaction dominates the particle-particle interaction, causing only small differences in the bed dynamics. For the more extreme situations considered in the simulations, the particle-particle interaction becomes more important, which results in different bed behaviour. The simulated cases mimic different stages of wetting during granulation processes, and it showed that the bed dynamics is highly affected by differences of the restitution coefficient. During granulation processes, however, regions of wet particles and dry particles prevail at different locations inside the bed and at different time-scales. Therefore, the DEM was further extended to simulate systems where

water is sprayed from the bottom via the spout into the bed. Here, both particles and droplets are considered as discrete elements in the DEM. The particles have restitution coefficients that vary in time and space, depending on the moisture content of each particle. These simulations revealed that the bed displays more heterogeneity as the particles are more moisturized, and additionally that due to the existence of distinct wet and dry zones the effect of the restitution coefficient is larger compared to the simulations with constant restitution coefficient. From these observations it can be concluded that the distribution of wet particles (*i.e.* distribution of the restitution coefficient) inside the bed influences the bed dynamics, and it is thus very important to incorporate these phenomena in the DEM. Furthermore, the size of regions of wet and dry particles depends on the flow regime that was applied. For the spouting-with-aeration regime, the impact of the simultaneous presence of dry and wet zones is most pronounced compared to the systems with constant restitution coefficient. Evaporation also affected the distribution of wet particles, since the particles in the annulus region were dried creating a dry annulus region and a wet spout region. For the jet-in-fluidized-bed regime (where the background velocity is rather high), the evaporation was most pronounced, showing the largest effect.

In the approach reported in this thesis, the restitution coefficient is solely dependent on the moisture content and is calculated for each particle. When two particles collide an effective restitution coefficient is calculated. However, during collisions of wet particles, part of the kinetic energy dissipates through the liquid layer. This implies that the rebound of particles depends on the impact velocity. In other words, if the impact velocity is low, less kinetic energy is left for rebound resulting in a lower rebound velocity. Consequently, the restitution coefficient depends on the moisture content and impact velocity, by which it should be regarded as a property of the collision event instead of a particle property. This is not yet accounted for in the model and it is foreseen that the influence of the restitution coefficient will increase if the impact velocity is also taken into account. The liquid viscosity should be considered as well, since this property influences the energy dissipation. The effect of impact velocity and liquid viscosity is described by Antonyuk et al. (2009). Additionally, solidification instead of evaporation of the liquid layer on the particles surface should be incorporated in the DEM to mimic the granulation process better and to enable the study of the quality of the produced granule in the future.

Nevertheless, the trends observed so far give already detailed understanding of the granulation processes which are applied in industry. In order to gain equal sized granules, mixing of the particles is very important, as well as drying (and solidification) of the liquid layer on the surface of the particles. These requirements plead to operate in the jet-in-fluidized-bed regime, since the larger background velocity provides good mixing and enhances evaporation of the liquid layer. Additionally, it prevents particles sticking to the distributor plate at the bottom of the granulator. The background velocity is of course limited to dust formation and operational costs, so that an optimum exists.

Experiments were conducted in the pseudo-2D and cylindrical 3D bed, where water was sprayed in the spout gas. Different wetting stages were studied and controlled by the humidity at the top of the bed by adjusting the water flow. It was very difficult to choose the correct wetting cases, since a too wet system causes particles to stick to each other and to the wall, hindering correct measurement of the particle velocity with PIV and PEPT. Additionally, formation of a water layer on the wall disturbs visualisation during PIV measurements, which should be avoided as well. Three wetting stages were used, corresponding to relative humidities of 65 %, 75 % and 85 %. A relative humidity of 90% showed too much sticking and floating of particles, and was therefore not studied. The background gas was humidified till $\sim 50\%$ relative humidity, resulting in a $RH = 40\%$ at the top of the bed for the dry case (due to mixing with the dry spout gas). The effect of water spray on the particle velocity in the pseudo-2D bed was measured for the spout-fluidization, the spouting-with-aeration and the jet-in-fluidized bed regime with Particle Image Velocimetry.

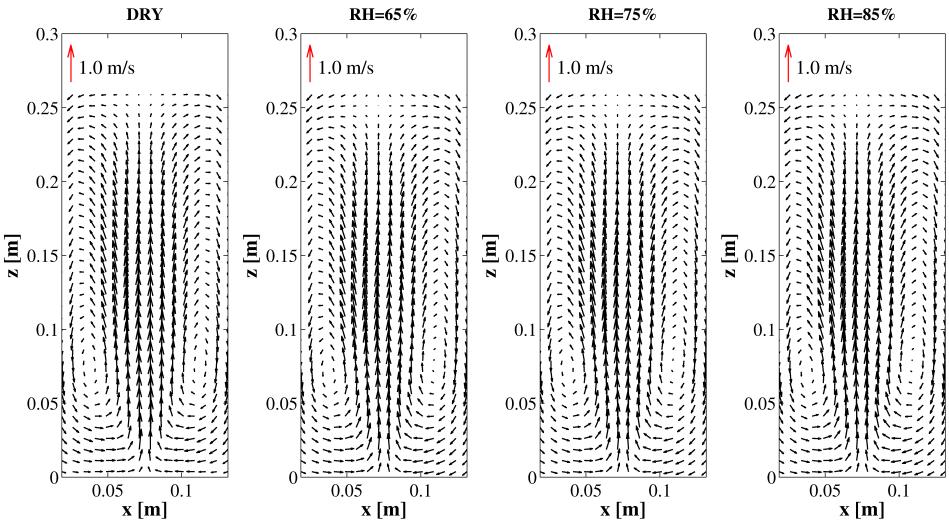

Figure E.1: Time-averaged particle velocity field in the pseudo-2D bed for the dry case ($RH = 40\%$), $RH = 65\%$, $RH = 75\%$ and $RH = 85\%$ (from left to right) obtained with PIV measurements for the jet-in-fluidized-bed regime.

It is shown in Figure E.1 that the time-averaged particle velocity fields are virtually the same for each wetting stage. The root mean square (RMS) of the particle velocity in the vertical (Figure E.2) and in the horizontal direction (Figure E.3) display large similarities as well, from which it can be concluded that the considered wetting stages did not result in wet particles causing different collision behavior. This was also the case for the spout-fluidization and spouting-with-aeration regime. In Figure E.4 the time-averaged vertical particle velocity profiles at one height in the central xz-plane are plotted for all three flow regimes, and it shows that the particle velocity is not affected by the water spray.

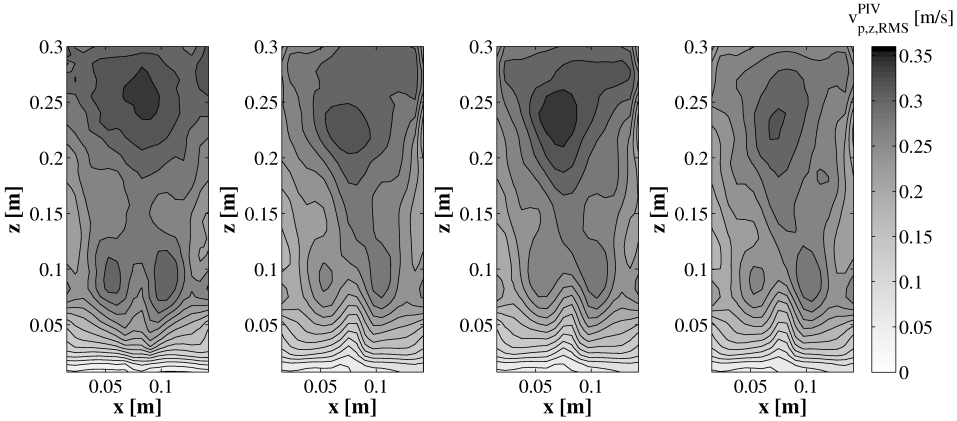

Figure E.2: Contour plot of the root mean square of the vertical particle velocity in the pseudo-2D bed for the dry case ($RH = 40\%$), $RH = 65\%$, $RH = 75\%$ and $RH = 85\%$ (from left to right) obtained with PIV measurements for the jet-in-fluidized-bed regime.

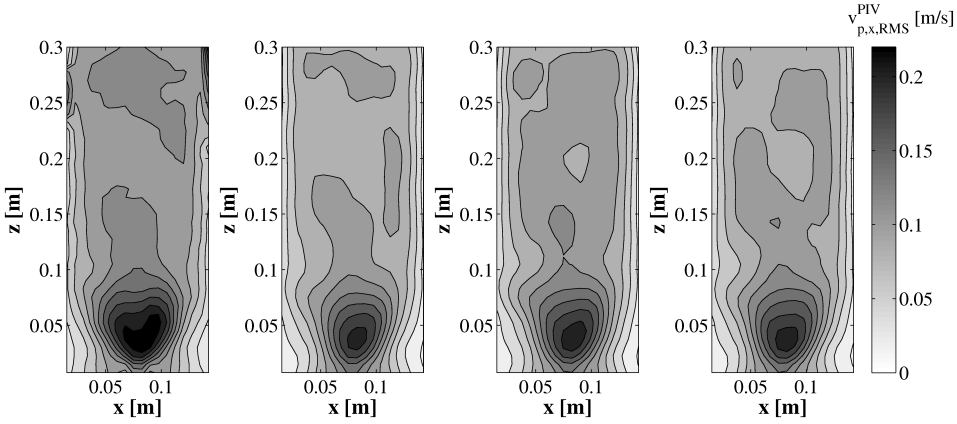

Figure E.3: Contour plot of the root mean square of the horizontal particle velocity in the pseudo-2D bed for the dry case ($RH = 40\%$), $RH = 65\%$, $RH = 75\%$ and $RH = 85\%$ (from left to right) obtained with PIV measurements for the jet-in-fluidized-bed regime.

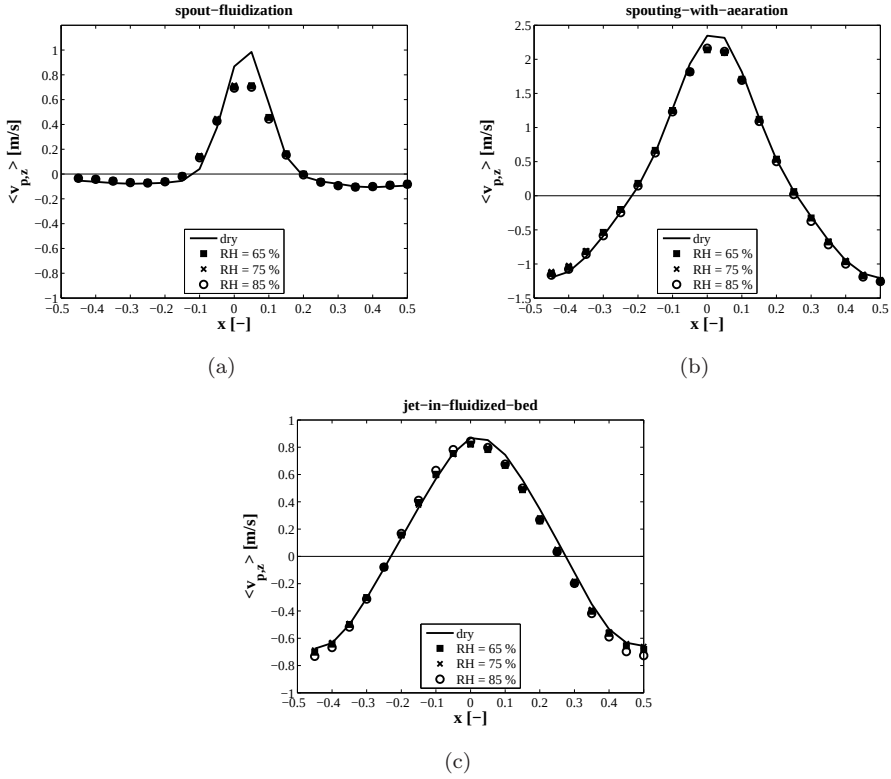

Figure E.4: Profiles of the time-averaged vertical particle velocity for the spout-fluidization regime in the central xz-plane at $z = 0.05$ m (a), for the spouting-with-aeration regime in the central xz-plane at $z = 0.10$ m (b) and for the jet-in-fluidized-bed regime in the central xz-plane at $z = 0.10$ m (c) for all the wetting stages in the pseudo-2D bed obtained from PIV measurements.

It is thus demonstrated that the water spray for these wetting stages did not influence the particle velocity inside the pseudo-2D bed. The results obtained from PEPT showed the same trends in both the pseudo-2D and cylindrical 3D bed. Unfortunately, the desired conditions to study the effect of wet particle-particle interactions on the bed dynamics were not reached, due to limitations of the experimental techniques. Hence, too dry conditions were chosen, resulting in experiments that gave similar results. The positive side of these observations, however, is that for measuring dry systems that are fluidized with humidified air to avoid electrostatic charging, relative humidity up to 85 % is still feasible for similar systems as described in this work. This was confirmed by pressure drop fluctuation measurements, where only a characteristic peak appeared for measurements with $RH < 35\%$, indicating that below this value electrostatic charging occurred.

To experimentally study the effect of liquid spraying in spout fluidized beds, more extreme wetting cases should be considered. Measurements in a pseudo-2D bed are very difficult since the particle-wall effects are more pronounced and the optical accessibility should be preserved. To the author's knowlegde, PEPT is the only non-invasive technique that could measure the particles velocity under wet conditions. However, very long measurement periods (approximately $>$ 10 hours) should be taken into account. X-ray tomography could be used to capture the temporal and spatial evolution of the particle volume fraction and thus the bubble behaviour.

The geometry of the spout fluidized bed was studied as well, to assess the effect of multiple spouts and the effect of spout elevation on the bed dynamics. A new flow regime map was constructed for the triple-spout fluidized bed, demonstrating that new flow regimes appear due to interaction of the spouts. It was shown that the background velocity influences the mutual interaction of the spouts, and the spout velocity affects the stability of the contraction into a single spout channel. The multiple-interacting-spouts regime was studied for double- and triple-spout fluidization, which is a fully new flow regime that does not appear in single-spout fluidized beds. Two flow patterns have been observed, *viz* particle circulation in between the spouts near the bottom of the bed, and the typical spout fluidization motion at a higher location upwards in the bed. Hence, the presence of multiple spouts in a spout fluidized bed highly affects the flow behaviour.

Simulation results were compared to the experimental results and it was shown that the simulation results deviate, in particular in the areas containing densely packed particles and near a wall. It was observed in the experiments that densely packed ensembles of particles are moving down in a pulsed manner, which shows that in this particular case static friction may be relevant. This is not accounted for in the model and should be included.

In this thesis, simulations and experiments were conducted on a pseudo-2D triple- and double-spout fluidized bed, with an intra-spout distance of 14 cm. Additionally, simulations were conducted for a double-spout fluidized bed with a distance between the spouts of 25 and 35 cm, respectively. It appeared that the spouts were less attracted to each other as the intra-spout distance increases, resulting in a downwards particle flux in between the spouts at a distance of 35 cm. However, it was shown that the downwards flux in between the spouts was still much smaller than the downward flux in the annulus region, which means that most of the particles are still hindered to move downwards by the attraction of the spout channels. These observations demonstrate that for a pseudo-2D bed as used in this work, up to an intra-spout distance of 35 cm, the spout channels still interact, although to lesser extent.

It should be stressed that these results were obtained for the typical pseudo-2D bed as used in this work. In a pseudo-2D bed, the spout channels can only move in the lateral direction of the bed, due to the small depth of the bed. As a result, the spout channels are more inclined to attract each other compared to full 3D systems. It is nevertheless very likely that the spout interaction also occurs in 3D systems, although this should be verified in future work.

After all, new insights were obtained for the multiple-spout fluidized bed granulators. If the spouts interact, an extra circulation pattern near the bottom of the bed could arise that worsens the mixing inside the granulator and increases the chance for deposition of wet particles on the bottom plate. This could be avoided by applying a relatively high background velocity, considering the earlier mentioned limitations and the fact that the spouts interact more at a higher background velocity. Therefore, it is recommended (in the frame of this work) to operate in between the multiple-interacting-spouts and multiple-jets-in-fluidized-bed regime.

The effect of spout elevation in spout fluidized beds was studied in both pseudo-2D and cylindrical 3D beds. For the pseudo-2D bed, the spout-fluidization and jet-in-fluidized-bed regime have been examined, from which it was concluded that the spout-fluidization regime did not show any dependency on spout height in the sense that increasing the spout height leads to the creation of dead zones up to the entrance of the spout. In the jet-in-fluidized-bed regime the background gas velocity is relatively high, producing bubbles in the annulus that interact with the spout channel. In case of a non-elevated spout, this interaction occurs near the bottom of the bed. As the spout is elevated, this interaction is shifted upwards in the bed, which allows the bubbles to remain undisturbed providing the motion of the particles in the annulus near the bottom of the bed. Consequently, no dead zones are created and additionally, circulation patterns are vertically stretched. These findings are also observed in the cylindrical 3D bed, though, to lesser extent. The bubbles in the pseudo-2D bed are more pronounced due to the more dominant particle-wall effects, and therefore enhance the effect of the spout elevation. To avoid stagnant zones in industrial granulators where the spouts are elevated, it is again recommended to operate in the jet-in-fluidized-bed regime.

The effect of particle wetness, multiple-spout and elevated spout were separately studied, although in principle these aspects should be considered simultaneously. Question is, how these aspects influence each other, and if the observed effects are strengthened or weakened. Below the expected behavior is discussed. In case of the multiple-interacting-spouts regime for a triple-spout fluidized bed, an additional circulation pattern occurs near the bottom of the bed, due to the interaction of the spouts. As the spouts are elevated, interaction of the spouts starts at a higher location in the bed and the particles near the bottom of the bed will become stagnant since the background velocity in this regime is in the order of the minimum fluidization velocity. As recommended earlier, the background velocity should be higher, however not too high to avoid too much disturbance of the spout channels. In case of elevated spouts, more pronounced bubble formation occurs, resulting in larger disturbances of the spouts, which should be accounted for. If a liquid is sprayed in the spout, the spout channel closes more often due to the smaller restitution coefficient of the particles in this zone. In the annulus region, bubbling becomes more pronounced, and the bed heterogeneity increases. If the background velocity is large enough, better mixing occurs by which the dry and wet zones are less distinctive and hence the effect of the restitution coefficient is less pronounced. The presence of wet particles will increase the interaction of the

spouts, due to the presence of more bubbles. However, the stability of merging to a single spout will not increase since the spouts will close more often than in the dry case, enabling to split again into separate channels. Of course these hypotheses should be verified by further numerical and experimental study. All the findings in this thesis were obtained in laboratory scale systems. As demonstrated in the experimental results for the pseudo-2D and cylindrical 3D spout fluidized bed, wall effects significantly influence the bed behaviour and enhance the effect of the studied aspects. Therefore, next step is to extend this study to pilot and industrial scale to analyze particle behaviour in systems that aproach industrial conditions better. Simulation models that are available in our group for larger scale operations are very suitable for these studies, such as the Multi Fluid Model (MFM) and Discrete Bubble Model (DBM). From the DEM results information can be obtained to provide closures for the MFM and DBM.

Although future work on larger scale is desirable, the results that were discussed in this thesis provide fundamental knowledge of the particle behaviour as function of particle-particle interaction, number of spouts and spout elevation which serves as a building block for improving the granulation process in spout fluidized beds.

Bibliography

Agarwal, P. K., Hull, A. S. and Lim, K. S.: 1997, *Non-invasive monitoring of multiphase flows*, Elsevier Science B.V.

Antonyuk, S., Heinrich, S., Deen, N. G. and Kuipers, J. A. M.: 2009, Influence of liquid layers on energy absorption during particle impact, *Particuology* **7**, 245.

Bird, R. B., Steward, W. E. and Lightfoot, E. N.: 1960, *Transport phenomena*, John Wiley and Sons.

Bokkers, G. A., Van Sint Annaland, M. and Kuipers, J. A. M.: 2004, Mixing and segregation in a bidisperse gas-solid fluidised bed: A numerical and experimental study, *Powder Technology* **140**, 176.

Chian, W. C., Seville, J. P. K., Yang, Z. and Baeyens, J.: 2009, Particle motion in the CFB riser with special emphasis on PEPT-imaging of the bottom section, *Powder Technology* **196**, 318.

Cundall, P. A. and Strack, O. D. L.: 1979, A discrete numerical model for granular assemblies, *Géotechnique* **29**, 47.

da Cunha, R. L. G., Pereira, M. M. C. and Rocha, S. C. S.: 2009, Conventional and modified fluidized bed: Comparison of the fluid dynamics and application in particle granulation, *Chemical Engineering and Processing* **48**, 1004.

Deen, N. G., van Sint Annaland, M. and Kuipers, J. A. M.: 2004, Multi-scale modeling of dispersed gas-liquid two-phase flow, *Chemical Engineering Science* **59**, 1853.

Deen, N. G., van Sint Annaland, M., van der Hoef, M. and Kuipers, J. A. M.: 2007, Review of discrete particle modeling of fluidized beds, *Chemical Engineering Science* **62**, 28.

Deng, R. and Wang, C. H.: 2003, Particle image velocimetry study on the pattern formation in a vertically vibrated granular bed, *Physics of Fluids* **15**, 3718.

Depypere, F., Pieters, J. G. and Dewettinck, K.: 2009, PEPT visualisation of particle motion in a tapered fluidised bed coater, *Journal of Food Engineering* **93**, 324.

Dijkhuizen, W., Bokkers, G. A., Deen, N. G., Van Sint Annaland, M. and Kuipers, J. A. M.: 2007, Extension of PIV for measuring granular temperature field in dense fluidized beds, *American Institute of Chemical Engineers Journal* **53**, 108.

Du, B., Warsito, W. and Fan, L. S.: 2004, ECT Studies of the Choking Phenomenon in a Gas-Solid Circulating Fluidized Bed, *American Institute of Chemical Engineers Journal* **50**, 1386.

Du, B., Warsito, W. and Fan, L. S.: 2005, ECT Studies of Gas-Solid Fluidized Beds of Different Diameters, *Industrial and Engineering Chemistry Research* **44**, 5020.

Ennis, B. J., Tardos, G. and Pfeffer, R.: 1991, A microlevel-based characterization of granulation phenomena, *Powder Technology* **65**, 257.

Fan, X., Parker, D. J., Yang, Y., K., S. J. P. and Baeyens, J.: 2008, The effect of bed materials on the solid/bubble motion in a fluidised bed, *Chemical Engineering Science* **63**, 943.

Fu, J., Adams, M. J., Reynolds, G. K., Salman, A. D. and Hounslow, M. J.: 2004, Impact deformation and rebound of wet granules, *Powder Technology* **140**, 248.

Geldart, D.: 1973, Types of gas fluidization, *Powder Technology* **7**, 285.

Godlieb, W.: 2010, *High pressure fluidization*, PhD thesis, Technical University Eindhoven.

Goldschmidt, M. J. V., Link, J. M., Mellema, S. and Kuipers, J. A. M.: 2003, Digital image analysis measurements of bed expansion and segregation dynamics in dense gas-fluidised beds, *Powder Technology* **138**, 135.

Gong, X., Hu, G. and Li, Y.: 2006, Hydrodynamic characteristics of a novel annular spouted with multiple air nozzles, *Industrial and Engineering Chemistry Research* **45**, 4830.

Gunn, D. J.: 1978, Transfer of heat or mass to particles in fixed and fluidized beds, *International Journal of Heat and Mass Transfer* **21**, 467.

Guo, Q. J., Zhang, J. and Werther, W.: 2003, Jetting transition velocity in a jetting fluidized bed with two nozzles, *Chemical Engineering Journal* **92**, 63.

Hong, R. Y., Guo, Q. J., Luo, G. H., Zhang, J. Y. and Ding, J.: 2003, On the jet penetration height in fluidized beds with two vertical jets, *Powder Technology* **133**, 216.

Hoomans, B. P. B., Kuipers, J. A. M., Briels, W. J. and van Swaaij, W. P. M.: 1996, Discrete particle simulation of bubble and slug formation in a two-dimensional gas-fluidised bed: A hard-sphere approach, *Chemical Engineering Science* **51**, 99.

Hoomans, B. P. B., Kuipers, J. A. M., Mohd Salleh, M. A., Stein, M. and Seville, J. P. K.: 2001, Experimental validation of granular dynamics simulations of gas-fluidised beds with homogenous in-flow conditions using Positron Emission Particle Tracking, *Powder Technology* **116**, 166.

Hu, G., Gong, X., Wei, B. and Li, Y.: 2008, Flow patterns and transitions of a novel annular spouted bed with multiple air nozzles, *Industrial and Engineering Chemistry Research* **47**, 9759.

Isaksen, O.: 1996, A review of reconstruction techniques for capacitances tomography, *Measurement Science and Technology* **7**, 325.

Iveson, S. M., Litster, J. D., Hapgood, K. and Ennis, B. J.: 2001, Nucleation, growth and breakage phenomena in agitated wet granulation processes: a review, *Powder Technology* **117**, 3.

Jain, N., Ottino, J. M. and Lueptow, R. M.: 2002, An experimental study of the flowing granular layer in a rotating tumbler, *Physics of Fluids* **14**, 572.

Kalwar, M. I., Raghavan, G. S. V. and Mujumbar, A. S.: 1993, Circulation of particles in two-dimensional spouted beds with draft plates, *Powder Technology* **77**, 233.

Koch, D. L. and Hill, R. J.: 2001, Inertial effects in suspension and porous-media flows, *Annual Reviews of Fluid Mechanics* **33**, 619.

Laverman, J. A.: 2010, *On the hydrodynamics in gas phase polymerization reactors*, PhD thesis, Technical University Eindhoven.

Laverman, J. A., Roghair, I., Van Sint Annaland, M. and Kuipers, J. A. M.: 2008, Investigation into the hydrodynamics of gassolid fluidized beds using particle image velocimetry coupled with digital image analysis, *The Canadian Journal of Chemical Engineering* **86**, 523.

Lei, J., Liu, S., Li, Z. and Sun, M.: 2009, An image reconstruction algorithm based on the extended Tikhonov regularization method for electrical capacitance tomography, *Measurement* **42**, 368.

Li, Y. and Yang, W.: 2008, Image reconstruction by nonlinear Landweber iteration for complicated distributions, *Measurement Science and Technology* **19**, 094014.

Link, J. M.: 2006, *Development and validation of a discrete particle model of a spout-fluid bed granulator*, PhD thesis, University of Twente.

Link, J. M., Cuypers, L. A., Deen, N. G. and Kuipers, J. A. M.: 2005, Flow regimes in a spout-fuid bed: A combined experimental and simulation study, *Chemical Engineering Science* **60**, 3425.

Link, J. M., Deen, N., Kuipers, J. A. M., Fan, X., Ingram, A., Parker, D., Wood, J. and Seville, J.: 2008, PEPT and Discrete Particle Simulation study of spout-fluid bed regimes, *American Institute of Chemical Engineers* **54**, 1189.

Link, J. M., Godlieb, W., Deen, N. G. and Kuipers, J. A. M.: 2007, Discrete element study of granulation in a spout-fluidized bed, *Chemical Engineering Science* **62**, 195.

Link, J. M., Zeilstra, C., Deen, N. G. and Kuipers, J. A. M.: 2004, Validation of a discrete particle model in a 2D spout-fluid bed using non-intrusive optical measuring techniques, *The Canadian Journal of Chemical Engineering* **82**, 30.

Liu, G. Q., Li, S. Q., Zhao, X. L. and Yao, Q.: 2008, Experimental studies of particle flow dynamics in a two-dimensional spouted bed, *Chemical Engineering Science* **63**, 1331.

Liu, S., Chen, Q., Wang, H. G., Jiang, F., Ismail, I. and Yang, W. Q.: 2005, Electrical capacitance tomography for gas-solids flow measurement for circulating fluidized beds, *Flow Measurement and Instrumentation* **16**, 135.

Makkawi, Y. T. and Wright, P. C.: 2002, Fluidization regimes in a conventional fluidized bed characterized by means of electrical capacitance tomography, *Chemical Engineering Science* **57**, 2411.

Mangwandi, C., Cheong, Y. S., Adams, M. J., Hounslow, M. J. and Salman, A. D.: 2007, The coefficient of restitution of different representative types of granules, *Chemical Engineering Science* **62**, 437.

Mavrovic, I., Shirley, R. and Coleman, G. R. B.: 2010, *Kirk-Othmer Encyclopedia of Chemical Technology*, John Wiley & Sons, Inc., chapter Urea.

Medina, A., Córdova, J. A., Luna, E. and Treviño, C.: 1998, Velocity field measurements in granular gravity flow in a near 2D silo, *Physics Letter A* **250**, 111.

Mörl, L., Heinrich, S. and Peglow, M.: 2007, *Granulation (Handbook of powder technology)*, Vol. 11, Elsevier Science B. V., Amsterdam, The Netherlands.

Mudde, R. F.: 2010, Advanced Measurement Techniques for GLS Reactors, *The Canadian Journal of Chemical Engineering* **88**, 638.

Parker, D. J., Allen, D. A., Benton, D. M., Fowles, P., McNeil, P. A., M. T. and Beynon, T. D.: 1997, Developments in particle tracking using the birmingham positron camera, *Nuclear Instruments and Methods in Physics Research A* p. 421.

Passos, M. L. and Mujumdar, A. S.: 2000, Effect cohesive forces on fluidized and spouted beds of wet particles, *Powder Technology* **110**, 222.

Seville, J. P. K., Ingram, A. and Parker, D. J.: 2005, Probing processes using positrons, *Chemical Engineering Research and Design* **83**, 788.

Stein, M., Ding, Y. L., Seville, J. P. K. and Parker, D. J.: 2000, Solids motion in bubbling gas fluidised beds, *Chemical Engineering Science* **55**, 5291.

Steingart, D. A. and Evans, J. W.: 2005, Measurements of granular flows in two-dimensional hoppers by Particle Image Velocimetry. Part I: Experimental method and results, *Chemical Engineering Science* **60**, 1043.

Talu, I., Tardos, G. I. and Khan, M. I.: 2000, Computer simulation of wet granulation, *Powder Technology* **59**, 222.

Tapp, H. S., Peyton, A. J., Kemsley, E. K. and Wilson, R. H.: 2003, Chemical engineering applications of electrical process tomography, *Sensors and Actuators B* **92**, 17.

Van de Velden, M., Baeyens, J., Seville, J. P. K. and Fan, X.: 2008, The solids flow in the riser of a Circulating Fluidised Bed (CFB) viewed by Positron Emission Particle Tracking (PEPT), *Powder Technology* **183**, 290.

Van der Hoef, M. A., Van Sint Annaland, M., Deen, N. G. and Kuipers, J. A. M.: 2008, Numerical simulation of dense gas-solid fluidized beds: A multiscale modeling strategy, *Annual Review of Fluid Mechanics* **40**, 47.

Vieira, M. G. A. and Rocha, S. C. S.: 2004, Influence of the liquid saturation degree on the fluid dynamics of a spouted-bed coater, *Chemical Engineering and Processing* **43**, 1275.

Vorhauer, N.: 2007, *Untersuchung des Einfluss von Flüssiskeitsschichten auf das Stoβverhalten elastisch-plastischer Granulate*, Master's thesis, Otto-von-Güricke-University Magdeburg.

Westerweel, J.: 1997, Fundamentals of digital particle image velocimetry data, *Measurement Science and Technology* **8**, 1379.

Yang, W. Q. and Peng, L.: 2003, Image reconstruction algorithms for electrical capacitance tomography, *Measurement Science and Technology* **14**, R1.

Zeilstra, C., Collignon, J. G., Van der Hoef, M. A., Deen, N. G. and Kuipers, J. A. M.: 2008, Experimental and numerical study of wall-induced granular convection, *Powder Technology* **184**, 166.

List of Publications

Journal Publications

1. Van Buijtenen, M.S., Deen, N.G., Heinrich, S., Antonyuk, S. and Kuipers, J.A.M.: 2009, A discrete particle simulation study on the influence of restitution coefficient on spout fluidized bed dynamics. *Chemical Engineering & Technology* **32**, 454.

2. Van Buijtenen, M.S., Deen, N.G., Heinrich, S., Antonyuk, S. and Kuipers, J.A.M.: 2009, A discrete element study of wet particle-particle interaction during granulation in a spout fluidized bed. *Canadian Journal of Chemical Engineering* **87**, 308.

3. Antonyuk, S., Heinrich, S., Tomas, J., Deen, N.G., van Buijtenen, M.S., Kuipers, J.A.M.: 2010, Energy absorption during compression and impact of dry elastic-plastic spherical granules. *Granular Matter* **12**, 15.

4. Van Buijtenen, M.S., Börner, M. Deen, N.G., Heinrich, S., Antonyuk, S. and Kuipers, J.A.M.: 2011, An experimental study of the effect of collision properties on spout fluidized bed dynamics. *Powder Technology*, 2011 **206**, 139.

5. Van Buijtenen, M.S., Van Dijk, W.J., Deen, N.G. and Kuipers, J.A.M., Numerical and experimental study on multiple-spout fluidized beds. *Chemical Engineering Science*, 2011, doi: 10.1016/j.ces.2011.02.055.

6. Van Buijtenen, M.S., Buist, K.A., Deen, N.G. and Kuipers, J.A.M., Numerical and experimental study on spout elevation in spout fluidized beds. *AIChE Journal* (submitted).

Publications in Conference Proceedings

1. Van Buijtenen, M.S., Deen, N.G., Heinrich, S., Kuipers, J.A.M., Tripp, P. and Schönherr, M.: Improvement of the discrete element model for the study of granulation in a spout fluidized bed. 6th International Conference on Multiphase Flow, ICMF 2007, Leipzig, Germany, July 9-13, 2007, paper no. 266

2. Heinrich, S., Deen, N.G., Van Buijtenen, M.S., Kuipers, J.A.M., Tripp, P., Schönherr, M. and Peglow, M.: Detailed investigation of granulation processes using a fibre-optical probe and discrete element simulations. 3rd International Conference on Population Balance Modelling, Québec City, Canada, September 19-21, 2007

3. Van Buijtenen, M.S., Deen, N.G., Heinrich, S., Antonyuk, S. and Kuipers, J.A.M.: A Discrete Element Study of Moisture Dependent Particle-Particle Interaction During Granulation in a Spout Fluidized Bed. 6th International Conference on Computational Fluid Dynamics in the Oil & Gas, Metallurgical and Process Industries Trondheim, Norway, June 10-12, 2008

4. Antonyuk, S., Heinrich, S., Dosta, M., Van Buijtenen, M.S., Deen, N.G. and Kuipers, J.A.M.: Effect of the liquid layer on the impact behaviour of particles. 9th International Symposium on Agglomeration, Sheffield, United Kingdom, June 22-26, 2009

5. Van Buijtenen, M.S., Börner, M., Deen, N.G., Heinrich, S., Antonyuk, S. and Kuipers, J.A.M.: An experimental study of the effect of collision properties on spout fluidized bed dynamics. 9th International Symposium on Agglomeration, Sheffield, United Kingdom, June 22-26, 2009

6. Van Buijtenen, M.S., Van Dijk, W.J., Deen, N.G. and Kuipers, J.A.M. Numerical and experimental study on the effect of multiple spouts on the spout fluidized bed dynamics. The World Congress on Particle Technology, Nürnberg, Germany, April 26 -29, 2010

Presentations

1. Van Buijtenen, M.S., Deen, N.G., **Heinrich, S.**, Tripp, P., Kuipers, J.A.M., Schönherr, M.: Analyse der Partikel- und Tropfenbewegungen in einer bedüsten-Wirbelschicht mittels Diskrete-Elemente-Modellierung

und faseroptischen Messungen. Plenary lecture at the "Arbeitstagung des GVC-Fachausschusses Agglomerations- und Schüttguttechnik", 2007

2. Van Buijtenen, M.S., Deen, N.G., **Heinrich, S.**, Tripp, P., Kuipers, J.A.M., Schönherr, M., Peglow, M.: Optimierung eines Diskreten-Elemente-Modells und Vergleich mit faseroptischen Messungen zur Analyse der Granulation in einer Wirbelschicht. Plenary lecture at the "Arbeitstagung des GVC-Fachausschusses Trocknungstechnik", 2007

3. Van Buijtenen, M.S., **Deen, N.G.**, Heinrich, S., Antonyuk, S. and Kuipers, J.A.M.: Improvement of the discrete element model for the study of granulation in a spout fluidized bed. Oral presentation at the 9^{th} International Conference on Circulating Fluidized Beds (CFB9), Hamburg, Germany, May 13-16, 2008

4. **Van Buijtenen, M.S.**, Deen, N.G., Heinrich, S., Antonyuk, S. and Kuipers, J.A.M.: A discrete element study of wet particle-particle interaction during granulation in a spout fluidized bed. Oral presentation at the Fifth International Symposium on Spouted Beds (ISSB-2008), Changping, Beijing, China, July 21-23, 2008

5. **Van Buijtenen, M.S.**, Deen, N.G. and Kuipers, J.A.M.: Collision considerations and moisture matters - Effect of the restitution coefficient on spout fluidized bed dynamics. Poster presentation at Netherlands Process Technology Symposium (NPS), Veldhoven, The Netherlands, October 28-29, 2008

6. **Van Buijtenen, M.S.**, Börner, M., Deen, N.G., Heinrich, S., Antonyuk, S. and Kuipers, J.A.M.: An experimental study of the effect of collision properties on spout fluidized bed dynamics. Oral presentation at the Second Impact-Fermat meeting, Enschede, the Netherlands, October 13-16, 2009

7. **Van Buijtenen, M.S.**, Van Dijk, W.J., Deen, N.G. and Kuipers, J.A.M. Numerical and experimental study on the effect of multiple spouts on the spout fluidized bed dynamics. Oral presentation at the The World Congress on Particle Technology, Nürnberg, Germany, April 26 -29, 2010

8. **Van Buijtenen, M.S.**, Deen, N.G. and Kuipers, J.A.M. Fundamentals of fluidized bed granulation processes. Oral presentation at the Burgersdag 2011, J.M. Burgerscentrum, Delft, The Netherlands, January 13, 2011

Dankwoord

“Hoe kom je als beginnend onderzoeker aan een goed promotie-onderwerp?” Dit vroeg ik mij opnieuw af toen ik begon aan dit dankwoord. Gelukkig hadden Hans Kuipers en Niels Deen in 2006 de financiering verkregen voor een voorstel, ingediend bij het onderzoeksprogramma ’Gedispergeerde meerfasestroming’ van FOM-STW-EZ, over Multiphase Flow in Spout Fluidized Bed Granulators. Juist dit project leek mij op het lijf geschreven. Doordat dit onderzoek een vervolg was op het promotie-onderzoek van Jeroen Link en doordat Yara Sluiskil BV door zijn financiële steun nauw betrokken was, kreeg het fundamentele onderzoek een zeer toegepast sausje. Deze combinatie sprak mij erg aan! Aanvankelijk lag de focus op de vocht-injectie in spout-wervelbedden, maar door de regelmatige besprekingen en discussies met Remco de Fouw, Ruud van Belzen en anderen van Yara Sluiskil, ontdekte ik dat in de industriële toepassing de spout verhoogd is en dat er meerdere spouts in de granulator aanwezig zijn. Het effect hiervan op de beweging van de deeltjes was niet geheel duidelijk. Verder realiseerde ik me dat deze geometrische aspecten nog nooit onderzocht waren en leek het mij van zowel academische als industriële waarde om dit in mijn onderzoek op te nemen. Hans en Niels reageerden zeer enthousiast op mijn voorstel. De vrijheid die mij gegeven werd om ook zelf richting te geven aan het onderzoek gaf mij het gevoel dat dit echt mijn eigen onderzoek was en dat werkte zeer stimulerend.

Ik wil daarom mijn promotor Hans Kuipers bedanken voor de mogelijkheid die hij mij heeft geboden om überhaupt te werken aan dit onderzoek, en voor het bieden van enerzijds de structuur en anderzijds de vrijheid in uitvoering. “Hans, onze besprekingen waren zeer nuttig en je zorgde ervoor dat we met een ’helicopter view’ naar de voortgang keken, zonder de details uit het oog te verliezen.” Uiteraard wil ik ook mijn copromotor Niels Deen bedanken, met wie ik wekelijks (zo niet vaker) over het onderzoek kon discussiëren. Daardoor bleef ik niet lang vastzitten met een probleem en behield het onderzoek continuïteit. “Niels, jouw inhoudelijke kennis en je kennis op het gebied van modelleren en experimentele

technieken hebben een grote bijdrage geleverd aan dit proefschrift.“

The collaboration with Prof. Heinrich and Dr. Antonyuk in the study of collision properties of wet and dry particles was very valuable, for which I owe them my gratitude.

Verder ben ik dank verschuldigd aan Prof. Westerweel die software beschikbaar stelde zodat ik synthetisch DIA beelden kon genereren voor de ontwikkeling van het DIA algoritme.

Tijdens het bekend raken met het DEM model, was collega-aio Willem Godlieb mijn vraagbaak. “Willem, gelukkig heb je geen punthoofd gekregen van mijn vragen (of toch wel?).” Voor mijn Linux en andere computer-perikelen kon ik altijd terecht bij Sebastian Kriebitzsch en Ivo Roghair. Tevens werd het rekencluster erg goed onderhouden door Robert Meijer, Wouter Dijkhuizen, Willem Godlieb, Sebastian Kriebitzsch, Ivo Roghair, Tom Kolkman en Yuk Man Lau, zodat er altijd veilig gequeue-ed, gesubmit en getarred kon worden.

Na een periode van achter de computer zitten werd het ook tijd voor experimenteren, en dus voor het ontwerpen en bouwen van nieuwe opstellingen. De bestaande opstelling werd door technicus Gerrit Schorfhaar gereed gemaakt, zodat mijn eerste afstudeerder Matthias Börner met metingen kon beginnen. Niels Hietberg heeft voor zijn Capita Selecta opdracht extra metingen gedaan in opvolging van Matthias. Het ontwerpen en bouwen van twee nieuwe opstellingen heb ik mede kunnen doen dankzij de bezielende begeleiding van de technici Robert Meijer en Wim Leppink. “Wat waren de besprekingen over het ontwerp leerzaam, en wat zijn de opstellingen mooi geworden (de constructie alleen al)!” Verder hebben we zelf een ECT sensor gemaakt, waarvoor Erik Analbers alle hulp heeft gegeven. Beide opstellingen werden gebruikt voor metingen aan de UT in Enschede, onder andere ook door een aantal studenten. Aan het pseudo-2D bed hebben Willem-Jan van Dijk en Kay Buist gewerkt. Willem-Jan heeft voor zijn afstudeeropdracht het effect van meerdere spouts op de beddynamica bekeken, waarbij hij het DIA algoritme verder verfijnd heeft. Daarnaast heeft hij o.a. het effect van de afstand tussen de spouts bestudeerd met behulp van simulaties. Kay Buist heeft voor zijn Bachelor opdracht metingen aan dezelfde opstelling uitgevoerd, waarbij hij de spouthoogte en vocht-injectie onderzocht heeft. Arjen Pille heeft in het kader van zijn Bachelor opdracht gewerkt aan de ECT sensor voor het 3D bed, en heeft laten zien dat de sensor goed presteert. Jeremy Timmer heeft een begin gemaakt met de verbetering van de beschrijving van de botsingen van natte deeltjes in het DEM model.

Ik heb dus een aantal studenten mogen begeleiden, wat niet alleen resulteerde in extra data en inzichten voor dit proefschrift, maar ook in extra plezier in het werk!

Naast het experimentele werk in Twente, heb ik ook experimenten uitgevoerd in Birmingham. I would like to thank Prof. Parker and Dr. Leadbeater for their availability and hospitality during my stay at the University of Birmingham, and I also appreciated the discussions with Dr. Leadbeater about the theory of the PEPT technique.

Het verschepen van de twee opstellingen (een heel busje vol!) heb ik natuurlijk niet in mijn eentje gedaan. Op de heenreis heeft Wim Leppink mij vergezeld en heeft hij de eerste opstelling in Birmingham in bedrijf gesteld. Robert Meijer heeft ervoor gezorgd dat de tweede opstelling bruikbaar was. Daarna hielp Robert met het weer keurig inpakken van de opstellingen voor de terugreis, die min of meer voorspoedig verliep. “Robert, het was alleen jammer dat de veerboot te vroeg vertrok....”

Om een promotie-onderzoek tot een goed einde te brengen is sociale cohesie binnen de onderzoeksgroep zeer belangrijk. Als promovendus ben je toch solistisch aan het werk, ondanks de samenwerking met verschillende mensen. Dit kwam tot uiting in de kantoortuin, waarin we met zijn allen werkten aan ons eigen ’meesterwerk’ met vaak overeenkomstige problemen die we dan eenvoudig met elkaar konden delen en oplossen. Ook niet-inhoudelijke punten kwamen aan bod, waar Willem en ik heerlijk over konden doorkletsen (waar de rest natúúrlijk geen last van had...). De vele borrels en aio-uitjes zorgden voor de extra gezelligheid.

Nu de promotie-datum nadert wil ik alvast mijn paranimfen Willem Godlieb en Sebastian Kriebitzsch bedanken voor hun assistentie tijdens mijn verdediging en daarna.

Verder ben ik mijn schoonouders en familie dankbaar voor hun interesse en steun, en mijn ouders die altijd rust en vertrouwen gaven. “Pap, wat is het toch bijzonder om samen over onze technische probleempjes te babbelen, en ook over TUD/UT dingen, jij als prof, ik als aio.” Ten slotte denk ik aan mijn lieve man Tymen. “Met jou aan mijn zijde kan ik de hele wereld aan en samen vormen we een super team. Jij bent mij voorgegaan met de voltooiing van jouw promotie. Daar heb ik veel van geleerd en ik hoop dat ik het net zo goed kan afronden als jij.”

Maureen van Buijtenen - Tiemersma

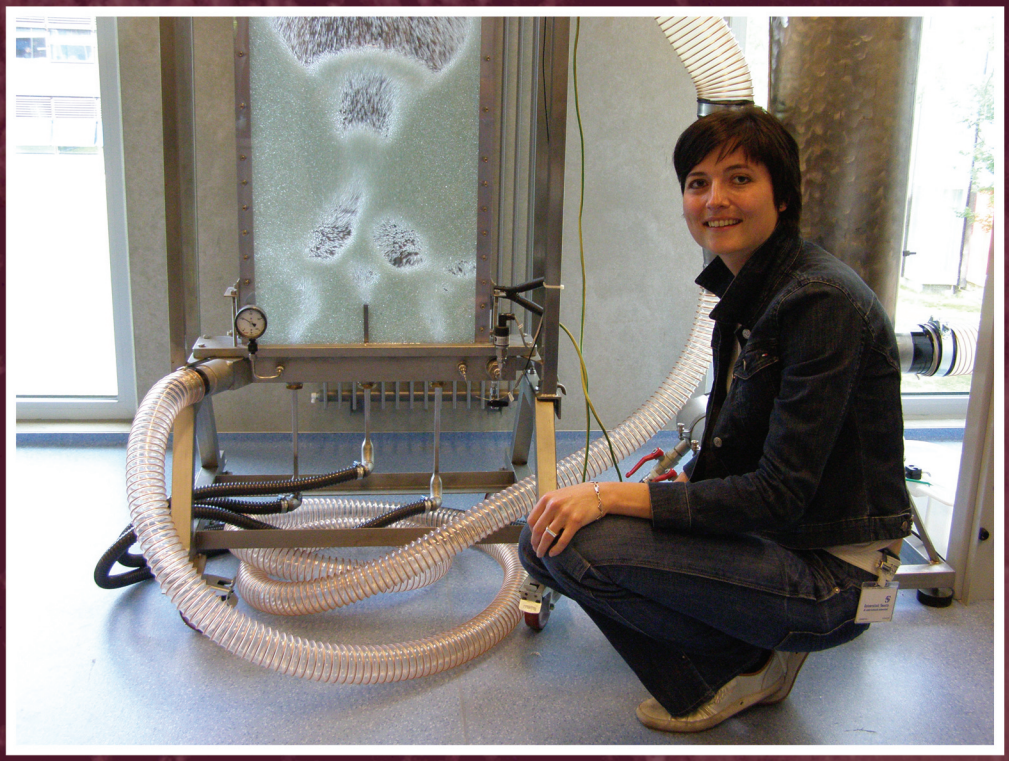

Maureen van Buijtenen-Tiemersma werd geboren op 21 februari 1980 in Warnsveld. Zij groeide op in Zutphen en Goor en volgde in Goor basisonderwijs op de Heeckerenschool. In 1997 nam ze het HAVO diploma en in 1999 het VWO diploma in ontvangst op het toenmalige Twickel College te Hengelo. In september 1999 begon Maureen aan de studie Chemische Technologie aan de Universiteit Twente in Enschede. Gedurende deze studie heeft zij stage gelopen bij KEMA Power Generation & Sustainables, en volgde de minor "Kennisoverdracht in Bedrijfs- en Kennisoverdrachtsituaties". In 2006 behaalde zij haar ingenieursdiploma bij de vakgroep Fundamentals of Chemical Reaction Engineering op een onderzoek getiteld "Numerical and experimental study of the lift and drag forces in gas-liquid systems".

Na de ingenieursopleiding trad zij in dienst van dezelfde vakgroep om als promovendus granulatie processen in een spout wervelbed zowel numeriek als experimenteel te onderzoeken. De resultaten van dit onderzoek staan beschreven in dit proefschrift. Sinds 1 maart 2011 is Maureen werkzaam als researcher bij AkzoNobel Chemicals B.V. in de Expert Capability Group Process Technology.

ISBN 978-90-386-2459-4